

Figure 62 Dimensionless temperature profiles  $\Delta^*$  versus the dimensionless gap  $\kappa$  using  $R_{\text{Ratio}} = 0.80$  and the dimensionless eccentricity,  $\varepsilon = 0.30$ , at various angles  $\beta$  and power law indexes n.

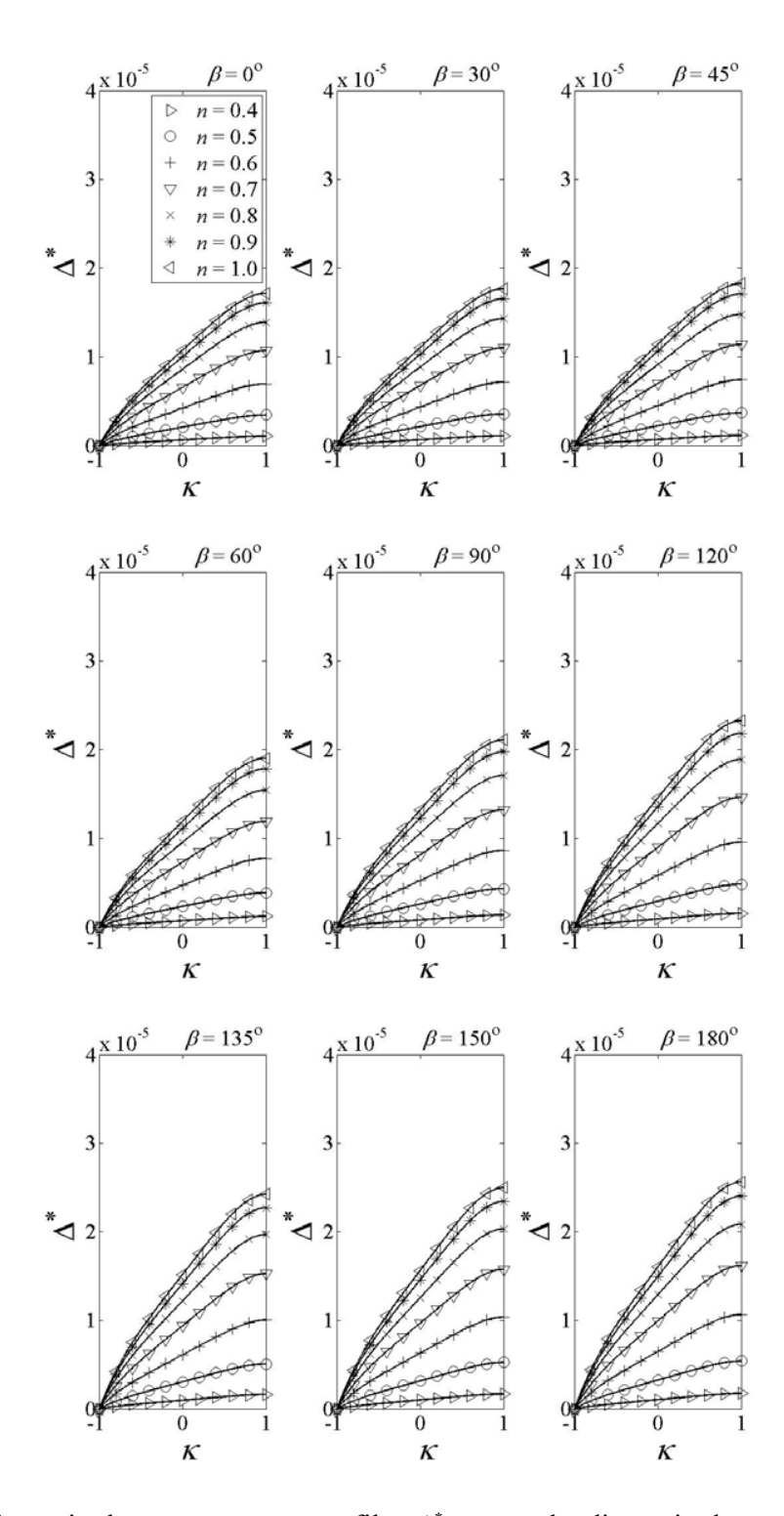


Figure 63 Dimensionless temperature profiles  $\Delta^*$  versus the dimensionless gap  $\kappa$  using  $R_{\text{Ratio}} = 0.85$  and the dimensionless eccentricity,  $\varepsilon = 0.05$ , at various angles  $\beta$  and power law indexes n.

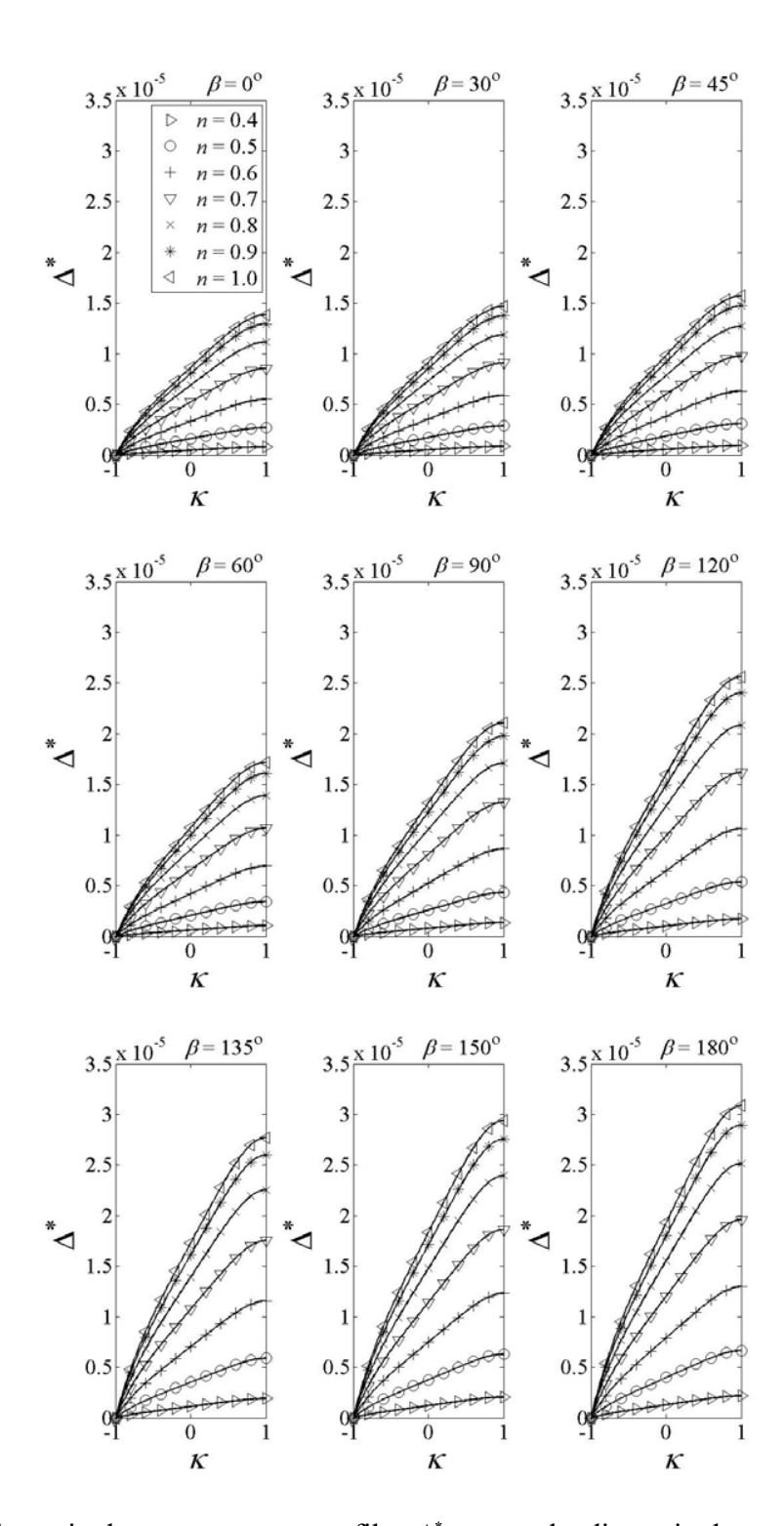


Figure 64 Dimensionless temperature profiles  $\Delta^*$  versus the dimensionless gap  $\kappa$  using  $R_{\text{Ratio}} = 0.85$  and the dimensionless eccentricity,  $\varepsilon = 0.10$ , at various angles  $\beta$  and power law indexes n.

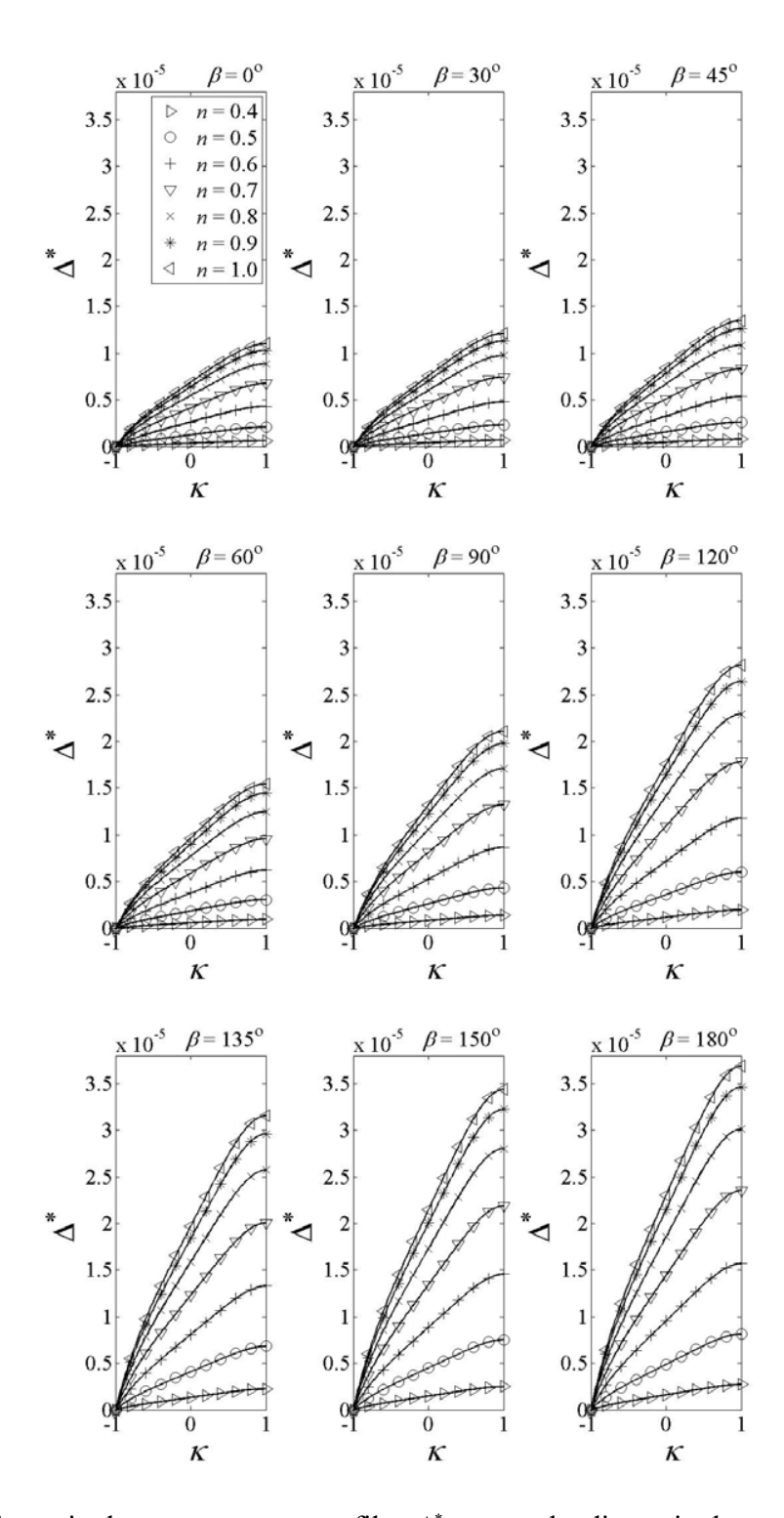


Figure 65 Dimensionless temperature profiles  $\Delta^*$  versus the dimensionless gap  $\kappa$  using  $R_{\text{Ratio}} = 0.85$  and the dimensionless eccentricity,  $\varepsilon = 0.15$ , at various angles  $\beta$  and power law indexes n.

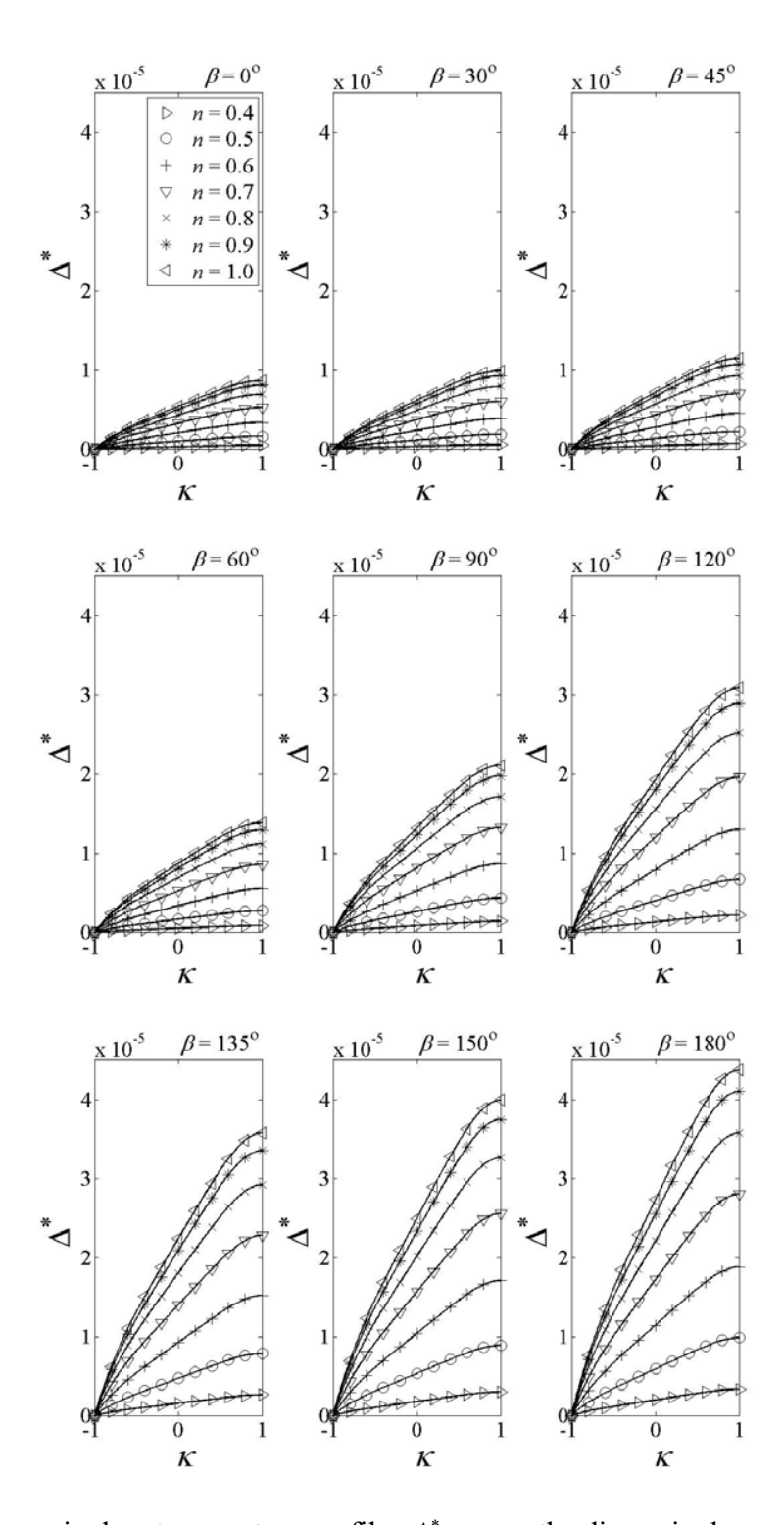


Figure 66 Dimensionless temperature profiles  $\Delta^*$  versus the dimensionless gap  $\kappa$  using  $R_{\text{Ratio}} = 0.85$  and the dimensionless eccentricity,  $\varepsilon = 0.20$ , at various angles  $\beta$  and power law indexes n.

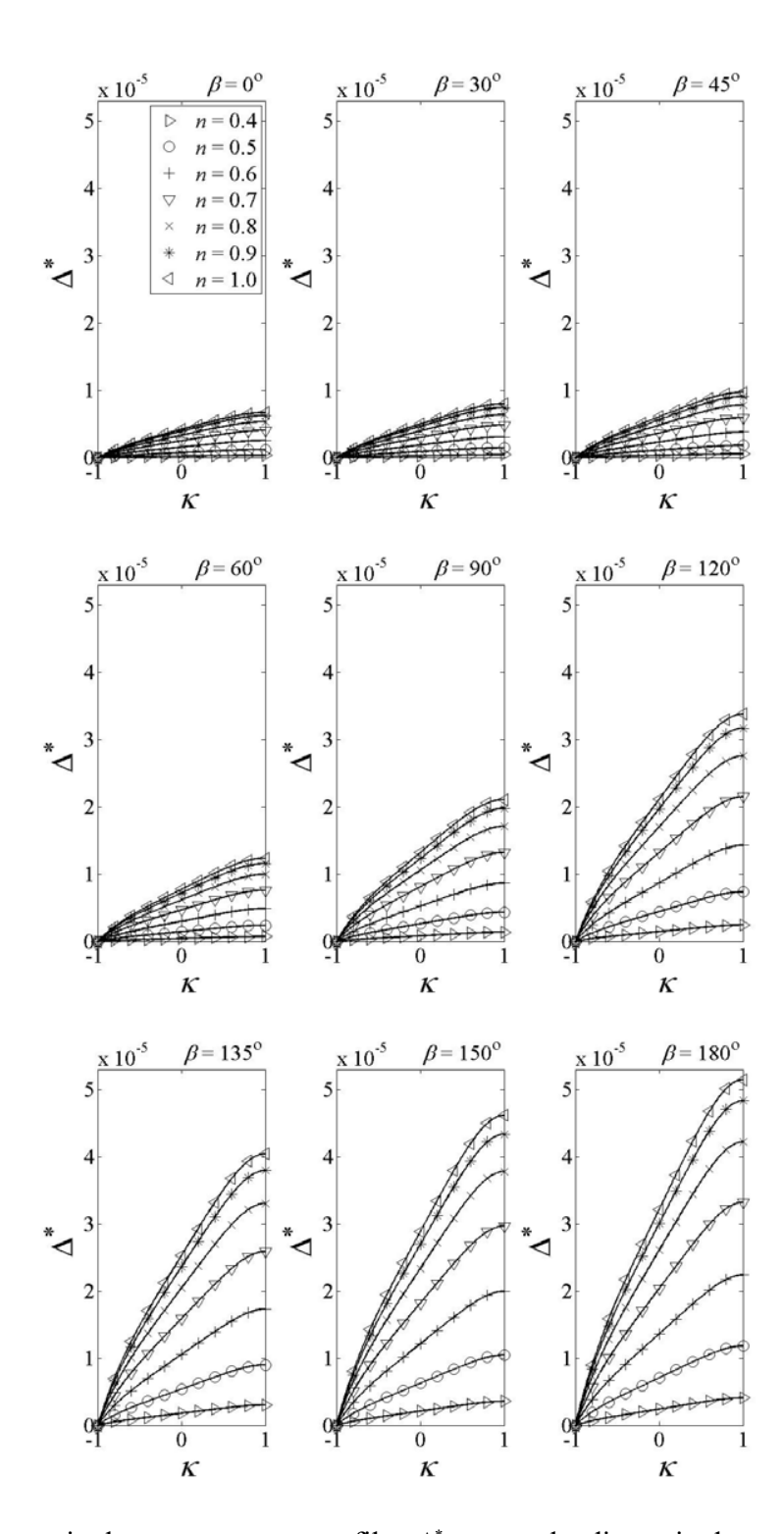


Figure 67 Dimensionless temperature profiles  $\Delta^*$  versus the dimensionless gap  $\kappa$  using  $R_{\text{Ratio}} = 0.85$  and the dimensionless eccentricity,  $\varepsilon = 0.25$ , at various angles  $\beta$  and power law indexes n.

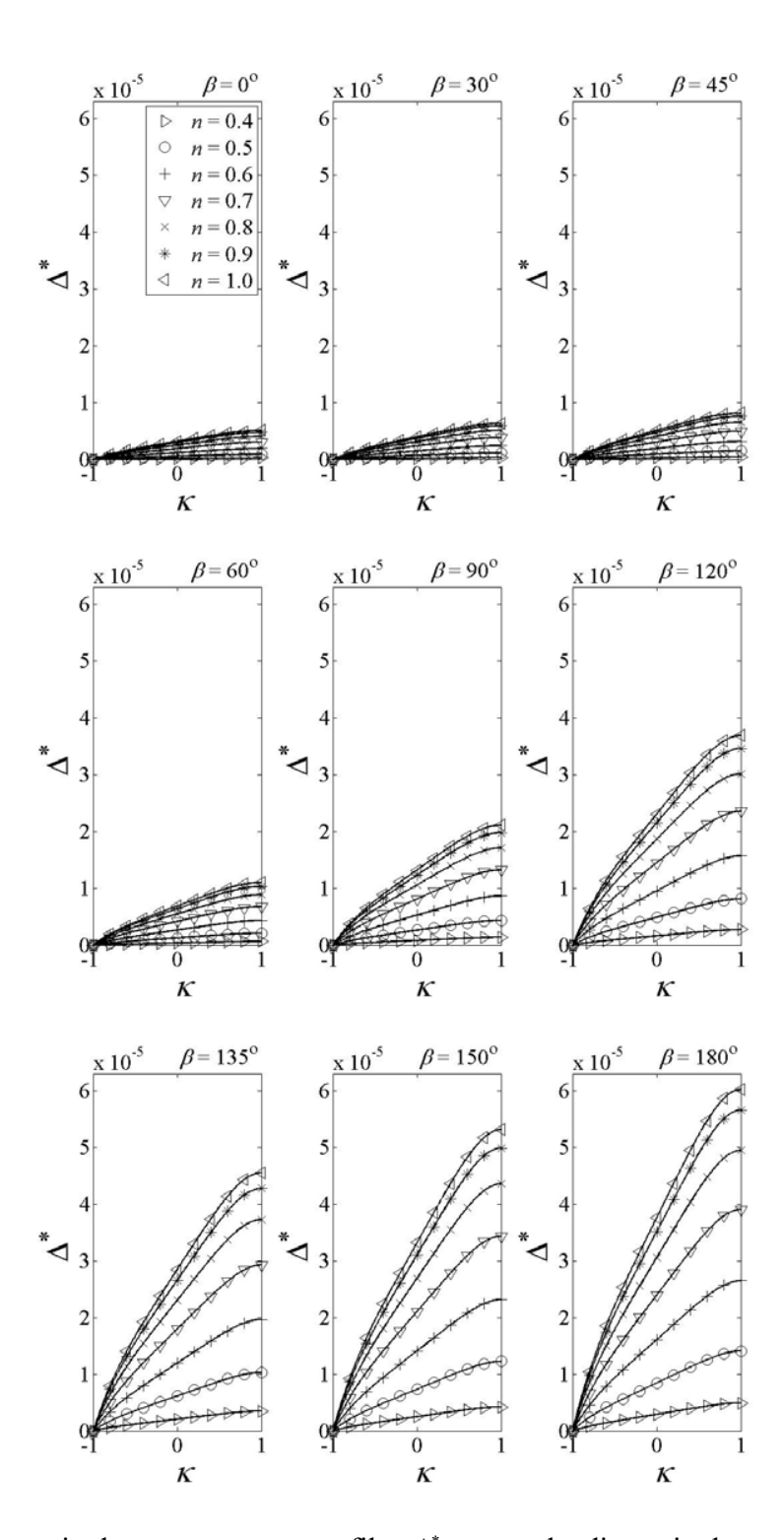


Figure 68 Dimensionless temperature profiles  $\Delta^*$  versus the dimensionless gap  $\kappa$  using  $R_{\text{Ratio}} = 0.85$  and the dimensionless eccentricity,  $\varepsilon = 0.30$ , at various angles  $\beta$  and power law indexes n.

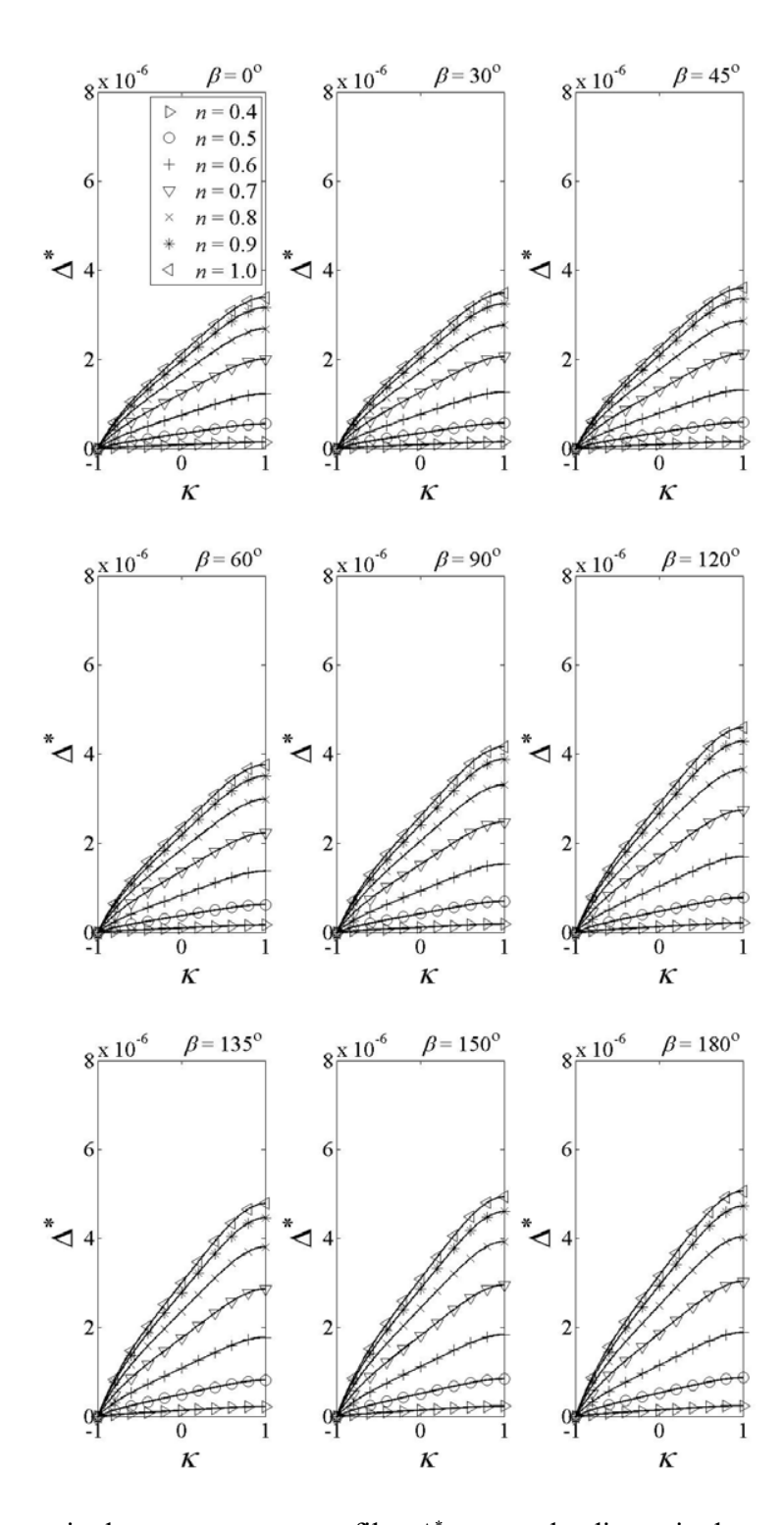


Figure 69 Dimensionless temperature profiles  $\Delta^*$  versus the dimensionless gap  $\kappa$  using  $R_{\text{Ratio}} = 0.90$  and the dimensionless eccentricity,  $\varepsilon = 0.05$ , at various angles  $\beta$  and power law indexes n.

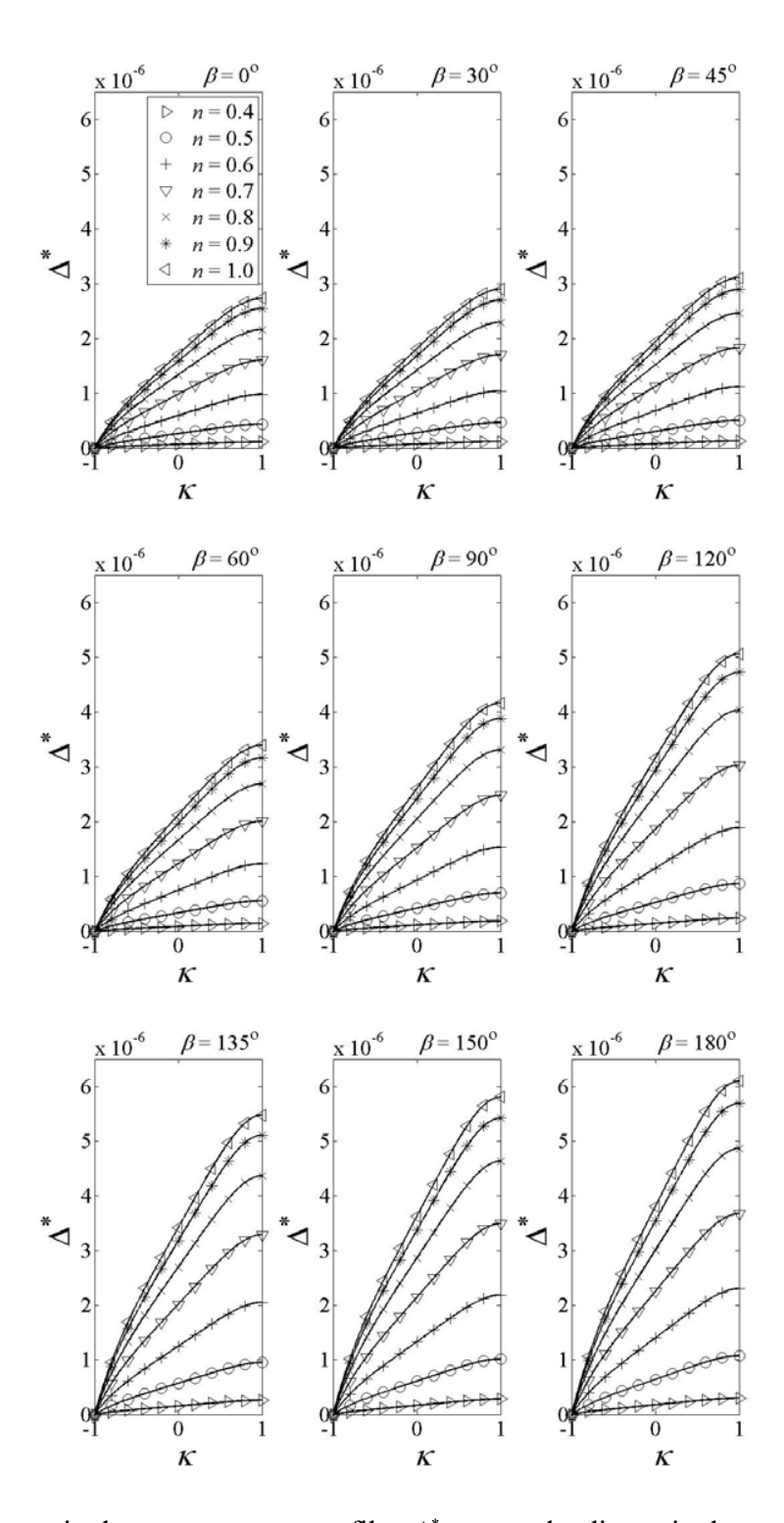


Figure 70 Dimensionless temperature profiles  $\Delta^*$  versus the dimensionless gap  $\kappa$  using  $R_{\text{Ratio}} = 0.90$  and the dimensionless eccentricity,  $\varepsilon = 0.10$ , at various angles  $\beta$  and power law indexes n.

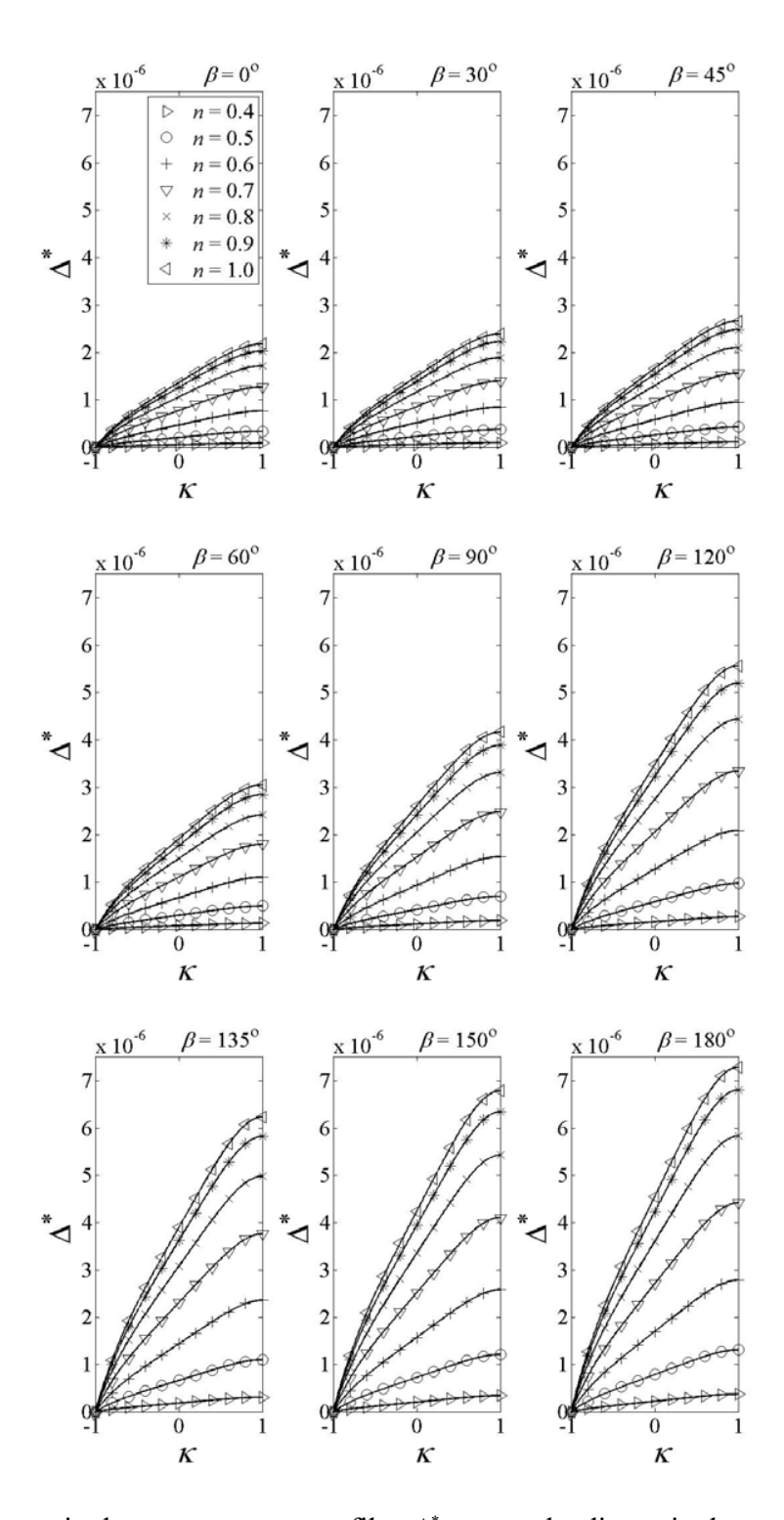


Figure 71 Dimensionless temperature profiles  $\Delta^*$  versus the dimensionless gap  $\kappa$  using  $R_{\text{Ratio}} = 0.90$  and the dimensionless eccentricity,  $\varepsilon = 0.15$ , at various angles  $\beta$  and power law indexes n.

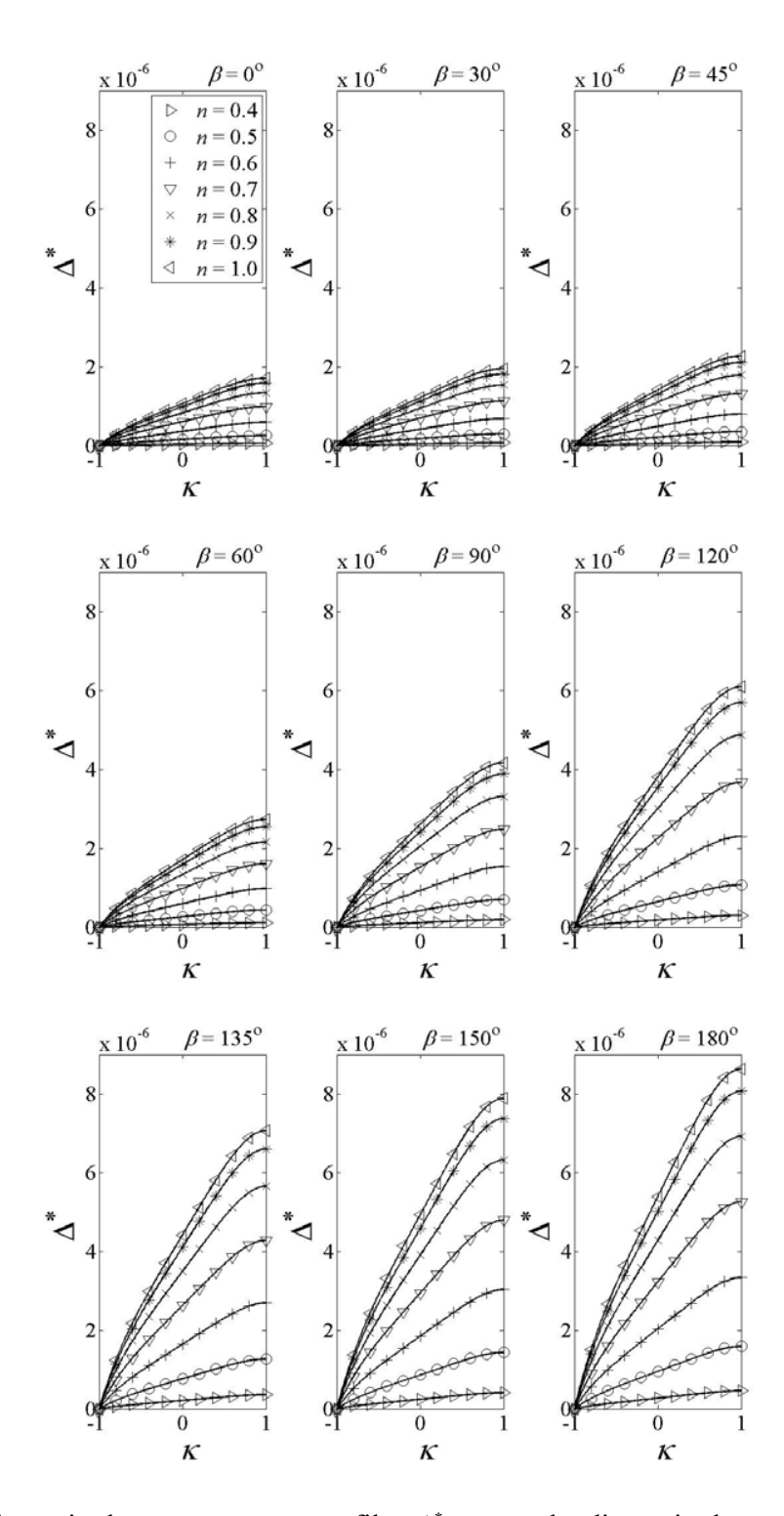


Figure 72 Dimensionless temperature profiles  $\Delta^*$  versus the dimensionless gap  $\kappa$  using  $R_{\text{Ratio}} = 0.90$  and the dimensionless eccentricity,  $\varepsilon = 0.20$ , at various angles  $\beta$  and power law indexes n.

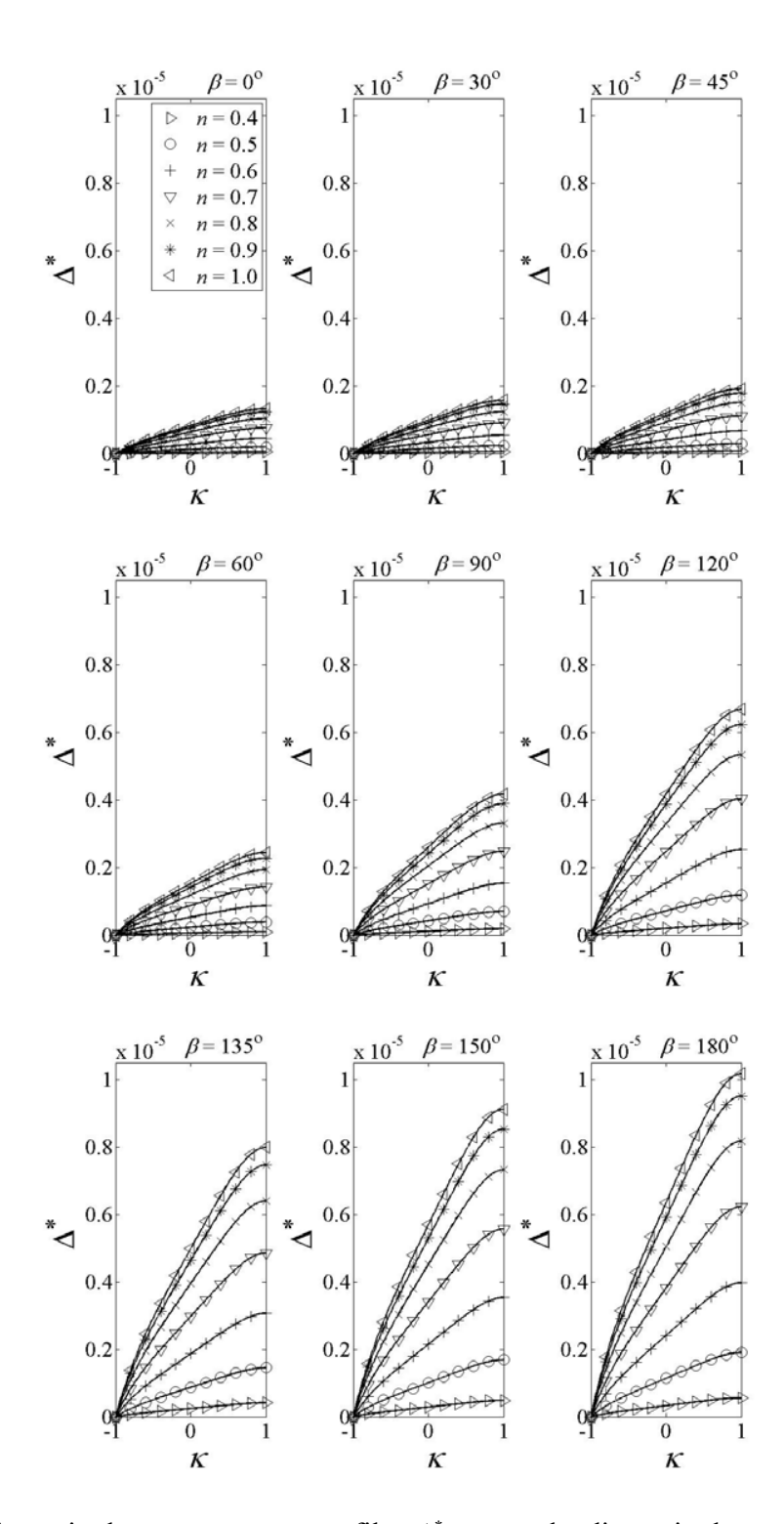


Figure 73 Dimensionless temperature profiles  $\Delta^*$  versus the dimensionless gap  $\kappa$  using  $R_{\text{Ratio}} = 0.90$  and the dimensionless eccentricity,  $\varepsilon = 0.25$ , at various angles  $\beta$  and power law indexes n.

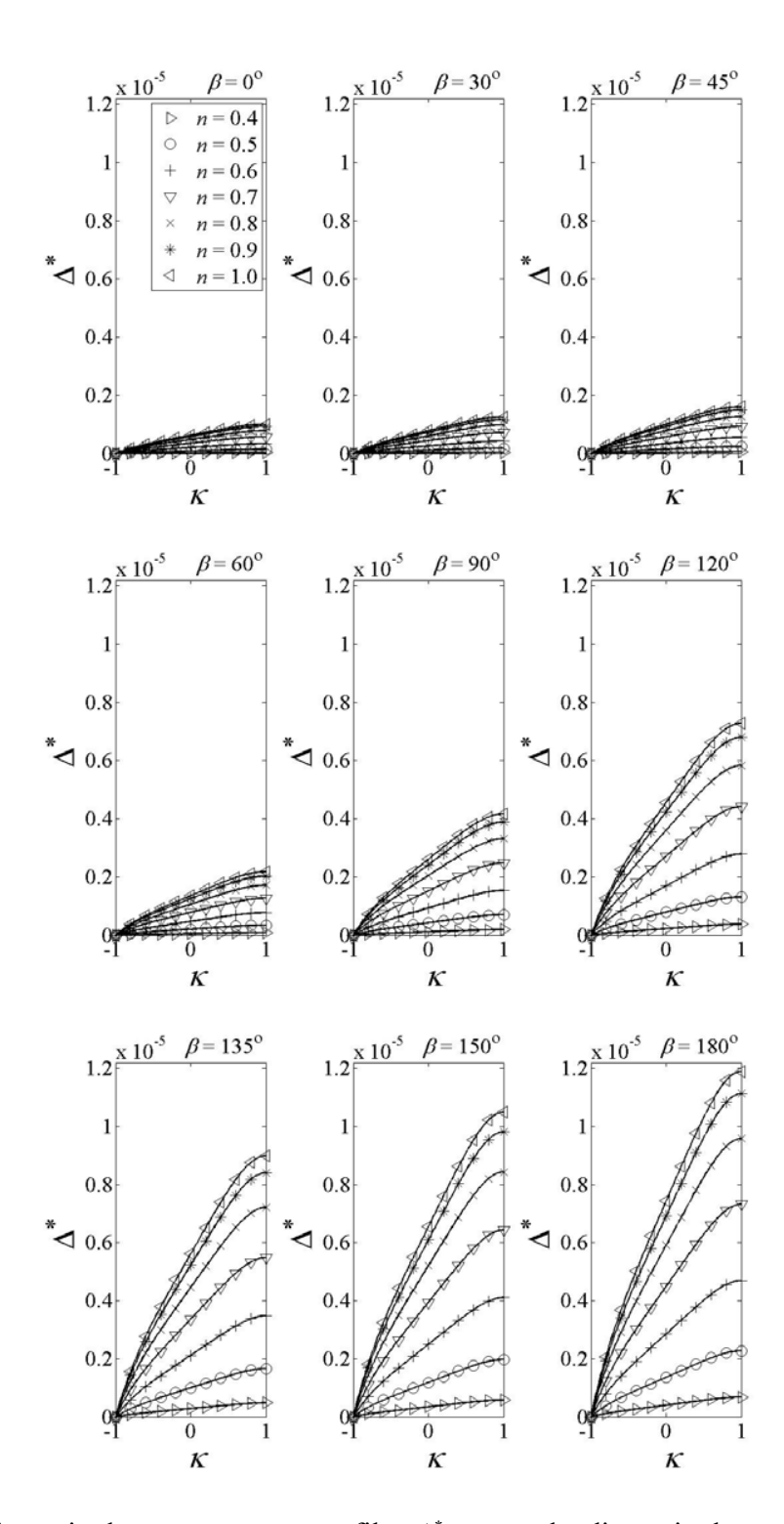


Figure 74 Dimensionless temperature profiles  $\Delta^*$  versus the dimensionless gap  $\kappa$  using  $R_{\text{Ratio}} = 0.90$  and the dimensionless eccentricity,  $\varepsilon = 0.30$ , at various angles  $\beta$  and power law indexes n.

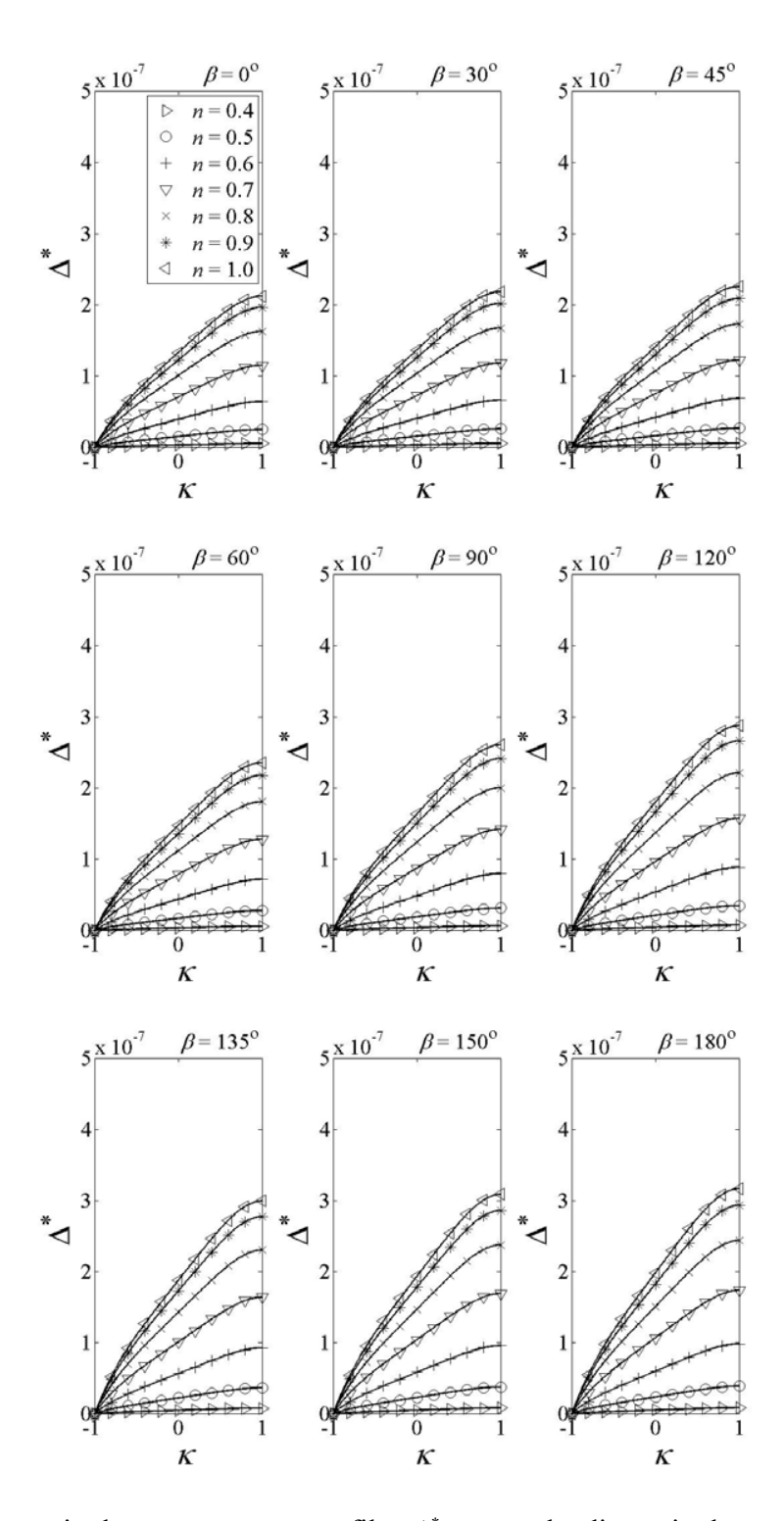


Figure 75 Dimensionless temperature profiles  $\Delta^*$  versus the dimensionless gap  $\kappa$  using  $R_{\text{Ratio}} = 0.95$  and the dimensionless eccentricity,  $\varepsilon = 0.05$ , at various angles  $\beta$  and power law indexes n.

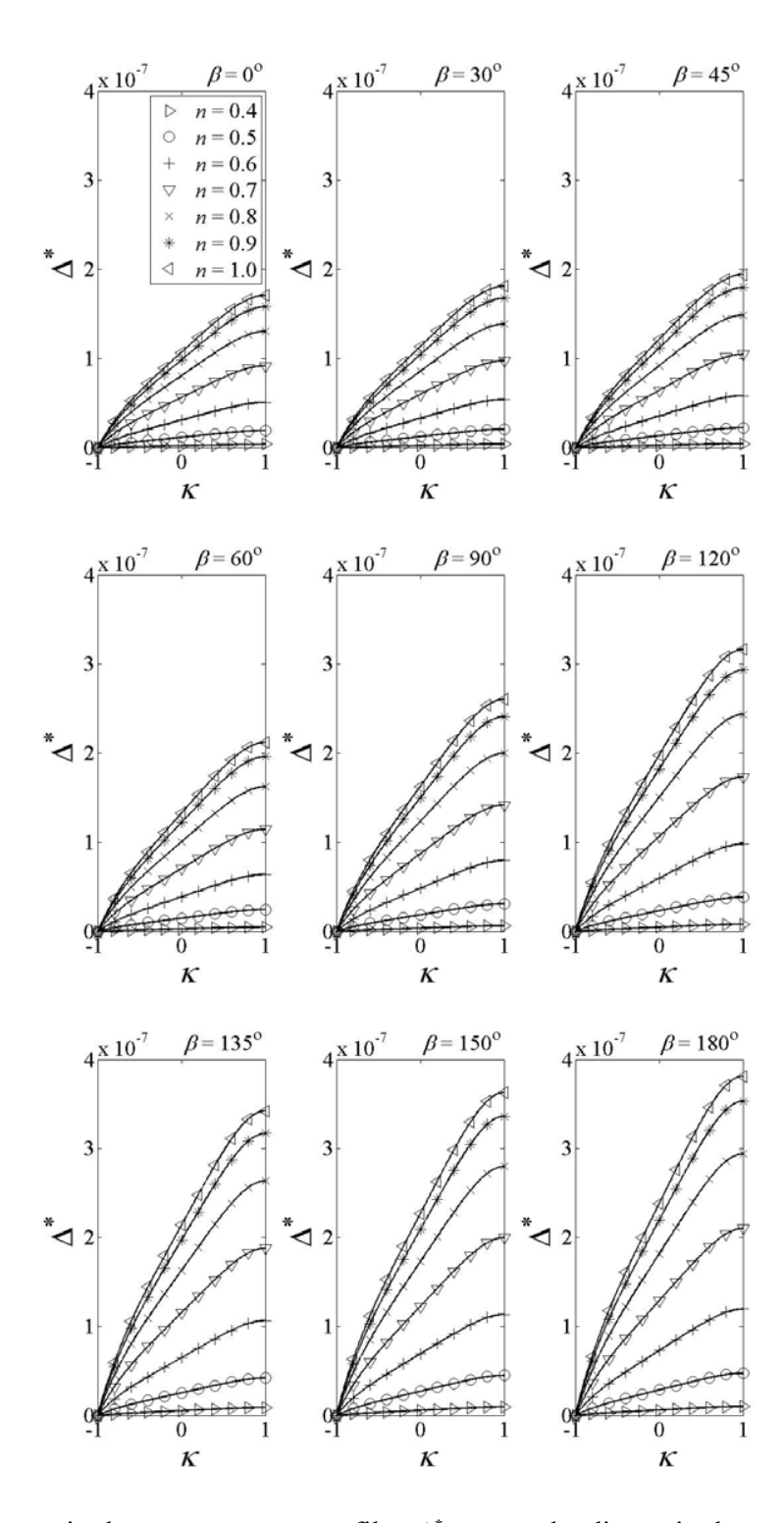


Figure 76 Dimensionless temperature profiles  $\Delta^*$  versus the dimensionless gap  $\kappa$  using  $R_{\text{Ratio}} = 0.95$  and the dimensionless eccentricity,  $\varepsilon = 0.10$ , at various angles  $\beta$  and power law indexes n.

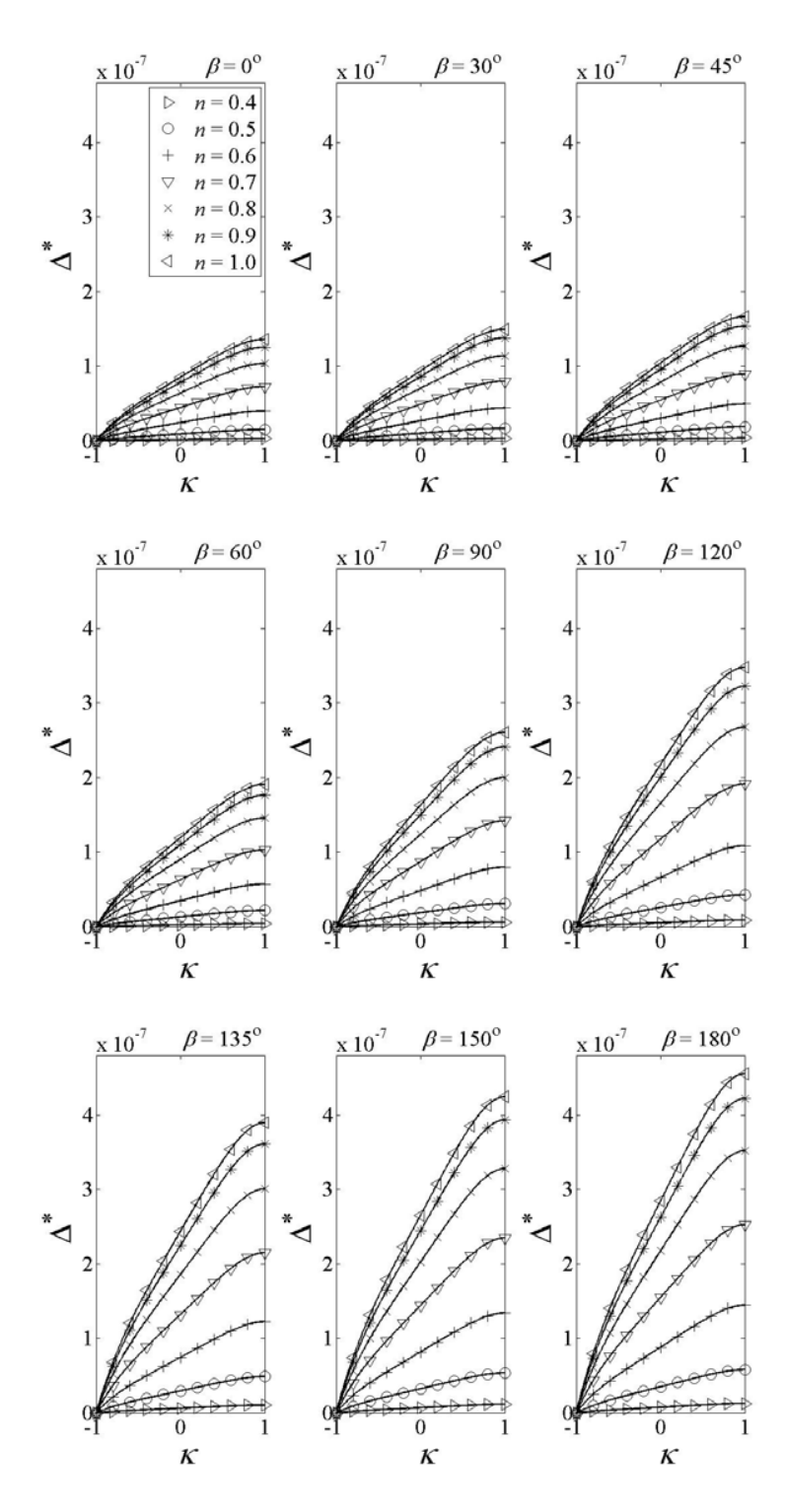


Figure 77 Dimensionless temperature profiles  $\Delta^*$  versus the dimensionless gap  $\kappa$  using  $R_{\text{Ratio}} = 0.95$  and the dimensionless eccentricity,  $\varepsilon = 0.15$ , at various angles  $\beta$  and power law indexes n.

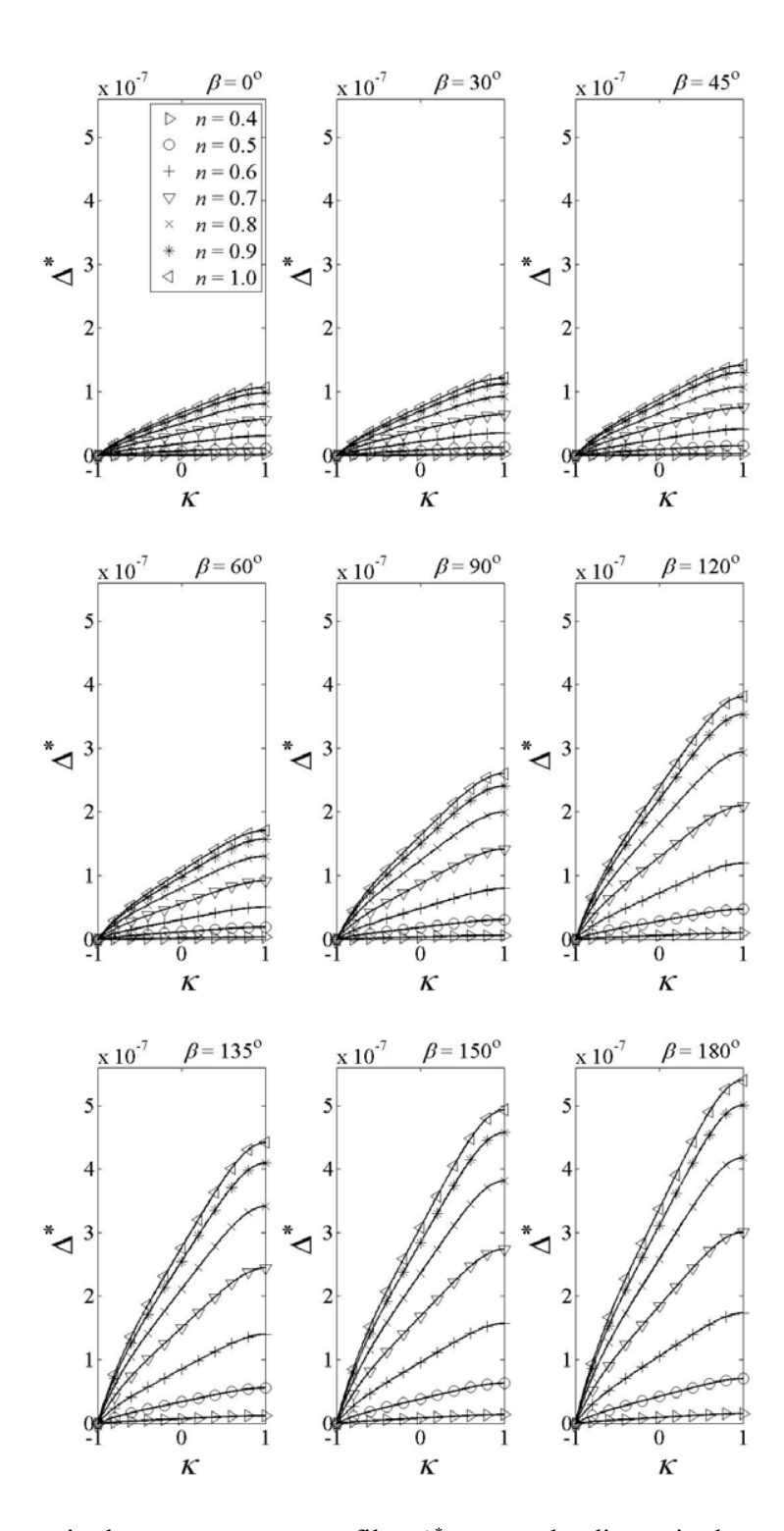


Figure 78 Dimensionless temperature profiles  $\Delta^*$  versus the dimensionless gap  $\kappa$  using  $R_{\text{Ratio}} = 0.95$  and the dimensionless eccentricity,  $\varepsilon = 0.20$ , at various angles  $\beta$  and power law indexes n.

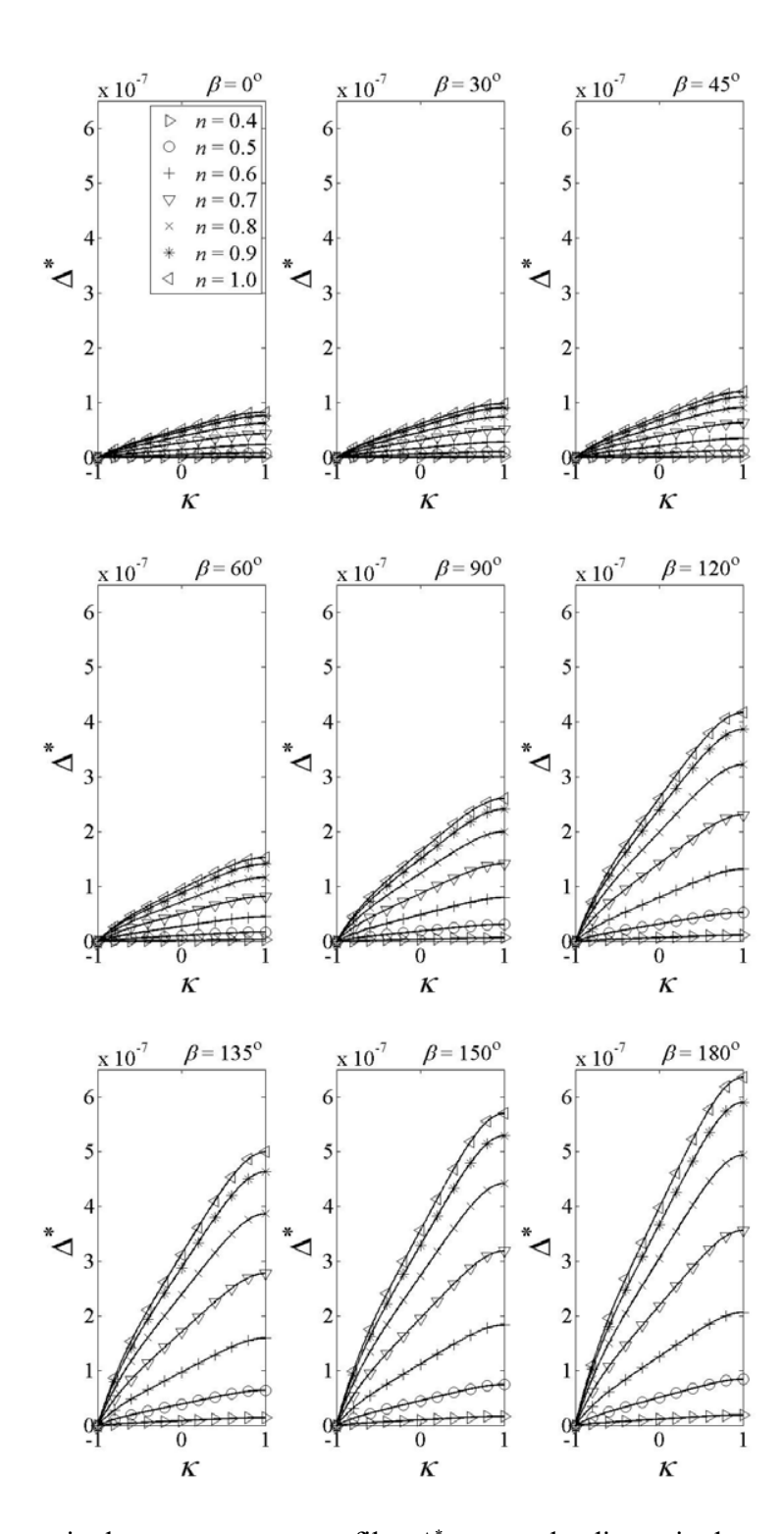


Figure 79 Dimensionless temperature profiles  $\Delta^*$  versus the dimensionless gap  $\kappa$  using  $R_{\text{Ratio}} = 0.95$  and the dimensionless eccentricity,  $\varepsilon = 0.25$ , at various angles  $\beta$  and power law indexes n.

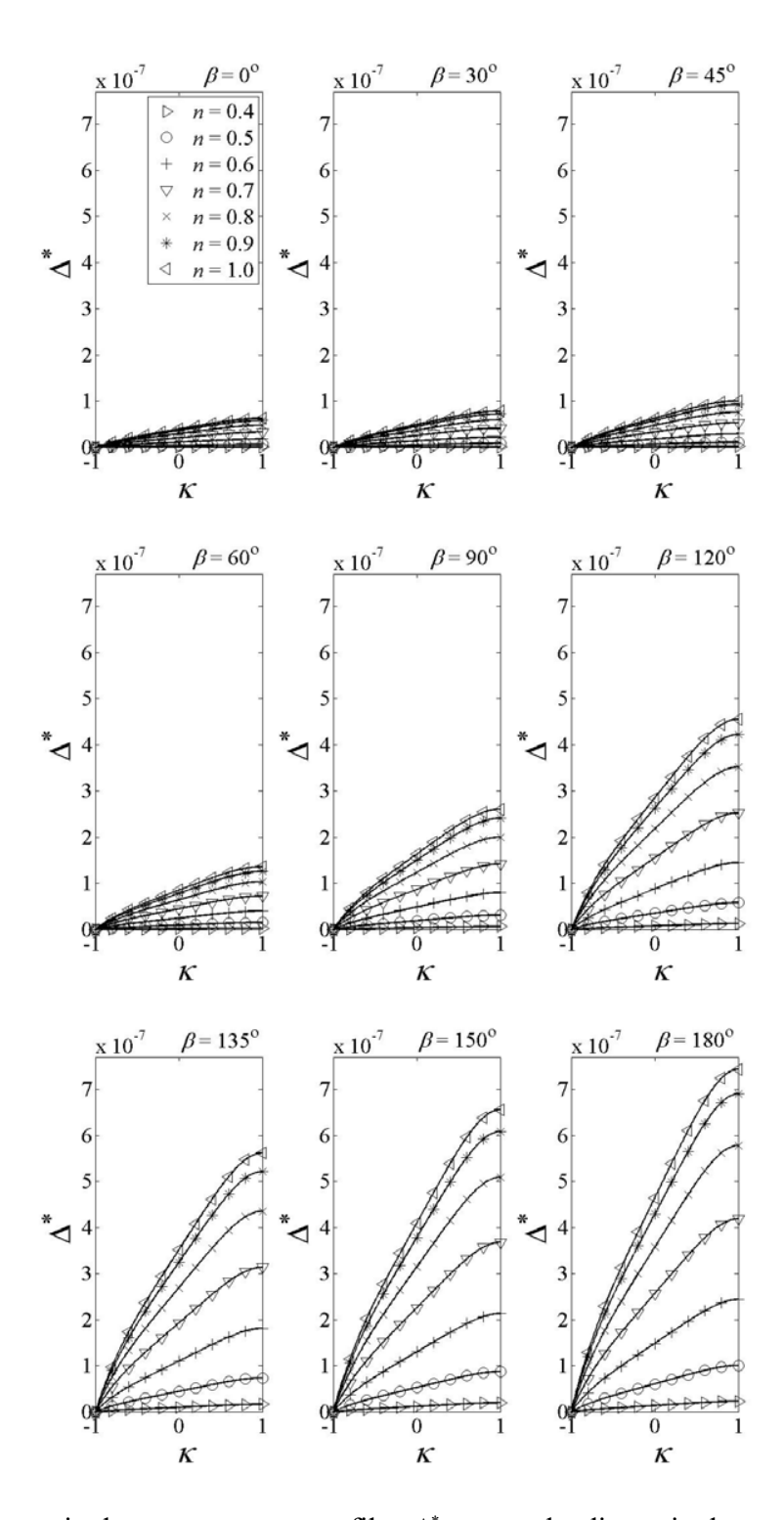


Figure 80 Dimensionless temperature profiles  $\Delta^*$  versus the dimensionless gap  $\kappa$  using  $R_{\text{Ratio}} = 0.95$  and the dimensionless eccentricity,  $\varepsilon = 0.30$ , at various angles  $\beta$  and power law indexes n.

Figures 57 to 80 show that the dimensionless temperature ( $\Delta^*$ ), in general, increases with the angular distance from the smallest gap,  $\beta$ , and the power law exponent, n, but decreases with the dimensionless radius ratio,  $R_{Ratio}$ . The temperature is risen up at the core since heat is accumulated at the inner wall according to the adiabatic heat flux. Moreover, the more eccentric the die (the higher the  $\varepsilon$ ), the greater the temperature difference between the fluid at the smallest gap ( $\beta = 0^{\circ}$ ) and the biggest gap ( $\beta = 180^{\circ}$ ). This is because of the convective flow in the eccentric die. In other words, the dimensionless temperature is proportional to the velocity in the die. The dimensionless temperatures also decrease by two decades [from  $O(10^{-4})$  to  $O(10^{-7})$ ] when the radius ratio ( $\varphi$ ) increases from 0.80 to 0.95. When the radius ratio increases, the inner and outer radii approach one another, and so the gap is very small all around the die. In this case, the convective effects in the die diminish, which is why the fluid temperature decreases as the radius ratio increases.

# 4.3 Design Example

### 4.3.1 Velocity Profile Determination in Isothermal Walls

A HDPE plastics pipe is extruded in an eccentric die of the outer cylinder diameter  $R_2 = 0.1$  meters and the gap, d = 0.01 meters with small dimensionless eccentricity of  $\varepsilon = 0.2$  to compensate the gravity sag. The HDPE plastics is considered as a power law polymer with the power law index, n = 0.56, and the consistency index,  $m = 6190 \ Pa-s^n$  [22, 23]. The polymer has the thermal conductivity,  $k = 0.045 \ W/(m-K)$ . The inner and outer wall temperatures,  $T_1$  and  $T_2$ , are uniform at  $180^{\circ}C$  (453.15 K). The pressure drop per unit

length within the extruded die is 5 MPa/m. Determine the temperature profiles of the polymer melt at various angle,  $\beta$ .

**Solution**: To solve for the dimensional temperature appearing in Eq. (3-8), we need to rearrange Eq. (3-20) to get

$$T_b = \lambda_0 \lambda_2 T_{Geo,Ind}$$

From Eqs. (2-34), (3-9), (3-11), and (3-15), at  $\beta = 0$ , for example,

$$hc = \frac{d(1 - \varepsilon \cos \beta)}{2} = \frac{(0.01m)(1 - 0.2\cos(0))}{2} = 4.00 \times 10^{-3} m$$

Then,

$$\lambda_0 = \frac{m}{k} \left(\frac{2}{hc}\right)^{n-1} \left[ -\frac{R_2^{n+1}}{m} \frac{dP}{d\zeta} \right]^{\frac{n+1}{n}}$$

$$\lambda_0 = \frac{\left(6190 \, Pa - s^n\right)}{\left(0.045 \, W \, / \, m - K\right)} \left(\frac{2}{4.00 \times 10^{-3} \, m}\right)^{0.56 - 1} \left[ -\frac{\left(0.1 \, m\right)^{0.56 + 1}}{\left(6190 \, Pa - s^n\right)} \left(-5 \times 10^6 \, Pa \, / \, m\right) \right]^{\frac{0.56 + 1}{0.56}}$$

$$\lambda_0 = 5.059 \times 10^7 \, K$$

$$\lambda_1 = \left[\frac{d(1 - \varepsilon \cos \beta)}{2R_2}\right]^{\frac{(n+1)^2}{n}} = \left[\frac{(0.01m)(1 - 0.2\cos(0))}{2(0.1m)}\right]^{\frac{(0.56+1)^2}{0.56}} = 8.413 \times 10^{-7}$$

$$\lambda_2 = \frac{\lambda_1}{\left(2 + \frac{1}{n}\right)\left(3 + \frac{1}{n}\right)} = \frac{8.413 \times 10^{-7}}{\left(2 + \frac{1}{0.56}\right)\left(3 + \frac{1}{0.56}\right)} = 4.644 \times 10^{-8}$$

Then the peak temperature at  $\beta = 0$  occurring when  $\kappa = 0$ can be calculated by letting  $T_{Geo,Ind} = 1$ ,

$$T_b = \lambda_0 \lambda_2 T_{Geo,Ind} = (5.059 \times 10^7 K)(4.644 \times 10^{-8})(1) = 2.349 K$$

$$T = T_b + T_1 = 2.349 K + 453.15 K = 455.499 K$$

Other peak temperatures at various angles,  $\beta$ , are constructed in Table 3.

Table 3 lists the peak temperatures of the HDPE melt flowing in the eccentric die at various angles,  $\beta$ .

| β   | $\lambda_0(K)$        | $\lambda_2$            | $T_{b \kappa=0}(K)$ | $T_{\kappa=0}(K)$ |
|-----|-----------------------|------------------------|---------------------|-------------------|
| 0   | $5.059 \times 10^7$   | $4.644 \times 10^{-8}$ | 2.349               | 455.499           |
| 30  | $5.133 \times 10^{7}$ | $5.358 \times 10^{-8}$ | 2.750               | 455.900           |
| 45  | $5.219 \times 10^7$   | $6.313 \times 10^{-8}$ | 3.295               | 456.445           |
| 60  | $5.328 \times 10^{7}$ | $7.747 \times 10^{-8}$ | 4.128               | 457.278           |
| 90  | $5.581 \times 10^{7}$ | $1.225 \times 10^{-7}$ | 6.835               | 459.985           |
| 120 | $5.820 \times 10^{7}$ | $1.853 \times 10^{-7}$ | 10.785              | 463.935           |
| 135 | $5.915 \times 10^7$   | $2.176 \times 10^{-7}$ | 12.871              | 466.021           |
| 150 | $5.987 \times 10^{7}$ | $2.452 \times 10^{-7}$ | 14.680              | 467.830           |
| 180 | $6.047 \times 10^7$   | $2.705 \times 10^{-7}$ | 16.355              | 469.505           |

Next, use the modified dimensionless temperature profiles with power-law index (n) at 0.56 from Figure 81, *i.e.* interpolated values of the modified dimensionless temperature profiles from Table 2, and then multiply them by the temperature amplitude  $T_{\kappa=0}$  in Table 3 to get the temperature rises at various  $\kappa$ . Then, superpose the wall temperature at 453.15 K (180 °C) on the temperature rises to get the temperature profile for each  $\beta$ . The calculated results are listed in Appendix B and shown in Figure 81.

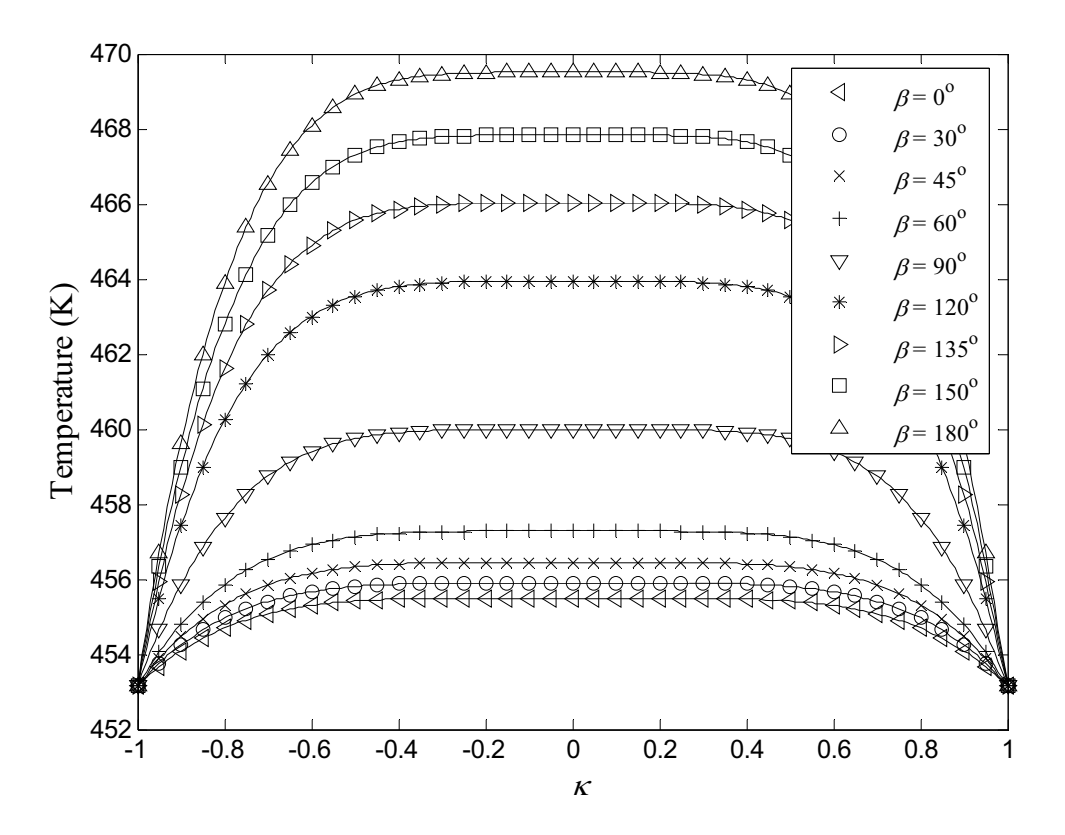


Figure 81 Temperature profiles of a HDPE power law polymer flow in an eccentric cylinders with wall temperature = 453.15 K.

## 4.3.2 Flow Rate Suggestion in Adiabatic Inner Wall

A high density polyethylene (HDPE) plastic pipe is extruded from an eccentric annular die of outer radius  $R_2 = 0.100$  m and inner radius  $R_1 = 0.08$  m with small dimensionless eccentricity of  $\varepsilon = 0.2$  to compensate for sag in the post-die cooling chamber. The HDPE melt obeys the power law with n = 0.56, the consistency index,  $m = 6190 \ Pa-s^n$  [22, 23] and its density,  $\rho = 850 \ kg/m^3$ . The polymer has thermal conductivity,  $k = 0.257 \ W/(m-K)$ . The bulk temperature of the fluid flowing into the die  $T_{b1}$  is  $190^{\circ}C$  (463.15 K). If the inner die wall is uncontrolled and left adiabatic at some period of time, determine an appropriate flow rate in kg/hr corresponding to the outer wall temperatures,  $T_2$ , for this process.

**Solution**: To solve for the appropriate dimensional flow rate appearing in Eq. (2-48), we need to determine from the *Nusselt Number* at the outer wall from Eq. (3-33). For this, we first solve for;

$$R_0 = \frac{R_1 + R_2}{2} = \frac{(0.10 \ m) + (0.08 \ m)}{2} = 0.09 \ m$$

$$d = R_2 - R_1 = (0.10 \ m) - (0.08 \ m) = 0.02 \ m$$

$$e = \varepsilon \cdot d = 0.2(0.02 \ m) = 0.004 \ m$$

We then can solve for the confocal length, a, in Eq. (2-42);

$$a = \frac{\sqrt{(0.08 \ m)^2 + (0.10 \ m)^2 - 4(0.08 \ m)^2 (0.10 \ m)^2}}{2(0.004 \ m)} = 0.441 \ m$$

From Eq. (2-40) and (2-41), we can solve for the corresponding circles;

$$\xi_1 = \sinh^{-1} \left\lceil \frac{a}{R_1} \right\rceil = \sinh^{-1} \left\lceil \frac{0.441 \, m}{0.08 \, m} \right\rceil = 2.408$$

$$\xi_2 = \sinh^{-1} \left[ \frac{a}{R_2} \right] = \sinh^{-1} \left[ \frac{0.441 \, m}{0.10 \, m} \right] = 2.189$$

$$c = \xi_1 - \xi_2 = 2.408 - 2.189 = 0.219$$

$$\psi_1 \equiv -\left(\frac{n}{2n-1}\right)\left(\frac{d}{2R_2}\right)^{\frac{(n+1)^2}{n}} = -\left(\frac{0.56}{2(0.56)-1}\right)\left(\frac{0.02 \ m}{2(0.08 \ m)}\right)^{\frac{(0.56+1)^2}{0.56}}$$

$$\psi_1 = -2.105 \times 10^{-4}$$

From Figure 6, we then read  $\Omega(0.56, 0.2) \approx 3.44$ . The dimensionless volumetric flow rate can be obtained from Eq. (2-46);

$$Q_p^* = \left(\frac{4(0.56)}{2(0.56) + 1}\right) \left(\frac{0.09 \ m}{0.10 \ m}\right) \left(\frac{0.02 \ m}{2(0.10 \ m)}\right)^{2 + \frac{1}{n}} (3.44) = 5.358 \times 10^{-4}$$

From Eqs. (2-48), (3-24) and (3-27), we can plot the *Nusselt Number* at the outer wall  $(Nu_2)$  versus the flow rate  $(Q_p)$  at various  $\Delta T_2$  as shown in Figure 82. The numerical values of the *Nusselt Number* and the flow rate are shown in Table 4. From Table 4, we can see that, to keep the melt at an uniform temperature, if the temperature difference  $\Delta T_2 = 2^{\circ}C$  [corresponding to the outer wall temperatures,  $T_2$ , at  $188^{\circ}C$  (443.15 K)], for example, the flow rate beyond 3.142 kg/hr gives the *Nusselt Number* greater than 1 in which the convective heat transfer of the melt is faster than the conduction one. Then, in this case, any processing flow rate beyond 3.142 kg/hr causes heat generation in the materials no matter how well the cooling system of the die is. The appropriate flow rate corresponding to the outer wall temperatures,  $T_2$ , for this process is shown in Table 2. Through higher temperature difference  $\Delta T_2$  improves the flow rate Q, but uncertain process control may occur. Thus increasing flow rate Q at minimum  $\Delta T_2$  are preferred.

This is why the pipe extrusion engineer normally works at the highest flow rate at the lowest controllable  $\Delta T_2$  and leaves the cooling system at the downstream cool down the heat.

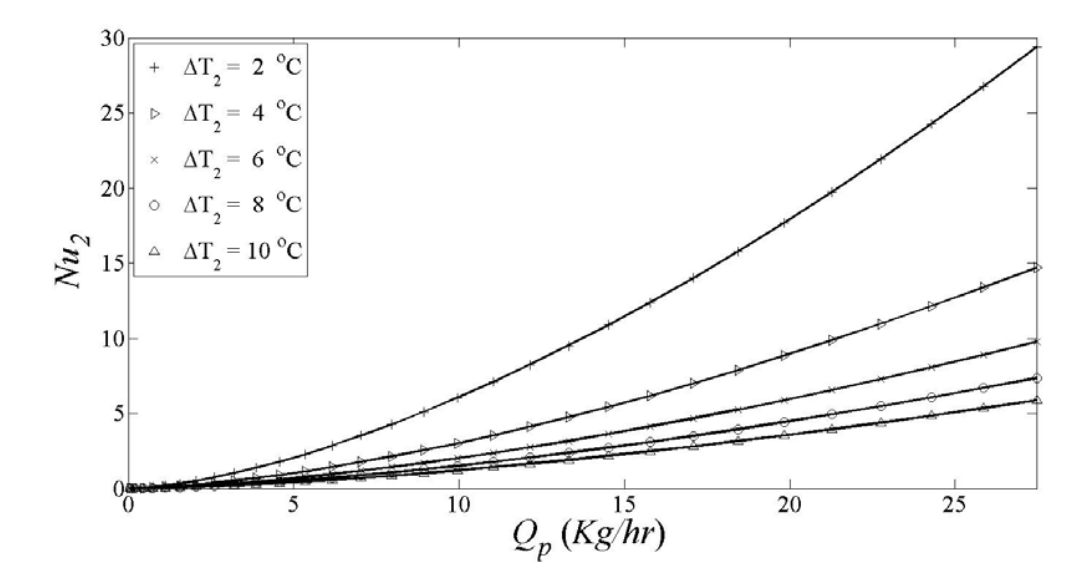


Figure 82 *Nusselt Number* at the outer wall  $Nu_2$  versus the flow rate  $Q_p$  at various  $\Delta T_2$  of the HDPE melt [n=0.56, m=6190  $Pa\cdot s^n$ , and k=0.257 W/(m-K)] flowing in the eccentric die with  $R_{Ratio}=0.8$ ,  $\varepsilon=0.2$ . The bulk temperature of the upcoming flow  $T_{b1}$  is  $190^{\circ}C$  (463.15 K).

Table 4 lists the numerical values of the *Nusselt Number* at the outer wall  $Nu_2$  and the flow rate  $Q_p$  at various  $\Delta T_2$  of the HDPE melt flowing in the eccentric die plotted in Figure 82.

| Q(kg/hr) | $Nu_2$                     |                            |                            |                            |                             |  |  |
|----------|----------------------------|----------------------------|----------------------------|----------------------------|-----------------------------|--|--|
|          | $\Delta T_2 = 2^{\circ} C$ | $\Delta T_2 = 4^{\circ} C$ | $\Delta T_2 = 6^{\circ} C$ | $\Delta T_2 = 8^{\circ} C$ | $\Delta T_2 = 10^{\circ} C$ |  |  |
| 0.063    | 2.256×10 <sup>-3</sup>     | 1.128×10 <sup>-3</sup>     | 7.519×10 <sup>-4</sup>     | 5.639×10 <sup>-4</sup>     | 4.511×10 <sup>-4</sup>      |  |  |
| 0.218    | 0.016                      | 7.777×10 <sup>-3</sup>     | 5.185×10 <sup>-3</sup>     | 3.889×10 <sup>-3</sup>     | 3.111×10 <sup>-3</sup>      |  |  |
| 0.450    | 0.048                      | 0.024                      | 0.016                      | 0.012                      | 9.626×10 <sup>-3</sup>      |  |  |
| 0.752    | 0.107                      | 0.054                      | 0.036                      | 0.027                      | 0.021                       |  |  |
| 1.120    | 0.200                      | 0.100                      | 0.067                      | 0.050                      | 0.040                       |  |  |
| 1.551    | 0.332                      | 0.166                      | 0.111                      | 0.083                      | 0.066                       |  |  |
| 2.042    | 0.510                      | 0.255                      | 0.170                      | 0.127                      | 0.102                       |  |  |
| 2.592    | 0.740                      | 0.370                      | 0.247                      | 0.185                      | 0.148                       |  |  |
| 3.199    | 1.027                      | 0.513                      | 0.342                      | 0.257                      | 0.205                       |  |  |
| 3.861    | 1.377                      | 0.689                      | 0.459                      | 0.344                      | 0.275                       |  |  |
| 4.577    | 1.796                      | 0.898                      | 0.599                      | 0.449                      | 0.359                       |  |  |
| 5.347    | 2.289                      | 1.144                      | 0.763                      | 0.572                      | 0.458                       |  |  |
| 6.168    | 2.860                      | 1.430                      | 0.953                      | 0.715                      | 0.572                       |  |  |
| 7.041    | 3.516                      | 1.758                      | 1.172                      | 0.879                      | 0.703                       |  |  |
| 7.964    | 4.261                      | 2.131                      | 1.420                      | 1.065                      | 0.852                       |  |  |
| 8.937    | 5.101                      | 2.550                      | 1.700                      | 1.275                      | 1.020                       |  |  |
| 9.959    | 6.039                      | 3.019                      | 2.013                      | 1.510                      | 1.208                       |  |  |
| 11.029   | 7.081                      | 3.541                      | 2.360                      | 1.770                      | 1.416                       |  |  |
| 12.147   | 8.232                      | 4.116                      | 2.744                      | 2.058                      | 1.646                       |  |  |
| 13.312   | 9.497                      | 4.748                      | 3.166                      | 2.374                      | 1.899                       |  |  |
| 14.524   | 10.879                     | 5.440                      | 3.626                      | 2.720                      | 2.176                       |  |  |
| 15.782   | 12.385                     | 6.192                      | 4.128                      | 3.096                      | 2.477                       |  |  |
| 17.086   | 14.017                     | 7.009                      | 4.672                      | 3.504                      | 2.803                       |  |  |
| 18.435   | 15.782                     | 7.891                      | 5.261                      | 3.945                      | 3.156                       |  |  |
| 19.829   | 17.682                     | 8.841                      | 5.894                      | 4.421                      | 3.536                       |  |  |
| 21.268   | 19.724                     | 9.862                      | 6.575                      | 4.931                      | 3.945                       |  |  |
| 22.751   | 21.910                     | 10.955                     | 7.303                      | 5.478                      | 4.382                       |  |  |
| 24.277   | 24.247                     | 12.123                     | 8.082                      | 6.062                      | 4.849                       |  |  |
| 25.847   | 26.736                     | 13.368                     | 8.912                      | 6.684                      | 5.347                       |  |  |
| 27.460   | 29.385                     | 14.692                     | 9.795                      | 7.346                      | 5.877                       |  |  |

Table 5 shows the suggested flow rate  $Q_s$  corresponding to the outer wall temperature  $T_2$  at  $Nu_2=1$  from the Table 4.

| $T_2$ (° $C$ ) | $Q_s\left(kg/hr\right)$ |  |  |  |
|----------------|-------------------------|--|--|--|
| 188            | 3.142                   |  |  |  |
| 186            | 4.896                   |  |  |  |
| 184            | 6.355                   |  |  |  |
| 182            | 7.641                   |  |  |  |
| 180            | 8.821                   |  |  |  |

# **Chapter 5 Conclusion**

## 5.1 Discussion

For bipolar cylindrical coordinate, the energy equation coupled with the velocity profiles of the power law constitutive model is used to determine the temperature profiles in the pipe extrusion die. The dimensionless temperature profiles of a steady, laminar, incompressible and fully developed flow of a power law polymer can be found by the analytic method with assumptions such that there are no velocities in the  $\xi$  and  $\theta$  directions, no heat convection terms, and uniform wall temperatures. The solution reveals that the dimensionless temperature distribution is a function of the dimensionless radius ratio,  $R_{Ratio}$ , the dimensionless eccentricity,  $\varepsilon$ , the angular distance from the smallest gap,  $\beta$ , the power law exponent, n, and a strong function of, the dimensionless gap,  $\kappa$ .

For isothermal walls, the temperature profile is flat at the middle of the gap and suddenly drops to reach the wall temperature near the wall region. The temperature rises at the gap center due to heat dissipation of the non-Newtonian effects. This temperature rise is higher if the gap, or in other word the angular distance from the smallest gap,  $\beta$ , is increased. This is because the bigger gap allows the polymer to easily flow and thus get more temperature dissipation from the molecular frictions. Moreover, the temperature rise also increases with the power law exponent, n, to reach the Newtonian temperature profile at n = 1. Thus, the less the power law exponent, n, the temperature profile shows plateau at the gap center, or in other word, it shows non-Newtonian effects when the

power law exponent, n, is less. The modified dimensionless temperature  $T_{Geo,Ind}$  is independent to the die geometry, so it can easily be used to approximate the temperature profiles of the polymer melt in the gap of the eccentric cylinders as illustrated in the designed example in section 4.3.

For adiabatic inner wall, the solution reveals that the dimensionless temperature distribution is a function of the dimensionless radius ratio,  $\varphi$ , the dimensionless eccentricity,  $\varepsilon$ , the angular distance from the smallest gap,  $\beta$ , the power law exponent, n, and is a strong function of, the dimensionless gap,  $\kappa$ . The temperature rises in the gap due to viscous dissipation. This temperature rise increases if the gap is increased. This is because the radial path length for thermal conduction to the wall is lengthened.

Moreover, the temperature rise also increases with the power law exponent, n, to reach the Newtonian temperature profile at n = 1.

# 5.2 Recommendation

The unity dimensionless modified Brinkman number ( $Br_{Mo}$ ) is difficult to be reached, thus in most case, the convection terms in the left side of the energy equation may not be zero. This leads to an unsolved solution in this field. In short, an undeveloped temperature profile must be studied and experimental data or simulation technique of a polymer flow in a long annular pipe is necessary to validate the solution.

# Appendix A

The transformation of  $\theta$  and  $\beta$  in Figure 3 can be shown below. From the relation,

$$H = R_2 - R_1 - e\cos\beta \tag{A-1}$$

or rewritten in term of the gap d,

$$H = d(1 - e\cos\beta) \tag{A-2}$$

Thus, for small gap,

$$\cos \beta = \frac{\cos \theta + \varepsilon}{1 + \varepsilon \cos \theta} \tag{A-3}$$

$$\sin \beta = \frac{(1+\varepsilon^2)^{\frac{1}{2}}\sin \theta}{1+\varepsilon\cos \theta} \tag{A-4}$$

$$\cos \theta = \frac{\cos \beta - \varepsilon}{1 - \varepsilon \cos \beta} \tag{A-5}$$

$$\sin \theta = \frac{\left(1 - \varepsilon^2\right)^{\frac{1}{2}} \sin \beta}{1 - \varepsilon \cos \theta} \tag{A-6}$$

$$1 + \varepsilon \cos \theta = \frac{1 - \varepsilon^2}{1 - \varepsilon \cos \theta} \tag{A-7}$$

$$d\theta = \frac{\left(1 - \varepsilon^2\right)^{\frac{1}{2}} d\beta}{1 - \varepsilon \cos \theta} \tag{A-8}$$

$$X = \frac{1 + \varepsilon \cos \theta}{\varepsilon} = \frac{1 + \varepsilon^2}{\varepsilon (1 - \varepsilon \cos \beta)}$$
 (A-9)

$$\frac{X}{a} = \frac{1 + \varepsilon \cos \theta}{\varepsilon} \frac{\varepsilon}{R_0 \left(1 - \varepsilon^2\right)^{\frac{1}{2}}}$$
 (A-10)

$$\frac{X}{a} = \frac{1 + \varepsilon \cos \theta}{R_0 \left(1 - \varepsilon^2\right)^{\frac{1}{2}}} \tag{A-11}$$

# **Appendix B**

Table B-1 lists the calculated temperature profiles of a HDPE power law polymer flow in an eccentric cylinders with wall temperature = 453.15 K.

| K    | $T_{Geo,Ind}$ | $T_{\beta=0}$ | $T_{\beta=30}$ | $T_{\beta=45}$ | $T_{\beta=60}$ | $T_{\beta=90}$ | $T_{\beta=120}$ | $T_{\beta=135}$ | $T_{\beta=150}$ | $T_{\beta=180}$ |
|------|---------------|---------------|----------------|----------------|----------------|----------------|-----------------|-----------------|-----------------|-----------------|
|      | @ n= 0.56     | 1 p=0         | 1 p=30         | 1 p=43         | 1 p-60         | 1 p=90         | 1 p=120         | 1 p=133         | 1 p=130         | 1 p=180         |
| 0.00 | 1.00000       | 455.50        | 455.90         | 456.44         | 457.28         | 459.98         | 463.93          | 466.02          | 467.83          | 469.50          |
| 0.05 | 1.00000       | 455.50        | 455.90         | 456.44         | 457.28         | 459.98         | 463.93          | 466.02          | 467.83          | 469.50          |
| 0.10 | 0.99998       | 455.50        | 455.90         | 456.44         | 457.28         | 459.98         | 463.93          | 466.02          | 467.83          | 469.50          |
| 0.15 | 0.99989       | 455.50        | 455.90         | 456.44         | 457.28         | 459.98         | 463.93          | 466.02          | 467.83          | 469.50          |
| 0.20 | 0.99955       | 455.50        | 455.90         | 456.44         | 457.28         | 459.98         | 463.93          | 466.02          | 467.82          | 469.50          |
| 0.25 | 0.99869       | 455.50        | 455.90         | 456.44         | 457.27         | 459.98         | 463.92          | 466.00          | 467.81          | 469.48          |
| 0.30 | 0.99685       | 455.49        | 455.89         | 456.43         | 457.26         | 459.96         | 463.90          | 465.98          | 467.78          | 469.45          |
| 0.35 | 0.99342       | 455.48        | 455.88         | 456.42         | 457.25         | 459.94         | 463.86          | 465.94          | 467.73          | 469.40          |
| 0.40 | 0.98754       | 455.47        | 455.87         | 456.40         | 457.23         | 459.90         | 463.80          | 465.86          | 467.65          | 469.30          |
| 0.45 | 0.97810       | 455.45        | 455.84         | 456.37         | 457.19         | 459.83         | 463.70          | 465.74          | 467.51          | 469.15          |
| 0.50 | 0.96375       | 455.41        | 455.80         | 456.33         | 457.13         | 459.74         | 463.54          | 465.55          | 467.30          | 468.91          |
| 0.55 | 0.94279       | 455.36        | 455.74         | 456.26         | 457.04         | 459.59         | 463.32          | 465.29          | 466.99          | 468.57          |
| 0.60 | 0.91324       | 455.30        | 455.66         | 456.16         | 456.92         | 459.39         | 463.00          | 464.90          | 466.56          | 468.09          |
| 0.65 | 0.87275       | 455.20        | 455.55         | 456.03         | 456.75         | 459.11         | 462.56          | 464.38          | 465.96          | 467.42          |
| 0.70 | 0.81858       | 455.07        | 455.40         | 455.85         | 456.53         | 458.74         | 461.98          | 463.69          | 465.17          | 466.54          |
| 0.75 | 0.74761       | 454.91        | 455.21         | 455.61         | 456.24         | 458.26         | 461.21          | 462.77          | 464.12          | 465.38          |
| 0.80 | 0.65627       | 454.69        | 454.96         | 455.31         | 455.86         | 457.64         | 460.23          | 461.60          | 462.78          | 463.88          |
| 0.85 | 0.54057       | 454.42        | 454.64         | 454.93         | 455.38         | 456.84         | 458.98          | 460.11          | 461.09          | 461.99          |
| 0.90 | 0.39603       | 454.08        | 454.24         | 454.45         | 454.78         | 455.86         | 457.42          | 458.25          | 458.96          | 459.63          |
| 0.95 | 0.21767       | 453.66        | 453.75         | 453.87         | 454.05         | 454.64         | 455.50          | 455.95          | 456.35          | 456.71          |
| 1.00 | 0.00000       | 453.15        | 453.15         | 453.15         | 453.15         | 453.15         | 453.15          | 453.15          | 453.15          | 453.15          |

# **Appendix C**

For 
$$-1 \le \kappa \le 0$$
,  $\frac{\partial v_{\zeta p}}{\partial \kappa}$  is positive. Thus,  $\left| \frac{\partial v_{\zeta p}}{\partial \kappa} \right| = + \frac{\partial v_{\zeta p}}{\partial \kappa}$ , while  $|\kappa| = -\kappa$ . Then, Eq.

(2-35) becomes;

$$v_{\mathcal{L}P} = -\frac{n}{n+1} \left[ \frac{d(1-\varepsilon\cos\beta)}{2R_2} \right]^{1+\frac{1}{n}} \left( (-\kappa)^{1+\frac{1}{n}} - 1 \right)$$
 (C-1)

where its derivative with respect to  $\kappa$  is;

$$\frac{\partial v_{\mathcal{P}}}{\partial \kappa} = \left[ \frac{d(1 - \varepsilon \cos \beta)}{2R_2} \right]^{1 + \frac{1}{n}} (-\kappa)^{\frac{1}{n}}$$
 (C-2)

Substitute Eq. (C-2) into Eq. (3-7) to get;

$$\frac{\partial^2 T^*}{\partial \kappa^2} = -\lambda_1 \left(-\kappa\right)^{1+\frac{1}{n}} \tag{C-3}$$

One can integrate Eq. (C-3) twice to get;

$$T^* = -\frac{\lambda_1}{\left(2 + \frac{1}{n}\right)\left(3 + \frac{1}{n}\right)} \left(-\kappa\right)^{3 + \frac{1}{n}} + c_1 \kappa + c_2 \tag{C-4}$$

where  $c_1$  and  $c_2$  are the integration constants. On the other hand for  $0 \ge \kappa \ge 1$ ,  $\frac{\partial v_{\zeta p}}{\partial \kappa}$  is

negative. Thus,  $\left| \frac{\partial v_{\zeta p}}{\partial \kappa} \right| = -\frac{\partial v_{\zeta p}}{\partial \kappa}$ , while  $|\kappa| = +\kappa$ . Then, Eq. (2-35) becomes;

$$v_{\zeta P} = -\frac{n}{n+1} \left[ \frac{d(1-\varepsilon\cos\beta)}{2R_2} \right]^{1+\frac{1}{n}} \left( (+\kappa)^{1+\frac{1}{n}} - 1 \right)$$
 (C-5)

where its derivative with respect to  $\kappa$  is;

$$\frac{\partial v_{\mathcal{P}}}{\partial \kappa} = \left[ \frac{d(1 - \varepsilon \cos \beta)}{2R_2} \right]^{1 + \frac{1}{n}} (+\kappa)^{\frac{1}{n}}$$
 (C-6)

Substitute Eq. (C-6) into Eq. (3-7) to get;

$$\frac{\partial^2 T^*}{\partial \kappa^2} = -\lambda_1 (+\kappa)^{1+\frac{1}{n}} \tag{C-7}$$

One can integrate Eq. (C-7) twice to get;

$$T^* = -\frac{\lambda_1}{\left(2 + \frac{1}{n}\right)\left(3 + \frac{1}{n}\right)} \left(+\kappa\right)^{3 + \frac{1}{n}} + c_1 \kappa + c_2 \tag{C-8}$$

where  $c_1$  and  $c_2$  are the integration constants. Finally, Eqs. (C-4) and (C-8) can be combined to give Eq. (3-13), while Eqs. (C-3) and (C-7) are combined to give Eq. (3-10).

# Appendix D

Kolitawong, C., N. Kananai, A. J. Giacomin, and U. Nontakaew, Viscous dissipation of a power law fluid in axial flow between isothermal eccentric cylinders, *J. Non-Newtonian Fluid Mech.*, **166** (2011) 133-144.

J. Non-Newtonian Fluid Mech, 166 (2011) 133-144



Contents lists available at ScienceDirect

### Journal of Non-Newtonian Fluid Mechanics

journal homepage: www.elsevier.com/locate/jnnfm



# Viscous dissipation of a power law fluid in axial flow between isothermal eccentric cylinders

Chanyut Kolitawong a.\*, Nantarath Kananai a, A. Jeffrey Giacomin b, Udomkiat Nontakaew a

- Department of Mechanical and Aerospace Engineering, Polymer Research Center, King Mongkut's University of Technology North Bangkok, 1518 Piboolsongkram Rd., Bangsue, Bangkok 10800, Thailand
- Department of Mechanical Engineering, Rheology Research Center, University of Wisconsin, Madison, WI 53706-1572, United States

#### ARTICLE INFO

Received 20 August 2010 Received in revised form 2 November 2010 Accepted 4 November 2010

Keywords: Temperature profiles Plastic pipe extrusion Plastics tubing Flow in eccentric pipe die Viscous heating Viscous dissipation Bipolar cylindrical coordinates

#### ABSTRACT

We study the temperature distribution of a power law fluid in a pressure-driven axial flow between isothermal eccentric cylinders in bipolar cylindrical coordinates. We begin our analysis by writing the equation of energy in bipolar cylindrical coordinates. We then obtain a dimensionless algebraic analytic solution for temperature profiles under a steady, laminar, incompressible and fully developed flow [Eq. (64)]. We find that the dimensionless temperature profile depends upon the radius ratio of the inner to outer cylinders, the eccentricity, the angular position, and the power law exponent n. The temperature is a strong function of the gap between the cylinders. The temperature profiles are flat in the middle of the gap and then, near the wall, suddenly drop to the wall temperature.

© 2010 Elsevier B.V. All rights reserved.

#### 1. Introduction

In plastic pipe manufacture, if polymer were extruded from a concentric annular die, the pipe wall thickness would not be uniform, and specifically, thicker at the bottom [1-3]. This is because of the gravity flow of the molten plastic, inside the pipe, occurring during its long residence in the cooling chamber. This is why the die mandrel is normally displaced eccentrically downward, so that the extrudate entering the cooling chamber is thicker on top (see Fig. 1).

In curved hose manufacture, the hose is suspended freely from the die [4]. Fig. 2 shows curvature caused by making the die centerpiece eccentric. The extrudate bends away from the thicker side. To obtain a particular hose shape, the die eccentricity must be specifically programmed.

Many researchers have attacked the eccentric annular die problems analytically and numerically [5], For instance, Bird et al. [6-8]. Michaeli [9], and Baird and Collias [10] extensively review concentric axial annular flow of Newtonian and power-law fluids. Fredrickson and Bird [11] solved analytically for the axial flow of power-law (and Bingham) fluids through concentric annuli. Later, Guckes [12] studied the same fluids numerically through eccentric annuli for large gaps.

In blow molding, diverging annular dies are commonly used [13,14]. Parnaby and Worth [15] obtained an analytic solution for the power-law liquid flow between cones with common apexes (diverging or converging dies). For cones without common apexes (axial eccentricity), Parnaby and Worth derived a numerical approach, whereas Dijksman and Savenije [16] solved this analytically using toroidal coordinates. The axial flow through radial eccentricity converging or diverging dies has yet to be tackled.

Later, Kolitawong and Giacomin [17] mapped the eccentric cylinder cross-section in Fig. 3 into bipolar cylindrical coordinates in Fig. 4 [6]. They analytically obtain the dimensionless axial velocity profile between eccentric cylinders for power law liquids.

The temperature rise during plastics pipe and curved hose manufacture may cause plastic degradation. Uneven melt temperatures may also distort the velocity profile, flowing faster than otherwise predicted where the fluid is hotter. Here, we are interested in viscous heating of a power-law fluid flowing axially, under a pressure gradient, through an eccentric annulus. To study the heat transfer between the eccentric cylinders, the energy equation is first written in bipolar cylindrical coordinates. The temperature distribution in the fluid between the eccentric cylinders is then determined analytically from this energy equation. Here we investigate the heat convection of the axial flow in the eccentric annular die to help pipe die designers predict melt temperatures in such dies.

<sup>\*</sup> Corresponding author, Tel.; +66 86 789 8126; fax; +66 2 586 9541. E-mail addresses: ckw@kmutnb.ac.th, chanvut.k@gmail.com (C. Kolitawong).

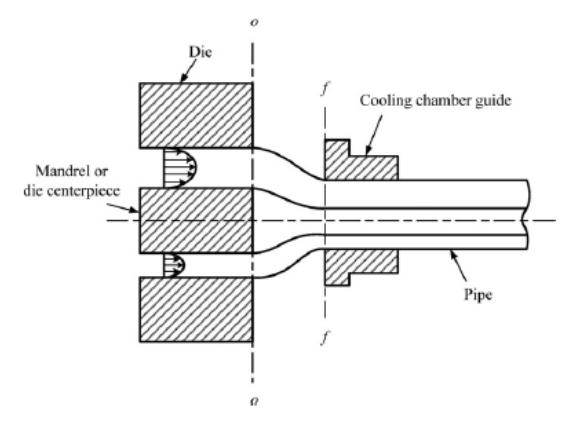


Fig. 1. A pipe extrusion die decentered to compensate for downstream sag.

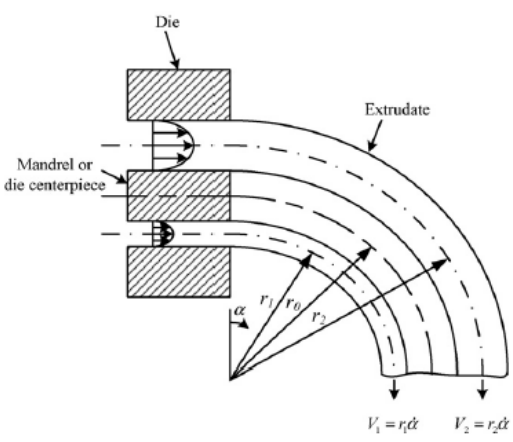


Fig. 2. The curvature in the emerging hose caused by die eccentricity.

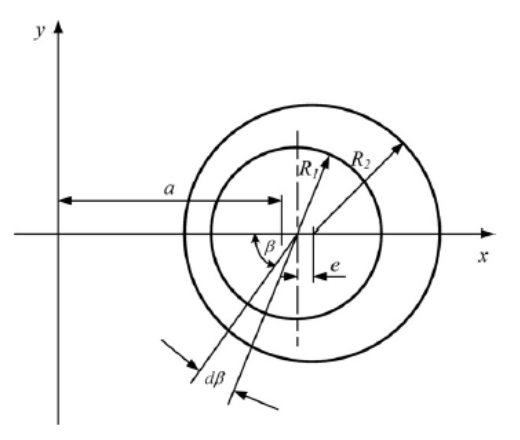


Fig. 3. Cross-section of an eccentric annulus,  $R_1$  and  $R_2$  are the inner and outer cylinder radii; and e is its eccentricity.

### 2. Methodology

### 2.1. Bipolar cylindrical coordinates

In bipolar cylindrical coordinates,  $\xi$  and  $\theta$  represent two orthogonal sets of circles. Figs. 3 and 4 show the inner and outer cylinders at constant  $\xi_1$  and  $\xi_2$ . The rectangular and the bipolar cylindrical coordinates are related by [18]

$$x = \frac{a \sinh \xi}{\cosh \xi - \cos \theta} \tag{1}$$

$$y = \frac{a\sin\theta}{\cosh\xi - \cos\theta} \tag{2}$$

$$z = \zeta$$
 (3)

where  $\theta \in [0, 2\pi)$ ,  $\xi \in (-\infty, \infty)$  and  $\zeta \in (-\infty, \infty)$ . There are several notation conventions for bipolar cylindrical coordinates. Arfken [19], for example, prefers  $(\eta, \xi, z)$ , while  $(\xi, \theta, \zeta)$  is used in this work [6]. We define the scale factors as,

$$h_{\theta} = \frac{a}{\cosh \xi + \cos \theta}$$

$$h_{\xi} = \frac{a}{\cosh \xi + \cos \theta}$$
(5)

$$h_{\xi} = \frac{a}{\cosh \xi + \cos \theta} \tag{5}$$

$$h_{\zeta} = 1$$
 (6)

Since the scale factors in Eqs. (4) and (5) match, we denote h –  $h_{\theta}$  –  $h_{\xi}$ . In bipolar cylindrical coordinates,  $\theta$  is a curvilinear coordinate at the intersection of two circles that are tangent to the circle of radius R centered at (0, p), while  $\xi$  is another curvilinear coordinate at the intersection of two circles that are tangent to the circle centered at (q, 0). The angle  $\theta$  is measured between the line (0, p)to (a, 0) and the y-axis. Hence:

$$\sin \theta = \frac{a}{R}$$
 (7)

$$\cos \theta = \frac{p}{R}$$
 (8)

$$tan \theta = \frac{a}{p} \tag{9}$$

$$p^2 + a^2 = R^2 (10)$$

The equation of a circle centered at (0, p) with radius R is:

$$(x-0)^{2} + (y-p)^{2} = R^{2}$$
(11)

Then, substitute p and R from Eqs. (7) and (9) into Eq. (11):

$$x^{2} + (y - a \cot \theta)^{2} = a^{2} \operatorname{cosec}^{2} \theta.$$
 (12)

After rearranging Eq. (12), one gets:

$$\tan \theta = \frac{2ay}{x^2 + y^2 - a^2} \tag{13}$$

that is:

$$\theta = \tan^{-1}\left(\frac{2ay}{x^2 + y^2 - a^2}\right). \tag{14}$$

The partial derivative of  $\theta$  with respect to x is,

$$\frac{\partial \theta}{\partial x} = \frac{\partial}{\partial x} \left( \tan^{-1} \left( \frac{2ay}{x^2 + y^2 - a^2} \right) \right),\tag{15}$$

or
$$\frac{\partial \theta}{\partial x} = \frac{-4axy}{(x^2 + y^2 - a^2)^2 + (2ay)^2}$$
After a symmetric the right of Eq. (16) one gets:

After rearranging the right side of Eq. (16), one gets: 
$$\frac{\partial \theta}{\partial x} = \frac{\partial}{\partial y} \left( \tanh^{-1} \left( \frac{2ax}{x^2 + y^2 + a^2} \right) \right) \tag{17}$$

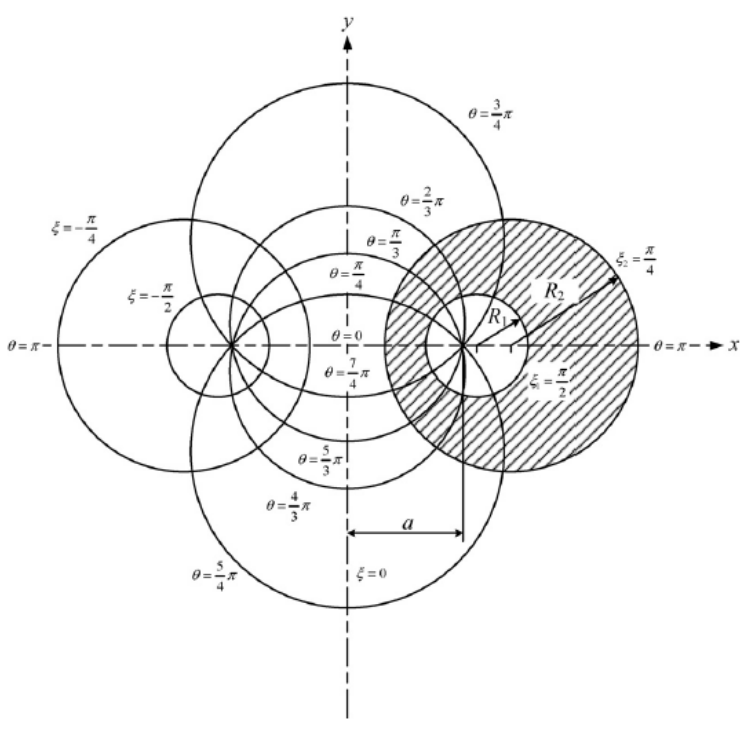


Fig. 4. Bipolar cylindrical coordinates showing the shaded die cross-section with the confocal length, a,

Then, to satisfy Eq. (79):

$$\xi = \tanh^{-1} \left( \frac{2ax}{x^2 + y^2 + a^2} \right) \tag{18}$$

Rearranging Eq. (18):

$$(x - a \coth \xi)^2 + y^2 = a^2 \operatorname{cosech}^2 \xi. \tag{19}$$

Finally, we solve Eqs. (12) and (19) to get:

$$x = \frac{y \cot \theta + a}{\coth \xi} \tag{20}$$

and

$$y = \frac{x \coth \xi - a}{\cot \theta} \tag{21}$$

then

$$x + iy = \frac{a(\sinh \xi + i \sin \theta)}{\cosh \xi + \cos \theta}$$
 (22)

or one can rewrite Eq. (22) to:

$$x + iy = a \tan \left(\frac{i\xi}{2} + \frac{\theta}{2}\right) \tag{23}$$

Eqs. (20)–(23) are the transformation relations between rectangular and bipolar cylindrical coordinates.

### 2.2. Dimensionless velocity profile

Kolitawong and Giacomin [17] developed the following dimensionless axial velocity profile between eccentric cylinders for power

law liquids in bipolar cylindrical coordinates,

$$v_{\zeta p}(\kappa, \beta) = -\frac{n}{n+1} \left( \frac{d(1-\varepsilon\cos\beta)}{2R_2} \right)^{1+(1/n)} \left( |\kappa|^{1+(1/n)} - 1 \right).$$

$$\varepsilon < \frac{1}{5}$$
 (24)

where n is the power law index of the power law viscosity;  $d-R_2-R_1$ , the annular gap;  $R_2$  and  $R_1$ , the outer and inner radii of the annulus, respectively.  $\beta$  is the bipolar angular coordinate measured from the x-axis as shown in Fig. 3, and  $\varepsilon$ , the dimensionless eccentricity:

$$\varepsilon \equiv \frac{e}{d}, \quad 0 < \varepsilon < 1$$
 (25)

They define the dimensionless axial velocity profile such that:

$$\nu_{\zeta p} = \frac{\nu_{\zeta}}{\left[ -(R_2^{n+1}/m)(dP/d\zeta) \right]^{1/n}}$$
 (26)

where m is the consistency index of the power law viscosity;  $v_{\zeta}$ , the dimensional velocity profile of the fluid between the eccentric cylinders;  $dP/d\zeta$ , the pressure gradient in the axial direction. They also introduce the dimensionless bipolar coordinate:

$$\kappa \equiv \frac{\xi - \xi_0}{\xi_1 - \xi_0} \tag{27}$$

where  $\xi$  represents a set of circles located between inner and outer circles, respectively at  $\xi_1$  and  $\xi_2$ . These circles  $\xi_1$  and  $\xi_2$  correspond to  $R_1$  and  $R_2$  as:

$$\xi_1 = \sinh^{-1} \left[ \frac{a}{R_1} \right] \tag{28}$$

and

$$\xi_2 = \sinh^{-1} \left[ \frac{a}{R_2} \right] \tag{29}$$

and

$$\xi_0 = \frac{\xi_1 + \xi_2}{2} \tag{30}$$

where the confocal length, a, is given by:

$$a = \frac{1}{2e} \sqrt{(R_1^2 + R_2^2 - e^2)^2 - 4R_1^2 R_2^2}$$
 (31)

The power law viscosity is defined such that:

$$\eta = m\dot{\gamma}^{n-1} \tag{32}$$

where n is the power law index and m is the consistency index of the power law viscosity. The magnitude of the rate of strain tensor is:

$$\dot{\gamma} \equiv \sqrt{\frac{1}{2}(\dot{\gamma} : \dot{\gamma})}$$
 (33)

where the rate of strain tensor is [6,7]:

$$\underline{\dot{\gamma}} = (\nabla \underline{v}) + (\nabla \underline{v})^{T} \tag{34}$$

### 2.3. Small dimensionless eccentricity approximation

For small dimensionless eccentricity,  $\varepsilon \ll 1$ , the scale factor simplifies to [17,20]:

$$h = \frac{a}{X} = \frac{R_0(1 - \varepsilon \cos \beta)}{(1 - \varepsilon^2)^{1/2}}$$
 (35)

where

$$X = \frac{1 + \varepsilon \cos \theta}{\varepsilon} = \frac{1 - \varepsilon^2}{\varepsilon (1 - \varepsilon \cos \beta)}$$
 (36)

and  $R_0$  is the average radius.

$$R_0 = \frac{R_1 + R_2}{2} \tag{37}$$

and  $\beta$  is measured from the x-axis as shown in Fig. 3. The relations between  $\beta$  and  $\theta$  are shown in Eq. (36) [17,20]. Let,

 $(38)c - \xi_1 - \xi_2$ then, for small eccentricity:

$$c = \frac{d}{2R_0} (1 - \epsilon^2)^{1/2}$$
(39)

From Eq. (27), one obtains:

$$\frac{\partial \kappa}{\partial \dot{\xi}} = \frac{2}{c}$$
 (40)

Finally, combining Eqs. (35) and (39):

$$hc = \frac{d(1 - \varepsilon \cos \beta)}{2} \tag{41}$$

### 2.4. Energy equation

We begin with the energy equation incorporating viscous heatng [7]:

$$\rho \hat{C}_{p} \frac{DT}{Dt} = -(\Delta \cdot \underline{q}) - T \left( \frac{\partial P}{\partial T} \right)_{\mu} (\Delta \cdot \underline{\nu}) - (\underline{\underline{\tau}} : \Delta \underline{\nu})$$
(42)

where  $\rho$  is the liquid density;  $\hat{C}_p$ , the specific heat at a constant pressure;  $\underline{r}$ , the extra stress tensor; and  $\underline{v}$ , the velocity vector. Also the heat flux for a constant thermal conductivity, k, is given by:

$$\underline{q} = -k\nabla T \tag{43}$$

The heat flux gradient in bipolar cylindrical coordinates is given y:

$$\nabla \cdot \underline{q} = \frac{1}{h^2} \left\{ \frac{\partial}{\partial \xi} (hq_{\xi}) + \frac{\partial}{\partial \theta} (hq_{\theta}) + \frac{\partial}{\partial \zeta} (h^2q_{\zeta}) \right\}$$
(44)

where  $q_{\xi}$ ,  $q_{\theta}$ , and  $q_{\zeta}$  are the heat flux components in the  $\xi$ ,  $\theta$ , and  $\zeta$  directions. The substantial derivative in Eq. (42) is given by:

$$\frac{DT}{Dt} = \frac{\partial T}{\partial t} + \frac{1}{h^2} \left\{ v_{\xi} \frac{\partial}{\partial \xi} (hT) + v_{\theta} \frac{\partial}{\partial \theta} (hT) + v_{\zeta} \frac{\partial}{\partial \zeta} (h^2 T) \right\}$$
(45)

where  $v_{\xi}$ ,  $v_{\theta}$ , and  $v_{\zeta}$  are the velocity components in the  $\xi$ ,  $\theta$ , and  $\zeta$  directions. In bipolar cylindrical coordinate, the gradient of a scalar function can be written in term of the scale factor  $h - h_{\theta} - h_{\xi}$ , defined in Eqs. (4) and (5), and thus the gradient of the temperature is:

$$\nabla T = \underline{\delta}_{\xi} \frac{1}{h} \frac{\partial T}{\partial \xi} + \underline{\delta}_{\theta} \frac{1}{h} \frac{\partial T}{\partial \theta} + \underline{\delta}_{\xi} \frac{\partial T}{\partial \zeta}$$
(46)

where  $\underline{\delta}_{\xi}$ ,  $\underline{\delta}_{\theta}$ , and  $\underline{\delta}_{\zeta}$  are unit vectors in the  $\xi$ ,  $\theta$ , and  $\zeta$  axes, respectively. Then, the Laplacian of the temperature is:

$$\nabla^2 T = \frac{1}{h} \frac{\partial}{\partial \xi} \left( \frac{1}{h} \frac{\partial T}{\partial \xi} \right) + \frac{1}{h} \frac{\partial}{\partial \theta} \left( \frac{1}{h} \frac{\partial T}{\partial \theta} \right) + \frac{\partial^2 T}{\partial \zeta^2} \tag{47}$$

The viscous dissipation term is the rightmost term in Eq. (42):

$$\underline{\underline{\tau}} : \nabla \underline{\underline{\nu}} = \tau_{\xi\xi} \left( \frac{1}{h} \frac{\partial \nu_{\xi}}{\partial \xi} \right) + \tau_{\theta\theta} \left( \frac{1}{h} \frac{\partial \nu_{\theta}}{\partial \theta} \right) + \tau_{\zeta\zeta} \left( \frac{\partial \nu_{\zeta}}{\partial \zeta} \right) \\ + \tau_{\xi\theta} \left( \frac{1}{h} \frac{\partial \nu_{\xi}}{\partial \theta} + \frac{1}{h} \frac{\partial \nu_{\theta}}{\partial \xi} \right) + \tau_{\xi\zeta} \left( \frac{\partial \nu_{\xi}}{\partial \zeta} + \frac{1}{h} \frac{\partial \nu_{\zeta}}{\partial \xi} \right) \\ + \tau_{\theta\zeta} \left( \frac{\partial \nu_{\theta}}{\partial \zeta} + \frac{1}{h} \frac{\partial \nu_{\zeta}}{\partial \theta} \right)$$

$$(48)$$

Substituting Eqs. (44), (47), and (48) into Eq. (42) yields:

$$\begin{split} & \rho \hat{\mathsf{C}}_{p} \left[ \frac{\partial T}{\partial t} + \frac{1}{h^{2}} \left\{ v_{\xi} \frac{\partial}{\partial \xi}(hT) + v_{\theta} \frac{\partial}{\partial \theta}(hT) + v_{\zeta} \frac{\partial}{\partial \zeta}(h^{2}T) \right\} \right] \\ & = k \left[ \frac{1}{h} \frac{\partial}{\partial \xi} \left( \frac{1}{h} \frac{\partial T}{\partial \xi} \right) + \frac{1}{h} \frac{\partial}{\partial \theta} \left( \frac{1}{h} \frac{\partial T}{\partial \theta} \right) + \frac{\partial^{2}T}{\partial \zeta^{2}} \right] \\ & - T \left( \frac{\partial P}{\partial T} \right)_{\psi} \left[ \frac{X}{h} \frac{\partial}{\partial \xi} \left( \frac{v_{\xi}}{X} \right) + \frac{X}{h} \frac{\partial}{\partial \theta} \left( \frac{v_{\theta}}{X} \right) + \frac{\partial v_{\zeta}}{\partial \zeta} \right] \\ & - \tau_{\xi\xi} \left( \frac{1}{h} \frac{\partial v_{\xi}}{\partial \xi} \right) - \tau_{\theta\theta} \left( \frac{1}{h} \frac{\partial v_{\theta}}{\partial \theta} \right) - \tau_{\zeta\zeta} \left( \frac{\partial v_{\zeta}}{\partial \zeta} \right) - \tau_{\zeta\zeta} \left( \frac{\partial v_{\zeta}}{\partial \zeta} \right) \\ & - \tau_{\xi\theta} \left( \frac{1}{h} \frac{\partial v_{\xi}}{\partial \theta} + \frac{1}{h} \frac{\partial v_{\theta}}{\partial \xi} \right) - \tau_{\xi\zeta} \left( \frac{\partial v_{\xi}}{\partial \zeta} + \frac{1}{h} \frac{\partial v_{\zeta}}{\partial \xi} \right) \\ & - \tau_{\theta\zeta} \left( \frac{\partial v_{\theta}}{\partial \zeta} + \frac{1}{h} \frac{\partial v_{\zeta}}{\partial \theta} \right) \end{split}$$

which is the energy equation written in bipolar cylindrical coordinates. Eq. (49) is the starting point for any heat transfer problem in bipolar cylindrical coordinates. For an incompressible fluid, the second term on the right side of the energy equation [Eq. (42)] is negligible. Then, the energy equation reduces to:

$$\rho \hat{C}_p \frac{DT}{Dt} = k \nabla^2 T - (\underline{\underline{\tau}} : \nabla \underline{\nu}) \qquad (50)$$

which can be combined with the equation of motion to solve problems in bipolar cylindrical coordinates.

136

### 3. Analysis

### 3.1. Assumption and modeling

For a steady, laminar, incompressible, fully developed flow, we assume that there is only axial velocity in the  $\zeta$  direction, i.e.  $v_{\zeta}=$  $v_{\zeta}(\xi, \theta), v_{\xi} = v_{\theta} = 0$ , and  $T(\xi, \theta)$ . For this case, Eq. (50) simplifies to:

$$0 = k \left\{ \frac{1}{h} \frac{\partial}{\partial \xi} \left( \frac{1}{h} \frac{\partial T}{\partial \xi} \right) + \frac{1}{h} \frac{\partial}{\partial \theta} \left( \frac{1}{h} \frac{\partial T}{\partial \theta} \right) \right\} - \left\{ \tau_{\xi\xi} \left( \frac{1}{h} \frac{\partial v_{\xi}}{\partial \xi} \right) + \tau_{\theta\xi \in \mathbb{Z}} \left( \frac{1}{h} \frac{\partial v_{\xi}}{\partial \theta} \right) \right\}$$

$$(51)$$

The shear stress can be written in terms of the velocity gradients such that [17,20]:

$$\tau_{\xi\xi} = -\eta \frac{1}{h} \frac{\partial v_{\xi}}{\partial \xi}$$
(52)

$$\tau_{\theta \xi} = -\eta \frac{1}{h} \frac{\partial v_{\xi}}{\partial \theta}$$
(53)

where  $\eta$  is the power law viscosity defined in Eq. (32);  $\nu_{\varepsilon}$ , the velocity profile for the flow between the eccentric cylinders. Substitute Eqs. (52) and (53) into Eq. (51) and rearrange to get,

$$\frac{\partial^2 T}{\partial \xi^2} + \frac{\partial^2 T}{\partial \theta^2} = -\frac{m}{k} \left| \frac{1}{h} \frac{\partial v_{\zeta}}{\partial \xi} \right|^{n-1} \left\{ \left( \frac{\partial v_{\zeta}}{\partial \xi} \right)^2 + \left( \frac{\partial v_{\zeta}}{\partial \theta} \right)^2 \right\}$$
(54)

For small dimensionless eccentricity,  $\varepsilon \ll 1$ , i.e.  $\partial v_{\xi}/\partial \theta \cong 0$ ,  $\partial^2 T/\partial \theta^2 \cong 0$ , Eq. (54) becomes:

$$\frac{\partial^2 T}{\partial \xi^2} = -\frac{m}{k} \left( \frac{1}{h} \right)^{n-1} \left| \frac{\partial \nu_{\xi}}{\partial \xi} \right|^{n+1} \tag{55}$$

Introducing the dimensionless variable from Eq. (27), into Eq.

$$\frac{\partial^2 T}{\partial \kappa^2} = -\frac{m}{k} \left(\frac{2}{hc}\right)^{n-1} \left| \frac{\partial v_{\zeta}}{\partial \kappa} \right|^{n+1} \tag{56}$$

Rearranging Eq. (26) for dimensional velocity,  $v_{\zeta}$ , and substituting into Eq. (56), one gets,

$$\frac{\partial^2 T}{\partial \kappa^2} = -\frac{m}{k} \left(\frac{2}{hc}\right)^{n-1} \left[ \left[ -\frac{R_2^{n+1}}{m} \frac{dP_\zeta}{d\zeta} \right]^{1/n} \frac{\partial \nu_{\zeta p}}{\partial \kappa} \right]^{n+1}$$
 (57)

Furthermore, we can rearrange Eq. (57) such that,

$$\frac{\partial^2 T^*}{\partial \kappa^2} = - \left| \frac{\partial v_{\xi p}}{\partial \kappa} \right|^{n+1} \tag{58}$$

where the dimensionless temperature profile,  $T^*$ , is:

$$T^* = \frac{T}{\lambda_0} \tag{59}$$

$$\lambda_0 = \frac{m}{k} \left( \frac{2}{hc} \right)^{n-1} \left[ -\frac{R_2^{n+1}}{m} \frac{dP}{d\zeta} \right]^{(n+1)/n}$$
 (60)

We differentiate Eq. (24) with respect to  $\kappa$  and then substitute

$$\frac{\partial^2 T^*}{\partial \kappa^2} = - \left[ \left[ \frac{d \left( 1 - \varepsilon \cos \beta \right)}{2R_2} \right]^{1 + (1/n)} \kappa |\kappa|^{1/n - 1} \right]^{n + 1} \tag{61}$$

$$\frac{\partial^2 T^s}{\partial \kappa^2} = -\lambda_1 |\kappa|^{1+1/n}$$
(62)

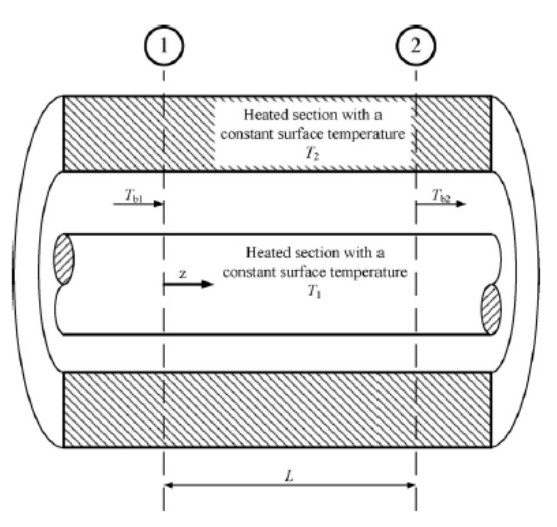


Fig. 5. illustrates heat transfer of the flow between eccentric cylinders.

where  $\lambda_1$  is always real and positive and defined such that:

$$\lambda_1 \equiv \left[ \frac{d(1 - \varepsilon \cos \beta)}{2R_2} \right]^{(n+1)^2/n} \tag{63}$$

By integrating Eq. (62) twice and assuming that the outer radius  $R_2$  ( $\kappa$  = -1), has a constant temperature  $T_2$ , corresponding to  $T^* =$  $T_2^*$ , and the inner radius  $R_2$  ( $\kappa$  – 1) has a constant temperature  $T_1$ , corresponding to  $T^* = T_1^*$ . Then:

$$T^* = -\lambda_2 (|\kappa|^{3+(1/n)} - 1) + \lambda_3 \kappa + \lambda_4$$
 (64)

$$\lambda_2 = \frac{\lambda_1}{(2 + (1/n))(3 + (1/n))} \tag{65}$$

$$\lambda_3 = \frac{T_1^* - T_2^*}{2}$$

$$\lambda_4 = \frac{T_1^* + T_2^*}{2}$$
(66)

$$\lambda_4 = \frac{{T_1}^* + {T_2}^*}{2} \tag{67}$$

Eq. (64) is the main result of this paper. Now, let the wall temperature be controlled uniformly over both cylinder walls so that  $T_1 - T_2$ , then, the dimensionless temperature profile in Eq. (64) is simplified to:

$$T^* = -\lambda_2 \left( |\kappa|^{3+(1/n)} - 1 \right) + T_1^*$$
(68)

$$\Delta^* = -\lambda_2 (|\kappa|^{3+(1/n)} - 1), \quad \Delta^* \equiv T^* - T_1^*$$
(69)

Dividing Eq. (69) by  $\lambda_2$  yields the angular position independent dimensionless temperature  $\Theta^\star$  :

$$\Theta^* = \frac{\Delta^*}{\lambda_2} = 1 - |\kappa|^{3 + (1/\pi)}$$
 (70)

## 3.2. Cooling system

In this work, all heat generated by the viscous energy dissipates through the inner and outer cylinder walls and then the cooling systems near the walls carry the energy out. Fig. 5 depicts this. Suppose that the fluid enters and leaves the die at bulk temperature  $T_{b1}$  and  $T_{b2}$ , respectively. The mandrel surface is controlled at

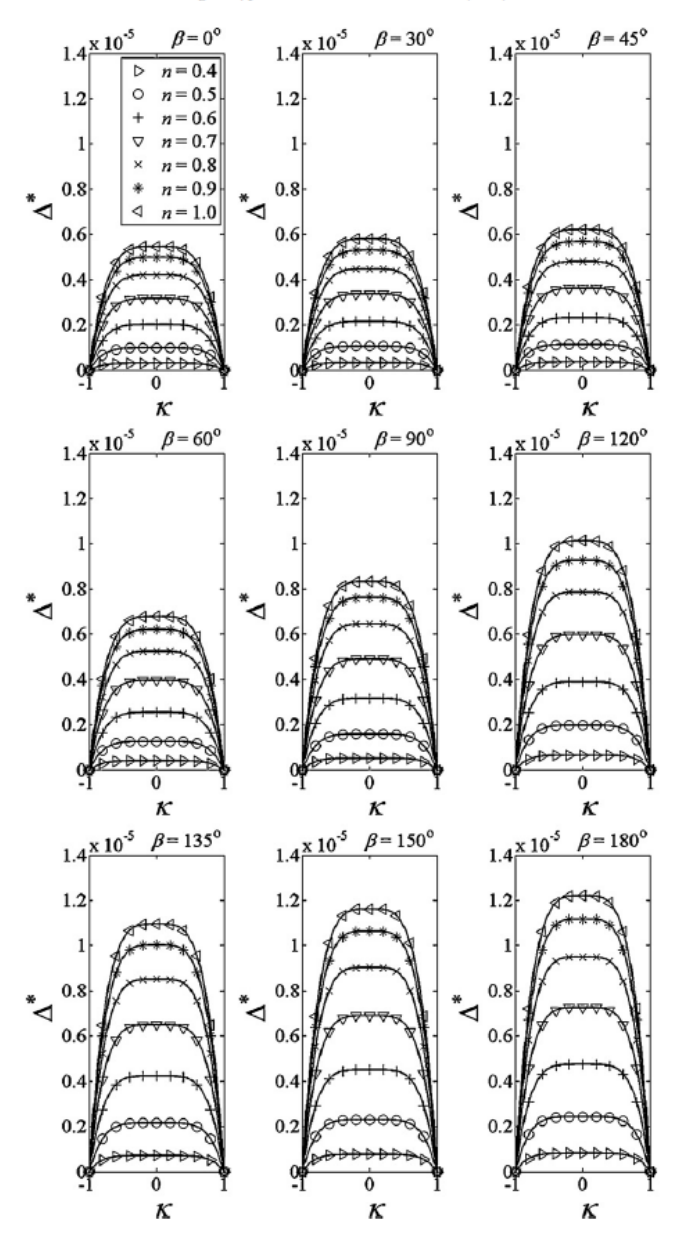


Fig. 6. Dimensionless temperature profiles  $\Delta^*$  versus the dimensionless gap  $\kappa$  using  $\varphi$  = 0.80 and the dimensionless eccentricity,  $\varepsilon$  = 0.10, at various angles  $\beta$  and power law indexes  $\rho$ 

a constant temperature  $T_1$ , while the die barrel is controlled at a constant temperature  $T_2$ . The heat flow from the fluid to the solid inner surface of the die (called the die mandrel) by the *Newton's law of cooling* is [7,8]:

$$h_1(\pi D_1 L)(T_{b1} - T_1) = \int_0^L \int_0^{2\pi} \left( k \frac{\partial T}{\partial \xi} h \, \mathrm{d}\theta \, \mathrm{d}\zeta \right)_{\xi = \xi_1} \tag{71}$$

and, at the outer wall of the die (called the die barrel):

$$h_2(\pi D_2 L)(T_{b1} - T_2) = \int_0^L \int_0^{2\pi} \left(k \frac{\partial T}{\partial \xi}\right) \int_{\xi = \xi}^{\xi = 0} h \, d\theta \, d\zeta$$
 (72)

where  $h_1$  and  $h_2$  are the heat transfer coefficient corresponding to the die mandrel and barrel surfaces, respectively. By using Eq. (40) and (59), we can easily show that the *Nusselt Number* corresponding

(74)

(75)

Fig. 7. Dimensionless temperature profiles  $\Delta^*$  versus the dimensionless gap  $\kappa$  using  $\varphi$  = 0.80 and the dimensionless eccentricity,  $\varepsilon$  = 0.20, at various angles  $\beta$  and power law indexes n.

ĸ

ĸ

to the outer surface of the mandrel is:

to the outer surface of the mandrel is: where, 
$$V_0 = \frac{m}{k} \left(\frac{2}{c}\right)^{n-1} \left[-\frac{R_2^{n+1}}{m} \frac{dP}{d\zeta}\right]^{(n+1)/n}$$
(74)
$$V_0 = \frac{m}{k} \left(\frac{2}{c}\right)^{n-1} \left[-\frac{R_2^{n+1}}{m} \frac{dP}{d\zeta}\right]^{(n+1)/n}$$
For uniform wall temperatures, i.e.  $T_1 - T_2$ , we differentiate Eq. (64) once and let  $\kappa - 1$ , Eq. (73) becomes: 
$$V_0 = \frac{m}{k} \left(\frac{2}{c}\right)^{n-1} \left[-\frac{R_2^{n+1}}{m} \frac{dP}{d\zeta}\right]^{(n+1)/n}$$
(74)
$$V_0 = \frac{m}{k} \left(\frac{2}{c}\right)^{n-1} \left[-\frac{R_2^{n+1}}{m} \frac{dP}{d\zeta}\right]^{(n+1)/n}$$
(75)
$$V_0 = \frac{m}{k} \left(\frac{2}{c}\right)^{n-1} \left[-\frac{R_2^{n+1}}{m} \frac{dP}{d\zeta}\right]^{(n+1)/n}$$
(75)

ĸ

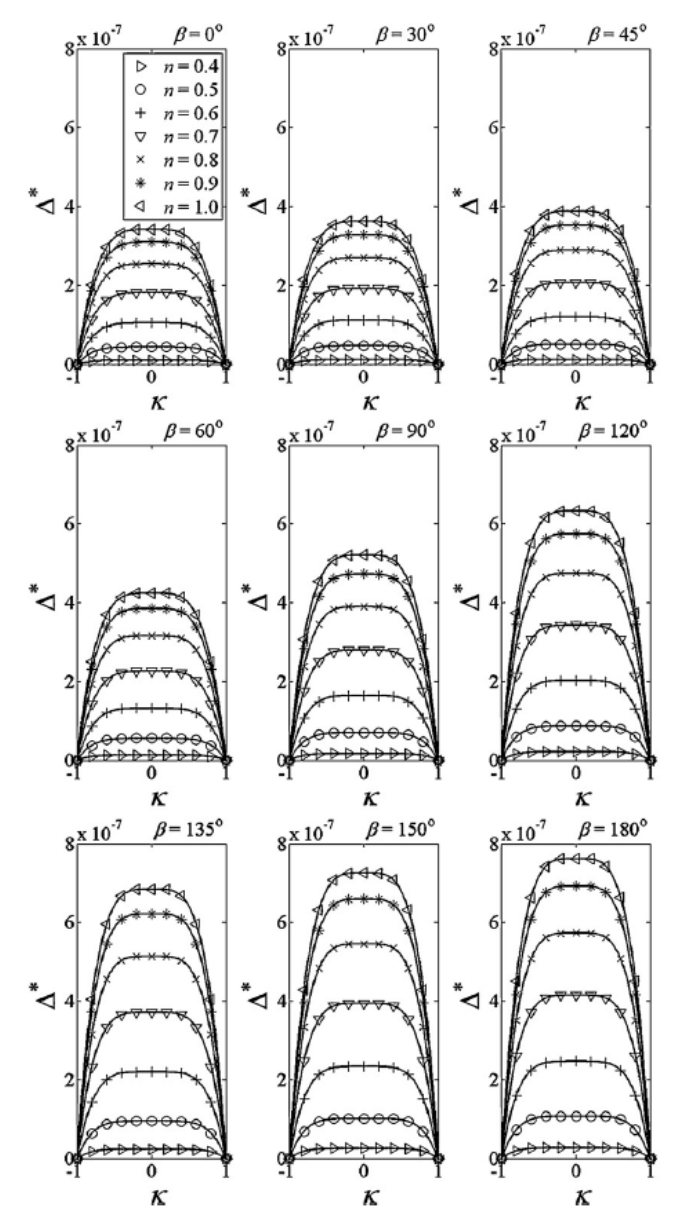


Fig. 8. Dimensionless temperature profiles  $\Delta^*$  versus the dimensionless gap  $\kappa$  using  $\varphi$  = 0.90 and the dimensionless eccentricity,  $\varepsilon$  = 0.10, at various angles  $\beta$  and power law

in which:

$$\psi_1 \equiv -\left(\frac{n}{2n-1}\right) \left(\frac{d}{2R_2}\right)^{(n+1)^2/n}$$
 (76)

and

$$\Omega(n,\varepsilon) = \int_0^{\pi} (1 - \varepsilon \cos \beta)^{3 + (1/n)} d\beta$$
 (77)

Furthermore, we can show that the *Nusselt number* corresponding to the inner surface of the die is:

$$Nu_{2} = \frac{4\psi_{0}\psi_{1}(1-\varepsilon^{2})^{(n-1)/2}}{\pi c(T_{b1}-T_{2})R_{0}^{n-2}}\Omega(n,\varepsilon)$$
 (78)

We can easily see that the *Nusselt numbers* are strongly dependent on the dimensionless eccentricity  $\varepsilon$ , the power law index n,

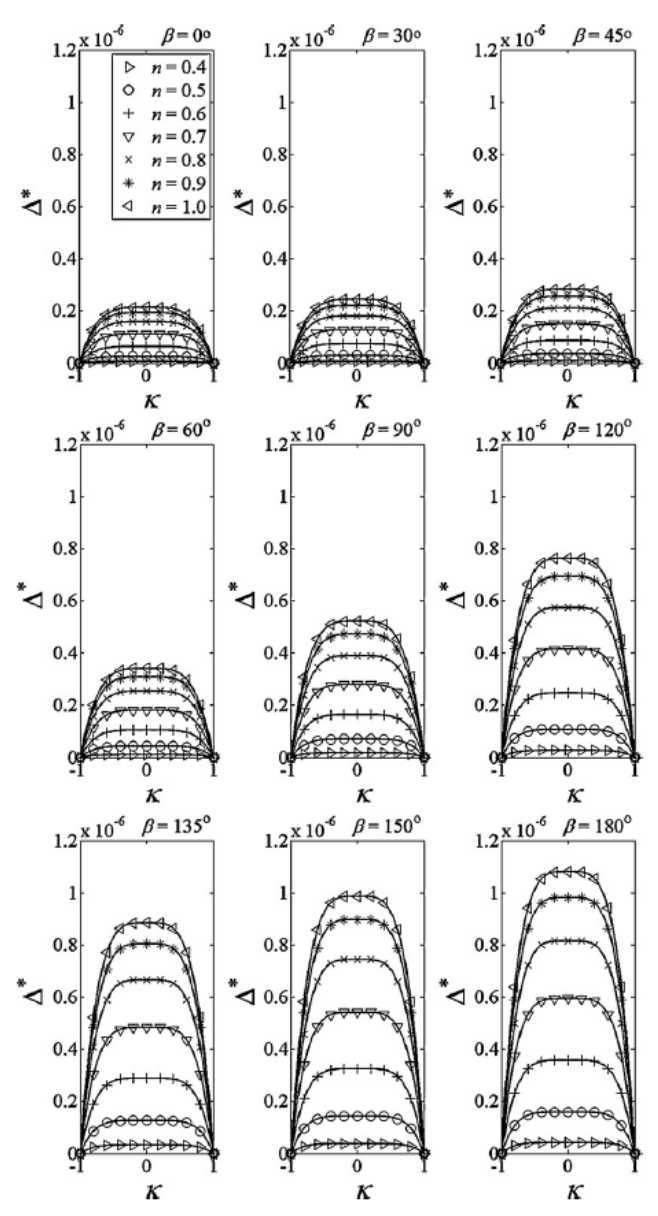


Fig. 9. Dimensionless temperature profiles  $\Delta^*$  versus the dimensionless gap  $\kappa$  using  $\varphi$  = 0.90 and the dimensionless eccentricity,  $\varepsilon$  = 0.20, at various angles  $\beta$  and power law indexes n.

the angular position  $\boldsymbol{\beta}$  and the different temperatures between the fluid and the wall.

### 3.3. Results and discussion

Figs. 6–9 plot the dimensionless temperature profiles,  $\Delta^*$  versus the dimensionless gap,  $\kappa$  [Eq. (69)] for 6 values of n over the range  $0.4 \le n \le 1$  at various angular positions from the smallest gap,  $\beta$ , with the dimensionless eccentricity ranging over from  $0.1 \le \varepsilon \le 0.2$ 

at the dimensionless radius ratio,  $\varphi \equiv R_1/R_2$ , values of 0.8 and 0.9.

Figs. 6–9 show that the dimensionless temperature  $(\Delta^*)$ , in general, increases with the dimensionless radius ratio,  $\varphi$ , the dimensionless eccentricity,  $\varepsilon$ , the angular distance from the smallest gap,  $\beta$ , and the power law exponent, n. In addition, the more shear thinning the fluid (the lower the n), the blunter the temperature profile. Moreover, the more eccentric the die (the higher the  $\varepsilon$ ), the greater the temperature difference between the fluid

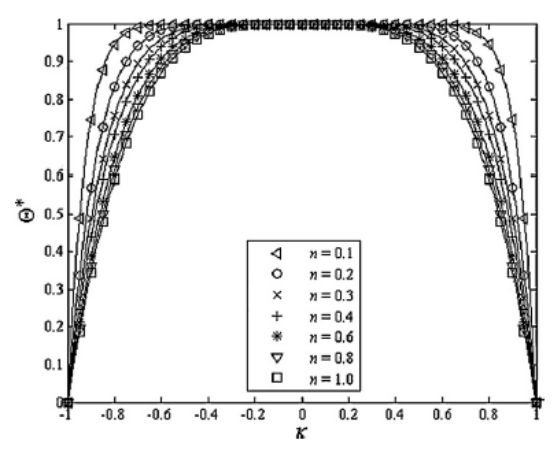


Fig. 10. Dimensionless temperature  $(\Theta^*)$  versus the dimensionless gap,  $\kappa$ , for various power law indexes (n).

at the smallest gap  $(\beta$ -0°) and the biggest gap  $(\beta$ =180°). This is because of the convective flow in the eccentric die. In other words, the dimensionless temperature is proportional to the velocity in the die.

The dimensionless temperatures also decrease by two decades [from  $O(10^{-5})$  to  $O(10^{-7})$ ] when the radius ratio  $(\varphi)$  increases from 0.80 to 0.90. When the radius ratio increases, the inner and outer radii approach one another, and so the gap is very small all around the die. In this case, the convective effects in the die diminish, which is why the fluid temperature decreases as the radius ratio increases.

Fig. 10 plots the dimensionless temperature profiles,  $\Theta'$ , versus the dimensionless gap,  $\kappa$ , [Eq. (70)] by varying the power-law index (n) over the range 0.1  $\leq$  1n  $\leq$  1. Fig. 10 shows that the dimensionless temperature is less than one for all power law indexes. From this, we can estimate the temperature distributions at any angular

Table 2 lists the peak temperatures of the HDPE melt flowing in the eccentric die at various angles,  $\beta$ .

| β(°) | λ <sub>0</sub> (K)    | λ2                     | $\Delta_{\kappa=0}$ (°C) | T <sub>κ</sub> =0 (°C) |
|------|-----------------------|------------------------|--------------------------|------------------------|
| 0    | $5.059 \times 10^{7}$ | $4.644 \times 10^{-8}$ | 2,349                    | 182,349                |
| 30   | $5,133 \times 10^{7}$ | $5.358 \times 10^{-8}$ | 2,750                    | 182,750                |
| 45   | $5,219 \times 10^{7}$ | $6.313 \times 10^{-8}$ | 3,295                    | 183,295                |
| 60   | $5.328 \times 10^{7}$ | $7.747 \times 10^{-8}$ | 4,128                    | 184,128                |
| 90   | $5,581 \times 10^{7}$ | $1,225 \times 10^{-7}$ | 6,835                    | 186,835                |
| 120  | $5.820 \times 10^{7}$ | $1.853 \times 10^{-7}$ | 10,785                   | 190,785                |
| 135  | $5,915 \times 10^{7}$ | $2,176 \times 10^{-7}$ | 12,871                   | 192,871                |
| 150  | $5.987 \times 10^{7}$ | $2,452 \times 10^{-7}$ | 14,680                   | 194,680                |
| 180  | $6.047 \times 10^{7}$ | $2,705 \times 10^{-7}$ | 16,355                   | 196,355                |

distance from the smallest gap,  $\beta$ , if we know the maximum temperature difference. Table 1 provides the numerical values of the angular position independent dimensionless temperature profiles,  $\Theta^*$ , versus the dimensionless gap,  $\kappa$ , for various power law indexes (n). How to use Fig. 10 for pipe die design is illustrated in an example in Section 3.4.

### 3.4. Design example

A high density polyethylene (HDPE) plastic pipe is extruded from an eccentric annular die of outer radius  $R_2$  – 0.100 m and inner radius  $R_1$  – 0.099 m with small dimensionless eccentricity of  $\varepsilon$  – 0.2 to compensate for sag in the post-die cooling chamber. The HDPE melt obeys the power law with n – 0.56, and the consistency index, m = 6190 Pa s<sup>n</sup> [21,22]. The polymer has thermal conductivity, k – 0.045 W/(m K). The inner and outer wall temperatures,  $T_1$  and  $T_2$ , are uniform at 180 °C (453.15 K). The pressure drop per unit length within the die is 5 MPa/m. Determine the temperature profiles in the molten plastic at various angular positions,  $\beta$ .

Solution: To solve for the dimensional temperature appearing in Eq. (59), we need to rearrange Eq. (70) to get:

$$\Delta = \lambda_0 \lambda_2 \Theta^*$$

**Table 1** provides the numerical values of the angular position independent dimensionless temperature ( $\Theta^*$ ) as a function of the dimensionless gap,  $\kappa$ , for various power law indexes n

| n   | K       | K       |         |         |         |         |         |         |         |         |         |
|-----|---------|---------|---------|---------|---------|---------|---------|---------|---------|---------|---------|
|     | 0,50    | 0.45    | 0.40    | 0,35    | 0,30    | 0.25    | 0,20    | 0,15    | 0,10    | 0.05    | 0,00    |
| 0.1 | 0,99988 | 0,99997 | 0,99999 | 1,00000 | 1,00000 | 1,00000 | 1,00000 | 1,00000 | 1,00000 | 1,00000 | 1,00000 |
| 0.2 | 0,99609 | 0,99832 | 0,99934 | 0,99977 | 0.99993 | 0.99998 | 1,00000 | 1,00000 | 1,00000 | 1,00000 | 1,00000 |
| 0,3 | 0,98760 | 0,99364 | 0.99698 | 0,99870 | 0.99951 | 0,99985 | 0,99996 | 0,99999 | 1,00000 | 1,00000 | 1,00000 |
| 0.4 | 0.97790 | 0.98762 | 0,99352 | 0.99689 | 0.99867 | 0,99951 | 0,99986 | 0,99997 | 1,00000 | 1,00000 | 1,00000 |
| 0,5 | 0,96875 | 0.98155 | 0,98976 | 0,99475 | 0.99757 | 0,99902 | 0,99968 | 0,99992 | 0,99999 | 1,00000 | 1,00000 |
| 0.6 | 0,96063 | 0,97592 | 0.98610 | 0,99255 | 0,99637 | 0.99845 | 0,99945 | 0,99986 | 0,99998 | 1,00000 | 1,00000 |
| 0.7 | 0,95356 | 0,97088 | 0,98271 | 0,99043 | 0,99517 | 0.99784 | 0,99920 | 0,99978 | 0,99996 | 1,00000 | 1,00000 |
| 0.8 | 0.94744 | 0,96641 | 0.97964 | 0,98846 | 0.99401 | 0.99724 | 0,99893 | 0,99968 | 0,99994 | 1,00000 | 1,00000 |
| 0.9 | 0.94213 | 0.96248 | 0.97688 | 0,98665 | 0.99291 | 0.99665 | 0,99866 | 0.99959 | 0,99992 | 1.00000 | 1,00000 |
| 1.0 | 0.93750 | 0,95899 | 0.97440 | 0,98499 | 0,99190 | 0,99609 | 0,99840 | 0,99949 | 0.99990 | 0,99999 | 1,00000 |
| _   |         |         |         |         |         |         |         |         |         |         |         |
| n   | К       |         |         |         |         |         |         |         |         |         |         |
|     | 1.00    | 0,95    | 0,80    | 0,85    | 0,80    |         | 0.75    | 0,70    | 0,65    | 0,60    | 0,55    |
| 0.1 | 0.00000 | 0.48666 | 0.74581 | 0.87909 | 0.945   | 02      | 0.97624 | 0.99031 | 0.99630 | 0.99869 | 0.99958 |
| 0.2 | 0.00000 | 0,33658 | 0,56953 | 0,72751 | 0,832   | 23      | 0.89989 | 0,94235 | 0.96814 | 0,98320 | 0.99163 |
| 0.3 | 0.00000 | 0,27737 | 0.48690 | 0.64274 | 0,756   | 65      | 0.83830 | 0.89554 | 0.93467 | 0,96065 | 0.97732 |
| 0.4 | 0.00000 | 0,24581 | 0.43981 | 0,59092 | 0,706   | 91      | 0.79449 | 0.85938 | 0.90645 | 0,93977 | 0.96268 |
| 0,5 | 0.00000 | 0,22622 | 0.40951 | 0,55629 | 0,672   | 32      | 0.76270 | 0.83193 | 0.88397 | 0,92224 | 0.94967 |
| 0.6 | 0.00000 | 0.21288 | 0.38840 | 0.53159 | 0.647   | 02      | 0.73881 | 0.81071 | 0.86605 | 0.90781 | 0.93857 |
| 0.7 | 0.00000 | 0,20320 | 0,37287 | 0,51311 | 0,627   | 76      | 0.72030 | 0,79393 | 0.85159 | 0.89588 | 0.92918 |
| 0.8 | 0.00000 | 0,19587 | 0,36096 | 0,49878 | 0,612   | 62      | 0,70555 | 0,78038 | 0,83972 | 0,88594 | 0,92120 |
| 0.9 | 0.00000 | 0,19012 | 0,35154 | 0,48734 | 0,600   | 43      | 0,69355 | 0,76923 | 0,82984 | 0,87755 | 0,91437 |
| 1.0 | 0.00000 | 0.18549 | 0,34390 | 0,47799 | 0,590   | 40      | 0,68359 | 0,75990 | 0.82149 | 0,87040 | 0,90849 |

Fig. 11. Temperature profiles of a HDPE power law polymer flow in eccentric cylinders with wall temperature of 180°C.

where  $\Delta - T - T_1$ . From Eqs. (41), (60), (63) and (65), at  $\beta$  - 0°, for example.

 $hc = d(1 - \varepsilon \cos \beta)/2 = (0.01 \text{ m})(1 - 0.2 \cos(0))/2 = 4.00 \times 10^{-3} \text{ m}.$ 

The

$$\begin{split} \lambda_0 &= \frac{m}{k} \left(\frac{2}{hc}\right)^{n-1} \left[ -\frac{R_2^{n+1}}{m} \frac{dP}{d\zeta} \right]^{n+1/n} \\ \lambda_0 &= \frac{(6190\,\text{Pa} - \text{s}^n)}{(0.045\,\text{W/m\,K})} \left(\frac{2}{4.00\times 10^{-3}\,\text{m}}\right)^{0.56-1} \\ &\times \left[ -\frac{(0.1\,\text{m})^{0.56+1}}{(6190\,\text{Pa}\,\text{s}^n)} (-5\times 10^6\,\text{Pa/m}) \right]^{(0.56+1)/0.56} \end{split}$$

$$\lambda_0 = 5.059 \times 10^7~K$$

$$\begin{split} \lambda_1 &= \left[\frac{d(1-\epsilon\cos\beta)}{2R_2}\right]^{(n+1)^2/n} \\ &= \left[\frac{(0.01\,m)(1-0.2\cos(0))}{2(0.1\,m)}\right]^{(0.56+1)^2/0.56} = 8.413\times 10^{-7} \\ \lambda_2 &= \frac{\lambda_1}{(2+(1/n))(3+(1/n))} = \frac{8.413\times 10^{-7}}{(2+(1/0.56))(3+(1/0.56))} \\ &= 4.644\times 10^{-8} \end{split}$$

We then calculate the peak temperature at  $\beta$  – 0°, occurring when  $\kappa$  – 0, by letting  $\Theta^*$  – 1,

$$\Delta = \lambda_0 \lambda_2 \Theta^* = (5.059 \times 10^7 \text{ K})(4.644 \times 10^{-8})(1)$$
  
= 2.349 K = 2.349 °C

$$T = \Delta + T_1 = 2.349 \,^{\circ}\text{C} + 180 \,^{\circ}\text{C} = 182.349 \,^{\circ}\text{C}$$

Other peak temperatures at various angles,  $\beta$ , are constructed in Table 2. Next, using the modified dimensionless temperature profiles with power-law index n = 0.56 from Fig. 10, i.e. interpolating values of the modified dimensionless temperature profiles from Table 1, and then multiply them by the peak temperature  $T_{\kappa=0}$  in Table 2 we get the temperature rises at various  $\kappa$ . We then, add the wall temperature at 180 °C (453.15 K) onto the temperature rises to get the temperature profile for each  $\beta$ . Fig. 11 shows that the

0.2 dimensionless eccentricity in this example would cause a 16  $^{\circ}\text{C}$  temperature imbalance around the die.

#### 4. Conclusion

The energy equation in bipolar cylindrical coordinates, coupled with the velocity profile of the power law viscosity model, is used to determine the temperature profile in an annular die for plastic pipe extrusion. The dimensionless temperature profile of a steady, laminar, incompressible and fully developed flow of a power law fluid can be found by the analytic method with assumptions such that there are no velocities in the  $\xi$  and  $\theta$  directions, no heat convection terms, and uniform wall temperatures. The solution reveals that the dimensionless temperature distribution is a function of the dimensionless radius ratio,  $\varphi$ , the dimensionless eccentricity,  $\varepsilon$ , the angular distance from the smallest gap,  $\beta$ , the power law exponent, n, and is a strong function of, the dimensionless gap,  $\kappa$ . The temperature profiles are blunt in the middle of the gap. The temperature rises in the gap due to viscous dissipation. This temperature rise increases if the gap is increased. This is because the radial path length for thermal conduction to the wall is lengthened. Moreover, the temperature rise also increases with the power law exponent, n, to reach the Newtonian temperature profile at n = 1. Thus, the lesser the power law exponent, n, the blunter the temperature profile.

Whereas this paper tackles the die with isothermal walls, there remains a need for the alternative case of constant heat fluxes at the walls. The temperature of the die mandrel is often uncontrolled, leaving it with zero heat flux at steady state. This is always the case for small die mandrels, where a temperature control unit cannot be installed.

### Acknowledgments

The authors gratefully acknowledge the Thailand Research Fund (TRF) and National Science and Technology Development Agency (NSTDA) for funding. The authors are also indebted to Suthinan Leewuthinan of the King Mongkut's University of Technology North Bangkok for his invaluable help and review of the manuscript.

## Appendix A.

If  $\xi$  and  $\theta$  are real single-valued functions of x and y and their four partial derivatives are continuous throughout a real domain of R, the Cauchy-Riemann equations [19,23] are thus:

$$\frac{\partial \theta}{\partial x} = \frac{\partial \xi}{\partial y}$$
(79)

and

$$\frac{\partial \xi}{\partial x} = -\frac{\partial \theta}{\partial y} \tag{80}$$

and these are both necessary and sufficient conditions for:

$$f(z) = \theta(x, y) + i\xi(x, y) \tag{81}$$

to be analytic in R. Under these conditions, the partial derivatives of f(z) are given by:

$$f'(z) = \frac{\partial \theta}{\partial x} + i \frac{\partial \xi}{\partial x}$$
 (82)

and

$$f'(z) = \frac{\partial \xi}{\partial y} - i \frac{\partial \theta}{\partial y}$$
 (83)

### References

 D.N. Githuku, A.J. Giacomin, Elimination of sag in plastic pipe extrusion, Int. Polym. Proc. VII (2) (1992) 140–143.

- [2] D.N. Githuku, A.J. Giacomin, Simulation of slump in plastic pipe extrusion, J. Eng. Mater. Technol. 114 (1) (1992) 81–83.
   [3] D.N. Githuku, A.J. Giacomin, A spectral element simulation of gravitational flow during plastic pipe extrusion, J. Eng. Mater. Technol. 115 (4) (1993) 433–439.
   [4] L.A. Goettler, A.J. Lambright, R.I. Leib, P.J. DiMauro, Rubber Chem. Technol. 54

- La. Goettler, A.J. Lambright, R.I. Leib, P.J. DiMauro, Rubber Chem. Technol. 54 (2) (1981) 277.
  W.T. Snyder, An analysis of slug flow heat transfer in an eccentric annulus, AlChe J. 9 (4) (1963) 503–506.
  R.B. Bird, R.C. Armstrong, O. Hassager, Dynamics of Polymeric Liquids, vol. I: Fluid Mechanics, second ed., John Wiley and Sons, Inc., New York, 1987, pp. 181–183, 595–596.
  R.B. Bird, W.E. Stewart, E.N. Lightfoot, Transport Phenomena, John Wiley and Sons, Inc., New York, 1960, pp. 42–54, 68.
  R.B. Bird, W.E. Stewart, E.N. Lightfoot, Transport Phenomena, second ed., John Willey and Sons Inc., New York, 2007, pp. 53–56, 64.
  W. Michaeli, Extrusion Dies for Plastics and Rubber, second ed., Hanser Publishers, New York, 1992, pp. 58–60.
  D.G. Baird, D.I. Collias, Polymer Processing: Principles and Design, John Willey and Sons, Inc., New York, 1998, pp. 14–16.
  A.G. Fredrickson, R.B. Bird, Ind. Eng. Chem. 50 (1958) 347.
  T.L. Guckes, Trans, ASME (B) 97 (1975) 498.

- [13] J.M. Dealy, K.F. Wissbrun, Melt Rheology and Its Role in Plastics Processing, Van Nostrand Reinhold, New York, 1990, pp. 512–519.
  [14] D.V. Rosato, D.V. Rosato, Blow Molding Handbook, Hanser Publishers, New York, 1989, pp. 664–669.
  [15] J. Parnaby, R.A. Worth, Proc. Inst. Mech. Eng. 188 (25) (1974) 357.

- [15] J. Parnaby, R.A. Worth, Proc. Inst. Mech. Eng. 188 (25) (1974) 357.
  [16] J.F. Dijksman, E.P.W. Savenije, Rheol. Acta 24 (1985) 105.
  [17] C. Kolitawong, A.J. Giacomin, Polym. Plast. Technol. Eng. 40 (3) (2001) 363–384.
  [18] P. Moon, D.E. Spencer, Field Theory for Engineers, D. Van Nostrand Company, Inc., New York, 1961, pp. 361–368.
  [19] G.B. Arfken, Mathematical Methods for Physicists, Academic Press, Orlando, Fl., 1970, pp. 97–102.
  [20] C. Kolitawong, A.J. Giacomin, Axial Flow Between Eccentric Cylinders, RRC Report 167, Rheology Research Center, University of Wisconsin, Madison, USA, 1999.
- 1999.
  [21] Z. Tadmor, C.G., Gogos, Principles of Polymer Processing, John Wiley and Sons, New York, 1973, p. 695.
  [22] Z. Tadmor, C.G. Gogos, Principles of Polymer Processing, second ed., John Wiley and Sons, New York, 2006, pp. 889–913.
  [23] C.R. Wylie, L.C. Barrett, Advanced Engineering Mathematics, sixth ed., McGraw-Hill Education (ISE Editions), 1995, pp. 1134–1135.

Kolitawong, C., Kananai, N, Giacomin, A. J. and Nontakaew, U, "Temperature Profiles of Axial Flows Between Eccentric Cylinders," Abstracts, *Commemorative International Conference on the Occasion of the 4<sup>th</sup> Cycle Celebration of KMUTT, SDSE 2008*, Bangkok, Thailand, pp. 1062-1069 (April 7-9, 2009).





# COMMEMORATIVE INTERNATIONAL CONFERENCE

ON THE OCCASION OF THE 4<sup>™</sup> CYCLE CELEBRATION OF KMUTT

# SUSTAINABLE DEVELOPMENT TO SAVE THE EARTH TECHNOLOGIES AND STRATEGIES VISION 2050 PROCEEDINGS

7-9 APRIL 2009 MILLENNIUM HILTON BANGKOK HOTEL BANGKOK THAILAND



Commemorative International Conference on the Occasion of the 4th Cycle Celebration of KMUTT Sustainable Development to Save the Earth: Technologies and Strategies Vision 2050: (SDSE2008) 7-9 April 2009, Bangkok, Thailand

### Temperature Profiles of Axial Flow Between Eccentric Cylinders

Chanyut Kolitawong<sup>1,\*</sup>, Nantarath Kananai<sup>1</sup>, A. J. Giacomin<sup>2</sup> and Udomkeat Nontakaew<sup>1</sup>

Department of Mechanical and Aerospace Engineering, Polymer Research Center, King Mongkut's University of Technology North Bangkok, Thailand 10800 Tel: (662) 5870026 Ext 411, Fax: (662) 5869541

Department of Mechanical Engineering, Rheology Research Center, University of Wisconsin, Madison, WI 53706-1572, USA.

\*\*Corresponding author: ckw@kmutnb.ac.th

Abstract: Here we study heat distribution of a power law fluid axially flows between eccentric cylinders by mapping the eccentric cylinder cross-sectional area with bipolar cylindrical coordinates. The bipolar cylindrical coordinates allow us to solve for an algebraic analytic solution of temperature profiles of a power law fluid flow under a steady, laminar, incompressible, and fully developed situation. The solution reveals that the temperature distribution is a function of the radius ratio of the inner and outer cylinders, the eccentricity, the angular distance from the smallest gap, the power law exponent n, and also a strong function of the gap between the cylinders. The temperature profiles are flat at the middle of the gap and suddenly drop to reach the wall temperature near the wall region. This behavior occurs due to heat dissipation of the non-Newtonian effects.

Keywords: Temperature profiles, Plastics flows in eccentric pipe die, Bipolar cylindrical coordinates.

### 1. INTRODUCTION

In plastic pipe manufacturer, when polymer is extruded from a concentric annular die, the pipe wall thickness is not uniform, and specially, thicker at the bottom. This is because of the gravity flow of the molten plastic, inside the pipe, occurring during the long residence in the cooling chamber. For this reason, the die concentric (mandrel) is displaced eccentrically downward, so that the extrudate entering the chamber is thicker at the top (see Figure 1).

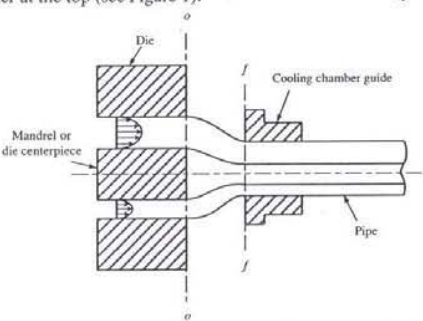


Figure 1 A pipe extrusion die decentered to compensate for downstream sag.

In curved hose manufacture, the hose is suspended freely from the die. Figure 2 shows curvature caused by making the die centerpiece eccentrie. The extrudate bends away from the thicker side. To obtain a particular hose shape, the die eccentricity must be specifically programmed.

Many researchers have been attacked and reviewed the eccentric annular die problems analytically and numerically. For instance, Bird et al. [1, 2], Michaeli [3], and Baird and Collias [4] extensively review concentric axial annular flow of Newtonian and power-law fluids. Fredrickson and Bird [5] solved analytically for the axial flow of power-law (and Bingham) fluids through concentric annuli. Later, Guckes [6] studied the same fluids through eccentric annuli numerically for large gaps.

In blow molding, diverging annular dies are commonly

used [7, 8]. Parnaby and Worth obtained an analytic solution for the power-law liquid flow between cones with common apices (diverging or converging dies). For cones without common apices (axial eccentricity), Parnaby and Worth [9] derived a numerical approach, whereas Dijksman and Savenije [10] solved this analytically using toroidal coordinates. The axial flow through radial eccentricity converging or diverging dies has yet to be tackled.

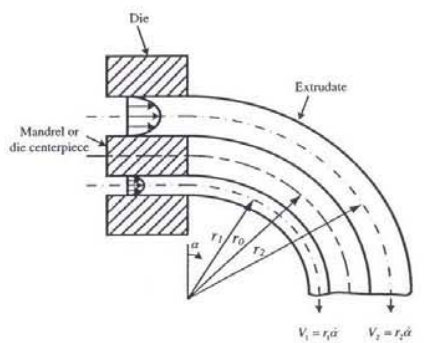


Figure 2 The curvature in the emerging hose caused by die eccentricity.

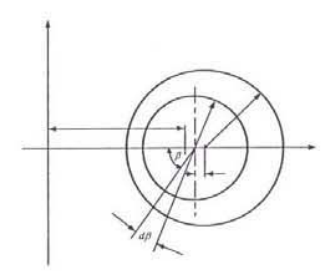


Figure 3 Cross section of an eccentric annulus.  $R_1$  and  $R_2$  are the inner and outer cylinder radii; and e is its eccentricity.

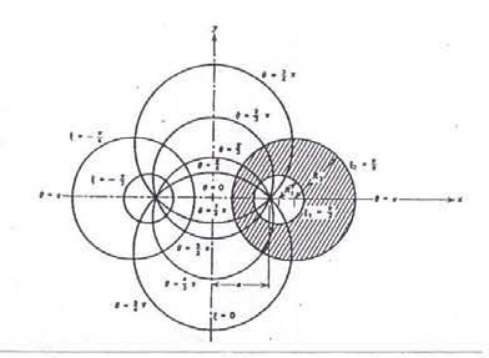


Figure 4 Bipolar cylindrical coordinates showing the shaded die cross section with the confocal length, a.

Later, Kolitawong and Giacomin [11] match the eccentric cylinder cross section in Figure 3 with bipolar cylindrical coordinates in Figure 4 [1]. They then calculate the dimensionless axial velocity profile in the eccentric cylinders for the power law liquids, which is,

$$v_{\mathcal{G}}(\kappa,\beta) = -\frac{n}{n+1} \left( \frac{d(1-\varepsilon\cos\beta)}{2R_2} \right)^{1+\frac{1}{n}} \left( |\kappa|^{1+\frac{1}{n}} - 1 \right)$$
(1)

where *n* is the power law index;  $d = R_2 - R_1$ , the annular gap.  $R_2$  and  $R_1$  are the outer and inner radii of the annular, respectively.  $\beta$  is the angle measured from the *x*-axis as shown in Figure 3; and  $\varepsilon$ , the dimensionless eccentricity defined as;

$$\varepsilon \equiv \frac{e}{d}$$
,  $0 < \varepsilon < 1$ . (2)

They also introduce the dimensionless variable  $\kappa$  as,

$$\kappa = \frac{\xi - \xi_0}{\xi_1 - \xi_0}$$
(3)

where,

$$\xi_0 \equiv \frac{\xi_1 + \xi_2}{2} \tag{4}$$

and the constant circles  $\xi_1$  and  $\xi_2$  corresponding to the  $R_1$  and  $R_2$  are;

$$\xi_1 = \sinh^{-1} \left[ \frac{a}{R_1} \right] \tag{5}$$

and

$$\xi_2 = \sinh^{-1} \left[ \frac{a}{R_2} \right] \tag{6}$$

where the confocal length, a, is the distance measured from the y-axis to the intersection of the  $\theta$  circles can be calculated from the  $R_1$  and  $R_2$  and the annular eccentricity e,

$$a = \frac{1}{2e} \sqrt{(R_1^2 + R_2^2 - e^2)^2 - 4R_1^2 R_2^2},$$
 (7)

while the dimensional axial velocity profile  $\nu_{\zeta}$  is defined such that,

$$v_{\varsigma} = v_{\varsigma p} \left[ -\frac{R_2^{n+1}}{m} \frac{dP}{d\zeta} \right]^{\frac{1}{n}}$$
(8)

where m is the consistency index of the power law viscosity and  $dP/d\zeta$  is the pressure gradient in the axial direction. Their solution is valid for the 0.2 dimensionless eccentricities or less.

Long residential time during plastics pipe and curved hose manufacturing may cause plastic degradation. Here, we are interested in heat flux of a power-law fluid axially flow in the eccentric annular. In other words, heat build up in the eccentric dies during the productions must be controlled. To study the heat transfer between the eccentric cylinders, energy equation is built in bipolar cylindrical coordinates. Temperature distribution between the eccentric cylinders is determined from the energy equation analytically. Here we investigate the heat convection of the axial flow between eccentric die to help pipe manufacturers to understand the heat behavior in the eccentric die.

### 2. METHODOLOGY

### 2.1 Bipolar cylindrical coordinates

In bipolar cylindrical coordinates,  $\xi$  and  $\theta$  represent two orthogonal sets of circles. Figures 3 and 4 show the inner and outer cylinders at constant  $\xi_1$  and  $\xi_2$ . The relations between the rectangular coordinates and the bipolar cylindrical coordinates are given by [12],

$$x = \frac{a \sinh \xi}{\cosh \xi - \cos \theta} \tag{9}$$

$$y = \frac{a\sin\theta}{\cosh\xi - \cos\theta} \tag{10}$$

$$z = \zeta$$
 (11)

where  $\theta \in [0, 2\pi)$ ,  $\xi \in (-\infty, \infty)$  and  $\zeta \in (-\infty, \infty)$ . There are several notation conventions. Arfken [13], for example, prefers  $(\eta, \xi, z)$ , while  $(\xi, \theta, \zeta)$  is used in this work [1]. The scale factors are,

$$h_{\theta} = \frac{a}{\cosh \xi + \cos \theta}$$
(12)

$$h_{\xi} = \frac{a}{\cosh \xi + \cos \theta}$$
(13)

$$h_{\xi} = 1.$$
 (14)

Since the scale factors in Eqs. (12) and (13) are the same, we denote  $h = h_B = h_B$ .

### 2.1.1 Functions for complex variables

Commemorative International Conference on the Occasion of the 4th Cycle Celebration of KMUTT Sustainable Development to Save the Earth: Technologies and Strategies Vision 2050: (SDSE2008) 7-9 April 2009, Bangkok, Thailand

If  $\xi$  and  $\theta$  are real single-valued functions of x and y which their four partial derivatives are continuous throughout a real domain of R. Then the Cauchy-Rieman equations,

$$\frac{\partial \theta}{\partial x} = \frac{\partial \xi}{\partial y} \tag{15}$$

and

$$\frac{\partial \xi}{\partial x} = -\frac{\partial \theta}{\partial y} \tag{16}$$

are both necessary and sufficient conditions that

$$f(z) = \theta(x, y) + i\xi(x, y)$$
(17)

is analytic in R. Under these conditions, the derivative of f(z) is given by either,

$$f'(z) = \frac{\partial \theta}{\partial x} + i \frac{\partial \xi}{\partial x}$$
(18)

and

$$f'(z) = \frac{\partial \xi}{\partial y} - i \frac{\partial \theta}{\partial y}.$$
 (19)

### 2.1.2 The intersection of two circles

In bipolar cylindrical coordinates,  $\theta$  is a coordinate at the intersection of two circles that tangent to the circle of origin (0, k), while  $\xi$  is a coordinate at the intersection of two circles that tangent to the circle of origin (h, 0). The angle  $\theta$  is measured between the line (0, k) to (a, 0) and the y-axis. Then,

$$\sin \theta = \frac{a}{R_s} \tag{20}$$

$$\cos \theta = \frac{k}{R}$$
 (21)

$$\tan \theta = \frac{a}{\iota} \tag{22}$$

$$k^2 + a^2 = R_i^2. (23)$$

The equation of a circle that center at (0, k) with radius  $R_1$  is,

$$(x-0)^2 + (y-k)^2 = R_1^2$$
. (24)

Then, substitute k and  $R_1$  from Eqs. (20) and (22) into Eq. (24),

$$x^{2} + (y - a \cot \theta)^{2} = a^{2} \csc^{2} \theta.$$
 (25)

After rearranging Eq. (25), one gets;

$$\tan \theta = \frac{2ay}{x^2 + y^2 - a^2},$$
 (26)

that is,

$$\theta = \tan^{-1} \left( \frac{2ay}{x^2 + y^2 - a^2} \right)$$
 (27)

The partial derivative of  $\theta$  with respect to x is,

$$\frac{\partial \theta}{\partial x} = \frac{\partial}{\partial x} \left( \tan^{-1} \left( \frac{2ay}{x^2 + y^2 - a^2} \right) \right),\tag{28}$$

then

$$\frac{\partial \theta}{\partial x} = \frac{-4axy}{\left(x^2 + y^2 - a^2\right)^2 + \left(2ay\right)^2}.$$
 (29)

After rearranging the terms at the right side of the Eq. (29), one gets

$$\frac{\partial \theta}{\partial x} = \frac{\partial}{\partial y} \left( \tanh^{-1} \left( \frac{2ax}{x^2 + y^2 + a^2} \right) \right)$$
 (30)

Then, to satisfy the Cauchy-Rieman in Eq. (15),

$$\xi = \tanh^{-1} \left( \frac{2ax}{x^2 + y^2 + a^2} \right). \tag{31}$$

Rearrange Eq. (31) to get,

$$(x - a \coth \xi)^2 + y^2 = a^2 \operatorname{csch}^2 \xi.$$
 (32)

Finally, we solve Eqs. (25) and (32) to get

$$x = \frac{y \cot \theta + a}{\coth \xi} \tag{33}$$

and

$$y = \frac{x \coth \xi - a}{\cot \theta} \tag{34}$$

then

$$x + yi = \frac{a(\sinh \xi + i \sin \theta)}{\cosh \xi + \cos \theta}$$
(35)

or one can rewrite Eq. (35) to

$$x + yi = a \tan(\frac{i\xi}{2} + \frac{\theta}{2}). \tag{36}$$

Eqs. (33) to (36) are the transformation relations between the rectangular coordinates and the bipolar cylindrical coordinates.

# 2.2 Small dimensionless eccentricity approximation

For small dimensionless eccentricity,  $\varepsilon << 1$ , the scale factor is simplified to [14]

$$h = \frac{a}{X} = \frac{R_0 \left(1 - \varepsilon \cos \beta\right)}{\left(1 - \varepsilon^2\right)_2^1}$$
(37)

where

$$X = \frac{1 + \varepsilon \cos \theta}{\varepsilon} = \frac{1 - \varepsilon^2}{\varepsilon (1 - \varepsilon \cos \beta)},$$
 (38)

and Ro is the average radius,

$$R_0 = \frac{R_1 + R_2}{2} \tag{39}$$

and  $\beta$  is measured from the x-axis as shown in the Figure 3. The relations between  $\beta$  and  $\theta$  are shown in [11, 14]. Let,

$$c = \xi_1 - \xi_2$$
 (40)

then, for the small eccentricity,

$$c = \frac{\delta}{2} (1 - \varepsilon^2)^{\frac{1}{2}} = \frac{d}{2R_0} (1 - \varepsilon^2)^{\frac{1}{2}}.$$
 (41)

From Eq. (3), one can get,

$$\frac{\partial \kappa}{\partial \xi} = \frac{2}{c}$$
 (42)

Finally, combine Eqs. (37) and (41) to get,

$$hc = \frac{d(1 - \varepsilon \cos \beta)}{2}.$$
 (43)

2.3 Energy equation

The rate of change of the fluid temperature depends on the heat conduction, change of the pressure, P, with respect to its temperature, T, at a constant volume  $\forall$ , and viscous heating of the fluid [2].

$$\rho \hat{C}_{p} \frac{DT}{Dt} = -\left(\nabla \cdot \underline{q}\right) - T\left(\frac{\partial P}{\partial T}\right)_{\underline{\nu}} \left(\nabla \cdot \underline{\nu}\right) - \left(\underline{r} : \nabla \underline{\nu}\right)$$
(44)

where  $\rho$  is the liquid density,  $\hat{C}_p$ ; the specific heat at a constant pressure,  $\underline{\tau}$ ; the deviatoric stress tensor,  $\underline{\nu}$ ; the velocity vector. Also the heat flux for a constant thermal conductivity, k, is defined as

$$q = -k\nabla T$$
. (45)

The gradient of the heat flux in the bipolar cylindrical coordinates is

$$\nabla \cdot \underline{q} = \frac{1}{h^2} \left\{ \frac{\partial}{\partial \xi} (hq_{\xi}) + \frac{\partial}{\partial \theta} (hq_{\theta}) + \frac{\partial}{\partial \zeta} (h^2 q_{\zeta}) \right\}. \quad (46)$$

The substantial derivative in the energy equation [Eq. (44)] is

$$\frac{DT}{Dt} = \frac{\partial T}{\partial t} + \frac{1}{h^2} \left\{ v_{\xi} \frac{\partial}{\partial \xi} (hT) + v_{\theta} \frac{\partial}{\partial \theta} (hT) + v_{\xi} \frac{\partial}{\partial \zeta} (h^2 T) \right\}. \tag{47}$$

In bipolar cylindrical coordinate, the gradient of a scalar function can be written in term of the transformation factor (scale factor)  $h = h_{\theta} = h_{\xi}$ , defined in Eqs. (12) and (13), and thus the gradient of the temperature is

$$\nabla T = \underline{\delta}_{\xi} \frac{1}{h} \frac{\partial T}{\partial \xi} + \underline{\delta}_{\theta} \frac{1}{h} \frac{\partial T}{\partial \theta} + \underline{\delta}_{\xi} \frac{\partial T}{\partial \zeta}$$
(48)

where  $\underline{\delta}_{\underline{\xi}}$ ,  $\underline{\delta}_{\theta}$ , and  $\underline{\delta}_{\underline{\xi}}$  are unit vectors in the  $\underline{\xi}$ ,  $\theta$ , and  $\zeta$  axes, respectively. Then, the Laplace equation on the temperature is

$$\nabla^{2}T = \frac{1}{h} \frac{\partial}{\partial \xi} \left( \frac{1}{h} \frac{\partial T}{\partial \xi} \right) + \frac{1}{h} \frac{\partial}{\partial \theta} \left( \frac{1}{h} \frac{\partial T}{\partial \theta} \right) + \frac{\partial^{2}T}{\partial \zeta^{2}}.$$
 (49)

The viscous dissipation term in the right side of Eq. (44) is

$$\underline{\tau} : \nabla \underline{v} = \tau_{\xi\xi} \left( \frac{1}{h} \frac{\partial v_{\xi}}{\partial \xi} \right) + \tau_{\theta\theta} \left( \frac{1}{h} \frac{\partial v_{\theta}}{\partial \theta} \right)$$

$$+ \tau_{\xi\xi} \left( \frac{\partial v_{\xi}}{\partial \zeta} \right) + \tau_{\xi\theta} \left( \frac{1}{h} \frac{\partial v_{\xi}}{\partial \theta} + \frac{1}{h} \frac{\partial v_{\theta}}{\partial \xi} \right)$$

$$+ \tau_{\xi\xi} \left( \frac{\partial v_{\xi}}{\partial \zeta} + \frac{1}{h} \frac{\partial v_{\xi}}{\partial \xi} \right) + \tau_{\theta\zeta} \left( \frac{\partial v_{\theta}}{\partial \zeta} + \frac{1}{h} \frac{\partial v_{\xi}}{\partial \theta} \right)$$

$$(50)$$

For incompressible fluid, the second term on the right side of the energy equation [Eq. (44)] is negligible. Then, the energy equation becomes.

$$\rho \hat{C}_{p} \frac{DT}{Dt} = k \nabla^{2} T - (\underline{r} : \nabla \underline{v}). \tag{51}$$

### 3. ANALYSIS

3.1 Assumption and modeling

Here, we study a polymer melt axially flowing in eccentric annuli shown in Figure 3, and thus map the physical flow with the bipolar cylindrical coordinates shown in Figure 4. For a steady, laminar, incompressible, fully developed flow, we assume that the velocities in  $\xi$  and  $\theta$  directions are very small compare to that in  $\zeta$  direction, and then,  $v_{\zeta} = v_{\zeta}(\xi, \theta)$ ,  $v_{\xi} = v_{\theta} = 0$ , and  $T(\xi, \theta)$ . Since the dimensionless modified Brinkman number (Br<sub>Mo</sub>), the heat generation balances with the molecular heat export, is unity. The energy equation [Eq. (51)] is simplified to,

$$0 = k \left\{ \frac{1}{h} \frac{\partial}{\partial \xi} \left( \frac{1}{h} \frac{\partial T}{\partial \xi} \right) + \frac{1}{h} \frac{\partial}{\partial \theta} \left( \frac{1}{h} \frac{\partial T}{\partial \theta} \right) \right\}$$

$$- \left\{ \tau_{\xi\xi} \left( \frac{1}{h} \frac{\partial v_{\xi}}{\partial \xi} \right) + \tau_{\theta\xi} \left( \frac{1}{h} \frac{\partial v_{\xi}}{\partial \theta} \right) \right\}.$$
(52)

The shear stress can be written in terms of shear rates which are related to the velocity gradients such that [11, 14]

$$\tau_{\xi\xi} = -\eta \frac{1}{h} \frac{\partial v_{\xi}}{\partial \xi}, \qquad (53)$$

$$\tau_{\theta\zeta} = -\eta \frac{1}{h} \frac{\partial v_{\zeta}}{\partial \theta}.$$
 (54)

Substitute Eqs. (53) and (54) into Eq. (52) and rearrange to

$$\frac{\partial^2 T}{\partial \xi^2} + \frac{\partial^2 T}{\partial \theta^2} = -\frac{m}{k} \left| \frac{1}{h} \frac{\partial v_{\xi}}{\partial \xi} \right|^{n-1} \left\{ \left( \frac{\partial v_{\xi}}{\partial \xi} \right)^2 + \left( \frac{\partial v_{\xi}}{\partial \theta} \right)^2 \right\}$$
(55)

where the viscosity  $\eta$  obeys the power law model;

Commemorative International Conference on the Occasion of the 4th Cycle Celebration of KMUTT Sustainable Development to Save the Earth: Technologies and Strategies Vision 2050: (SDSE2008) 7-9 April 2009, Bangkok, Thailand

$$\eta = m\dot{\gamma}^{n-1} \tag{56}$$

where, for a shear flow, the scalar function of the rate of deformation tensor is,

$$\dot{\gamma} = \sqrt{\frac{1}{2} \left( \dot{\underline{\gamma}} : \dot{\underline{\gamma}} \right)}$$
(57)

where the rate of deformation tensor is defined as [1, 2],

$$\underline{\dot{\gamma}} = (\nabla \underline{v}) + (\nabla \underline{v})^T$$
(58)

For very small dimensionless eccentricity,  $\varepsilon << 1$ , *i.e.*  $\frac{\partial v_{\xi}}{\partial \theta} \cong 0$ ,  $\frac{\partial^2 T}{\partial \theta^2} \equiv 0$ , Eq. (55) becomes,

$$\frac{\partial^{2} T}{\partial \xi^{2}} = -\frac{m}{k} \left( \frac{1}{h} \right)^{n-1} \left| \frac{\partial V_{\zeta}}{\partial \xi} \right|^{n+1}. \tag{59}$$

Introducing the dimensionless variable from Eq. (3), and then, Fq. (59) will be

$$\frac{\partial^2 T}{\partial \kappa^2} = -\frac{m}{k} \left( \frac{2}{hc} \right)^{n-1} \left| \frac{\partial v_{\zeta}}{\partial \kappa} \right|^{n+1}. \tag{60}$$

Substituting Eq. (8) into Eq. (60), one gets,

$$\frac{\partial^2 T}{\partial \kappa^2} = -\frac{m}{k} \left(\frac{2}{hc}\right)^{n-1} \left[ -\frac{R_2^{n+1}}{m} \frac{dP_\zeta}{d\zeta} \right]^{\frac{n+1}{n}} \frac{\partial v_{,p}}{\partial \kappa}$$
(61)

Furthermore, we can rearrange Eq. (61) such that,

$$\frac{\partial^2 T^*}{\partial \kappa^2} = - \frac{\left| \partial \nu_{\varphi_p} \right|^{n+1}}{\partial \kappa}$$
(62)

where the dimensionless temperature profile, T', is

$$T^* = \frac{T}{\frac{m}{k} \left(\frac{2}{h_C}\right)^{n-1} \left[ -\frac{R_2^{n+1}}{m} \frac{dP_s}{d\zeta} \right]^{\frac{n+1}{n}}}$$
 (63)

We differentiate Eq. (1) with respect to  $\kappa$  and then substitute into Eq. (62) to set

$$\frac{\partial^2 T^*}{\partial \kappa^2} = -\left[\frac{d(1 - \varepsilon \cos \beta)}{2R_2}\right]^{1 + \frac{1}{n}} \kappa |\kappa|^{\frac{1}{n} \cdot 1}$$
(64)

or,

$$\frac{\partial^2 T^*}{\partial \kappa^2} = -\lambda_1 |\kappa|^{1+\frac{1}{n}} \tag{65}$$

where  $\lambda_1$  is always real and positive and defined such that,

$$\lambda_1 = \left[ \frac{d(1 - \varepsilon \cos \beta)}{2R_2} \right]^{\frac{(n+1)^2}{n}}.$$
 (66)

By integrating Eq. (65) once, one gets

$$\frac{\partial T^*}{\partial \kappa} = -\frac{\lambda_1}{\left(2 + \frac{1}{n}\right)} |\kappa|^{2 + \frac{1}{n}} + c_1,$$
(67)

From Eq. (67), the dimensionless temperature profile  $T^*$  is,

$$T^* = -\frac{\lambda_1}{\left(2 + \frac{1}{n} \left(3 + \frac{1}{n}\right) \left|\kappa\right|^{3 + \frac{1}{n}} + c_1 \kappa + c_2\right)}$$
(68)

where  $c_1$  and  $c_2$  are the integration constants. Assume that the outer radius  $R_2$  ( $\kappa=-1$ ), has a constant temperature  $T_1$ , corresponding to  $T^*=T_1^*$ , and the inner radius  $R_1$  ( $\kappa=1$ ) has a constant temperature  $T_2$ , corresponding to  $T^*=T_2^*$ . Then,

$$T^* = -\lambda_2 \left( |\kappa|^{3+\frac{1}{n}} - 1 \right) + \lambda_3 (\kappa + 1)$$
 (69)

where

$$\lambda_2 = \frac{\lambda_1}{\left(2 + \frac{1}{n}\right)\left(3 + \frac{1}{n}\right)},\tag{70}$$

$$\lambda_3 = \frac{\left(T_2^* - T_1^*\right)}{2}.$$
 (71)

### 3.2 Results and discussion

Figures 5 to 8 are plotted the dimensionless temperature profiles,  $T^*$  versus the dimensionless gap,  $\kappa$  [Eq. (69)] by using the power-law index (n) from 0.5, and increasing by 0.1, to 0.9, at various angular distance from the smallest gap,  $\beta$ , with the dimensionless eccentricity,  $\varepsilon$ , from 0.10 to 0.20 at the dimensionless radius ratio,  $R_{\rm Ratio} = 0.80$  and 0.90.

The figures 5 to 8 show that the dimensionless temperature  $(T^*)$ , in general, increases with the dimensionless radius ratio,  $R_{\text{Ratio}}$ , the dimensionless eccentricity,  $\varepsilon$ , the angular distance from the smallest gap,  $\beta$ , and the power law exponent, n. In addition, the more non-Newtonian of the fluid (less n), the more flat at the tip of the temperature profile. Moreover, the more dimensionless eccentricity,  $\varepsilon$ , dimensionless temperature profiles decrease at the smallest gap ( $\beta$ =0) and increase at the biggest gap ( $\beta$ =180). This is because of the convective flow of the fluid in the eccentric die. In other words, the dimensionless temperature is proportional to the velocity profile in the die.

The dimensionless temperatures also decrease from 10E-5 to 10E-7 when the radius ratios (R<sub>Ratio</sub>) increase from 0.80 to 0.90. When the radius ratios increase, the inner radius and outer radius are almost the same. This means that the gaps in both upper and lower side are very small. Then, the convective effects in the die are diminish, which make the dimensionless temperature decreases when the radius ratio increases.

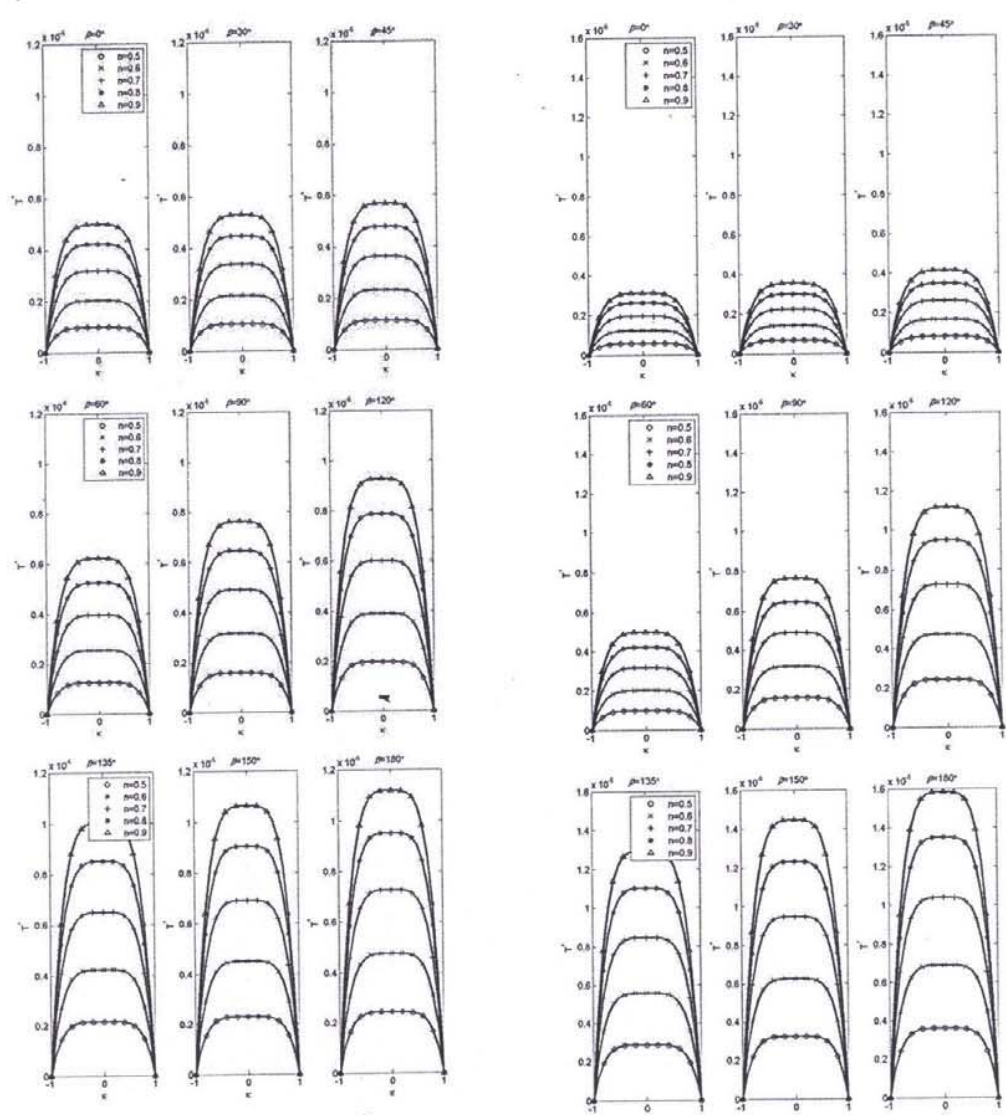


Figure 5 Dimensionless temperature profiles  $T^*$  versus the dimensionless gap  $\kappa$  using  $R_{Ratio} = 0.80$  and the dimensionless eccentricity,  $\varepsilon = 0.10$ , at various angle  $\beta$  and power law index n.

Figure 6 Dimensionless temperature profiles  $T^*$  versus the dimensionless gap  $\kappa$  using  $R_{\rm Ratio} = 0.80$  and the dimensionless eccentricity,  $\varepsilon = 0.20$ , at various angle  $\beta$  and power law index n.

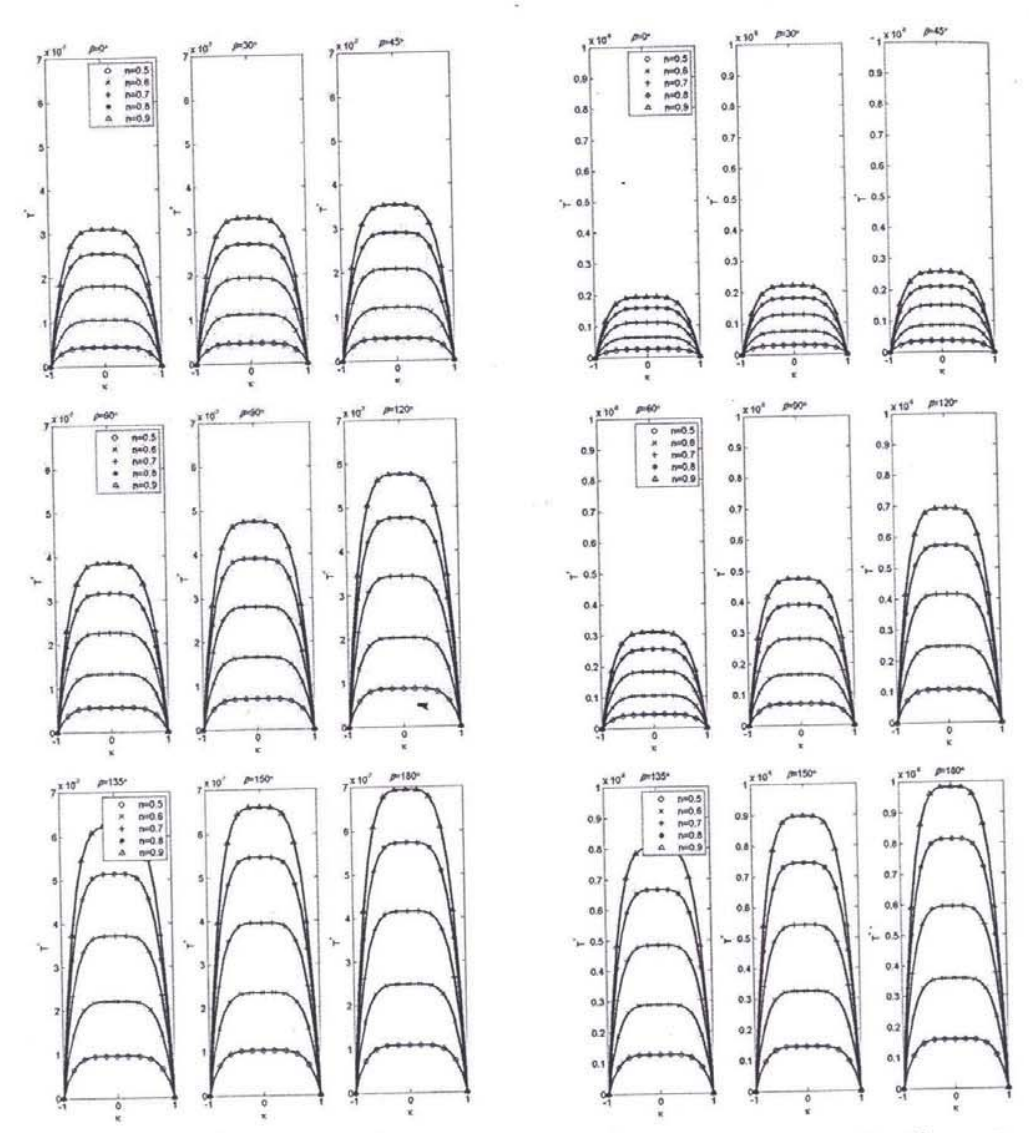


Figure 7 Dimensionless temperature profiles  $T^*$  versus the dimensionless gap  $\kappa$  using  $R_{\rm Ratio}$ = 0.90 and the dimension less eccentricity,  $\varepsilon$  = 0.10, at various angle  $\beta$  and power law index n.

Figure 8 Dimensionless temperature profiles  $T^*$  versus the dimensionless gap  $\kappa$  using  $R_{\rm Ratio} = 0.90$  and the dimension less eccentricity,  $\varepsilon = 0.20$ , at various angle  $\beta$  and power law index n.

Commemorative International Conference on the Occasion of the 4th Cycle Celebration of KMUTT Sustainable Development to Save the Earth: Technologies and Strategies Vision 2050: (SDSE2008) 7-9 April 2009, Bangkok, Thailand

### 4. CONCLUSION

For bipolar cylindrical coordinate, the energy equation coupled with the velocity profile of the power law constitutive model is used to determine the temperature profile in the pipe extrusion die. The dimensionless temperature profile of a steady, laminar, incompressible and fully developed flow of a power law polymer can be found by the analytic method with assumptions such that there are no velocities in the  $\xi$  and  $\theta$ directions, no heat convection terms, and uniform wall temperatures. The solution reveals that the dimensionless temperature distribution is a function of the dimensionless radius ratio, R<sub>Ratio</sub>, the dimensionless eccentricity, E, the angular distance from the smallest gap,  $\beta$ , the power law exponent, n, and a strong function of, the dimensionless gap,  $\kappa$ . The temperature profiles are flat at the middle of the gap and suddenly drop to reach the wall temperature near the wall region. The temperature rises at the gap center due to heat dissipation of the non-Newtonian effects. This temperature rise is higher if the gap, or in other words the angular distance from the smallest gap,  $\beta$ , is increased. This is because the bigger gap allows the polymer to easily flow and thus get more temperature dissipation from the molecular frictions. Moreover, the temperature rise also increases with the power law exponent, n, to reach the Newtonian temperature profile at n = 1. Thus, the less the power law exponent, n, the temperature profile shows plateau at the gap center, or in other words, it shows non-Newtonian effects when the power law exponent, n, is less.

## 5. ACKNOWLEDGMENTS

The authors gratefully acknowledge Thailand Research Fund (TRF) and National Science and Technology Development Agency (NSTDA) for funding supports.

# 6. REFERENCES

- Bird, R. B., Armstrong, R. C. and Hassager, O., (1987)
   Dynamics of Polymeric Liquids. Vol. 1: Fluid Mechanics, 2<sup>nd</sup>
   Ed., Wiley, New York, pp.181-183 and pp. 595-596.
   Bird, R. B., Stewart, W. E. and Lightfoot, E. N., (1960)
- [2] Bird, R. B., Stewart, W. E. and Lightfoot, E. N., (1960) Transport Phenomena, John Willey & Sons, Inc., New York, pp. 42-54, 68.
- [3] Michaeli, W., (1992) Extrusion Dies for Plastics and Rubber, 2<sup>nd</sup> Ed., Hanser Publishers, New York, pp. 58-60.
- [4] Baird, D. G. and Collias, D. I., (1998) Polymer Processing: Principles and Design, John Willey & Sons, Inc., New York, pp. 14-16.
- [5] Fredrickson, A. G. and Bird, R. B., (1958) Ind. Eng. Chem., 50, 347.
- [6] Guckes, T. L., (1975) Trans. ASME(B), 97, 498.
- [7] Dealy, J. M. and Wissbrun, K. F., (1990) Melt Rheology and Its Role in Plastics Processing, Van Nostrand Reinhold, New York, pp. 512-519.
- [8] Rosato, D. V. and Rosato, D. V., (1989) Blow Molding Handbook, Hanser Publishers, New York, pp. 664-669.
- [9] Parnaby, J. and Worth, R. A., (1974) Proc. Instr. Mech. Engrs., 188(25), 357.
- [10] Dijksman, J. F. and Savenije, E. P. W., (1985)
- Rheologica Acta, 24, 105.
- [11] Kolitawong, C. and Giacomin, A. J., (2001) Polym.-Plast. Technol. Eng., 40(3), 363-384.

- [12] Moon, P. and Spencer, D. E., (1961) Field Theory for Engineers, D. Van Nostrand Company, Inc., New York, pp. 361-368.
- [13] Arfken G., (1970) Mathematics Methods for Physicist, Academic Press, Orlando, FL, pp. 97-102.
- [14] Kolitawong, C. and Giacomin, A. J., (1999) Axial Flow Between Eccentric Cylinders, RRC Report 167, Rheology Research Center, University of Wisconsin, Madison, USA.

# References

- 1 R. B. Bird, R. C. Armstrong, and O. Hassager, *Dynamics of Polymeric Liquids. Vol. I: Fluid Mechanics*, 2<sup>nd</sup> Ed., Wiley, New York, pp.181-183 and pp.595-596 (1987).
- 2 R. B. Bird, W. E. Stewart, and E. N. Lightfoot, *Transport Phenomena*, John Wiley & Sons, Inc., New York, pp 42-54, 68 (1960).
- 3 R. B. Bird, W. E. Stewart, and E. N. Lightfoot, *Transport Phenomena*, 2<sup>nd</sup> Ed., John Wiley & Sons, Inc., New York, pp. 53-56, 64 (2007).
- 4 W. Michaeli, *Extrusion Dies for Plastics and Rubber*, 2<sup>nd</sup> Ed., Hanser Publishers, New York, pp. 58-60 (1992).
- 5 D. G. Baird and D. I. Collias, *Polymer Processing: Principles and Design*, John Wiley & Sons, Inc., New York, pp. 14-16 (1998).
- 6 A. G. Fredrickson and R. B. Bird, Ind. Eng. Chem., 50, 347 (1958).
- 7 T. L. Guckes, Trans. ASME(B), 97, 498 (1975).
- 8 C. Kolitawong and A. J. Giacomin "Axial Flow Between Eccentric Cylinders" RRC Report 167, Rheology Research Center, University of Wisconsin, Madison, USA (1999).
- 9 J. Happel and H. Brenner, *Low Reynolds Number Hydrodynamic*, 2<sup>nd</sup> Ed., Noordhoff International Publishing, Netherlands, pp.35-37 (1973).
- 10 J. Caldwell, Jour. Royal Tech. College (Glasgow), 2, p. 203 (1932).
- 11 Piercy, N. A. V., M. S. Hooper, and H. F. Winny, *Phil. Mag.*, 7(15), 647 (1933).
- 12 R. Berker, "Intégration des équations du mouvementy d'un fluide visqueux incompressible," S. Flügge, ed., VIII/2, *Handbuch Der Physik, "Strömungsmechanik II*," Springer-Verlag, Berlin, pp.74-75 (1963).
- 13 J. F. Heyda, Journal of the Franklin Institute, 26, 25 (1959).
- 14 W. T. Snyder and G. A. Goldstein, AIChE Journal, 11(3), 462 (1965).
- 15 J. M. Dealy and K. F. Wissbrun, *Melt Rheology and Its Role in Plastics Processing*, Van Nostrand Reinhold, New York, pp. 512-519 (1990).
- 16 D. V. Rosato and D. V. Rosato, *Blow Molding Handbook*, Hanser Publishers, New York, pp. 664-669 (1989).
- 17 J. Parnaby and R. A. Worth, *Proc. Instn Mech. Engrs.*, **188**(25), 357 (1974).
- 18 J. F. Dijksman and E. P. W. Savenije, Rheologica Acta, 24, 105 (1985).
- 19 C. Kolitawong and A. J. Giacomin, Polym.-Plast. Technol. Eng., **40**(3), 363-384 (2001).
- 20 P. Moon and D. E. Spencer, "Field Theory for Engineers," D. Van Nostrand Company, Inc., New York, pp. 361-368 (1961).
- 21 Arfken G. "Mathematics Methods for Physicist," Academic Press, Orlando, FL, pp. 97-102 (1970).
- 22 Z. Tadmor, and C. G. Gogos, "Principles of Polymer Processing," John Wiley and Sons, New York, pp. 695 (1973).
- 23 Z. Tadmor and C. G. Gogos, "Principles of Polymer Processing," 2<sup>nd</sup> Ed., John Wiley & Son, New York, pp. 889-913 (2006).